Electronic Applications of Single-Walled Carbon Nanotubes: Electropolymerised Transparent Electrodes and CNT Monolayers on Silicon

Tobias Lockwood   Department of Chemistry

McGill University, Montreal

October 2009

A thesis submitted to McGill University in partial fulfilment of the requirements of the degree of Master of Chemistry

CONTENTS

1. Carbon Nanotubes and their electronic applications

2. Conducting Polymers

3. Electropolymerisation

4. Transparent electrodes from electropolymerised PEDOT on CNT films

5. Covalently bound SWNT monolayers on silicon

ABSTRACT

The viability of two independent electronic applications of single-walled carbon nanotubes was studied. Firstly, the use of a transparent, conductive, nanotube film as an electrode on which to electrochemically synthesise a thin film of poly(ethylenedioxythiophene). Such an electrode, possessing advantageous properties of both the nanotube and polymer film, should prove useful for numerous organic devices. Polymer-nanotube electrodes were made with HipCO and arc-discharge CNTs, on glass and flexible substrates; showing up to 100 Ω/sq. improvement in sheet resistance over conventional spin-coated films was demonstrated on glass. Preliminary organic LED devices were fabricated and successfully tested. Secondly, covalently bound monolayers of SWNTs on silicon were synthesised with a view to exploring the electronic properties of vertically aligned SWNT arrays. Silicon surfaces with hydroxyl functionality were prepared by a radical reaction with hydroxyl terminated 1-alkenes, which were then ester couple to oxidised carbon nanotubes. The resulting substrates showed bound, but disordered nanotube films.

RÉSUMÉ

Nous avons étudié deux applications basées sur l’utilisation de nanotubes de carbone. Nous avons tout d'abord réalisé des couches conductives et transparentes de nanotubes servant de substrat pour le dépôt électrochimique d'une couche mince de poly(éthylenedioxythiophene). Une telle électrode, ayant les propriétés des nanotubes ainsi que du polymère, devrait être bénéfique pour divers dispositifs organiques. Les électrodes polymère-nanotubes ont été fabriquées avec les SWNTs HipCO et à l’arc électrique sur du verre et sur du plastique; le gain obtenu rapport aux couches déposées par enduction centrifuge en terme de résistance va jusqu’à 100 Ω/sq. Quelques DEL organiques fonctionnelles ont été fabriquées avec succès en utilisant ces électrodes. Ensuite, nous avons synthétisé des couches auto-assemblées de SWNTs sur du silicium, afin d'étudier les propriétés électriques des SWNTs alignés verticalement. Les surfaces de silicium fonctionnalisées avec des groupes hydroxyles ont été liées aux nanotubes par estérification. Les substrats obtenus ont des nanotubes liés à la surface qui sont désordonnés.

ACKNOWLEDGMENTS

My supervisor Prof. Perepichka for his unfailing and helpful advice, as well as all members of this research group for their invaluable help and assistance throughout the project.

Our collaborators in the research group of Ricardo Izquierdo at L'Université de Quebec à Montréal for their help and advice with PDMS stamping and OLED fabrication; particularly Yu-Mo Chien who conducted much of this work.

Line Mongeon and Gilles Bourret for help with SEM.

1. CARBON NANOTUBES AND THEIR ELECTRONIC APPLICATIONS

1.1 Introduction

Carbon nanotubes are an allotrope of carbon whose structure were first brought to light by Iijima in 1991 [1], although they had certainly been observed elsewhere in much earlier work [2]. They can be considered either as fullerene molecules elongated in one dimension, or equivalently as a single atomic layer of graphite (graphene) rolled up into a cylinder. Such a structure became known as a single-walled nanotube (SWNT) whereas similar fullerenes consisting of several of these cylinders stacked inside one another are called multi-walled nanotubes (MWNTs). It was soon recognised that the unique crystal structure of this material should lend it rather unusual mechanical and electronic properties, and the years following their discovery have seen great efforts to harness these properties for a diverse array of possible applications. These include their use as nanoscale components in molecular electronics, vessels for drug delivery, giving mechanical strength to polymer composite materials, and as electrode materials for fuel cells, field emission devices, photovoltaics and LEDs. Currently, very few of the applications thought to be able to benefit from this form of carbon have fully realised their expected potential. Indeed, it is clear that it is a considerable challenge to attempt to express the remarkable properties of a single tube on the nanoscale in the properties of a macroscale material; nevertheless there are fields in which the nanotube is beginning to show the significant impact it can make.

1.2 Electronic structure

Understanding the electronic nature of single-walled nanotubes requires some study of the exact structure of the sp^2 hybridised carbon cylinder from which they formed. In effect, this cylinder can be thought of as a graphene sheet rolled up along some direction which may be defined using the hexagonal lattice vectors: (m,n). This direction then defines whether the nanotube has a non-chiral structure known as ‘armchair’ (m, n=m), ‘zig-zag’ (m,0), or a chiral structure for any other m and n. Importantly, it turns out that the chirality of the nanotube has a crucial bearing on its electronic nature, in that whether they are metallic or semi-conducting depends on these vectors m and n: $\frac{(2m+n)}{3} = integer$ is the condition for a nanotube to be metallic. It follows that in a random assortment of nanotubes, roughly one in three will be metallic.

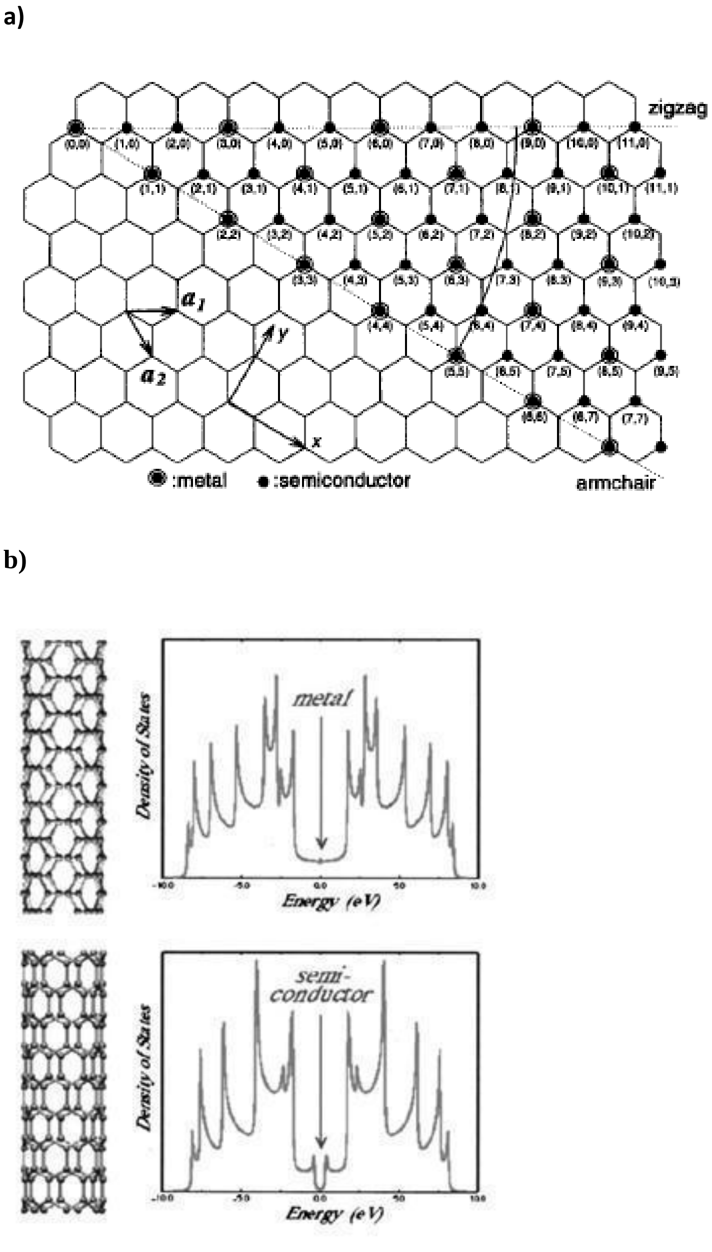

Figure 1.1 ***(a)*** *The vectors (m,n) as defined on a 2D hexagonal carbon lattice and (**b**) The structure and density of states for metallic and semi-conducting nanotubes* [3]

Figure 1.1 shows the electronic density of states (DOS) for typical semi-conducting and metallic nanotubes. Their one-dimensional nature gives rise to an electronic structure somewhere between that of an individual molecule and that of a crystal. In the direction of the axis, electrons are not confined and broad conduction and valence bands arise as a consequence. However, the confinement of electrons in the other two dimensions causes the sharp peaks in the DOS, known as Van Hove singularities which can be seen as somewhat analogous to the discreet energy levels observed in individual molecules. This quantisation of energy levels gives rise to the variation in the conducting properties of the nanotubes. A flat sheet of graphene possesses an energy surface which has zero band-gap at six symmetry points; whether the confined nanotube levels intersect these points or not determines whether or not they are metallic.

The semi-conducting nanotubes have a band gap between the valence and conduction bands, whereas the metallic tubes have some non-zero density of states in this region. For tubes of the same diameter it will be the case that the first singularities either side of the gap in a semi-conducting tube will be closer in energy than the first singularities in each ‘band’ of the metallic tubes. This has significant bearing on the type of transitions observed between states, which will be discussed further below. It is also important to note that a single-walled nanotube can possess a range of diameters (typically from 1 to 5 nm), and this diameter will affect the confinement of the electrons and thus the spacing of the energy levels. As for a simple particle in a box model, the thicker the nanotube, the closer together these levels will be.

Theoretically, the one-dimensional structure of carbon nanotubes should allow conduction of electrons along their axis without any scattering; a phenomenon known as ballistic conduction. The electron can be thought of as travelling along the nanotube as a coherent wave, just as light travels through a wave-guide. This type of transport can be described in quantum mechanical terms, in which the conductance corresponds to the number of electron modes with energies between the Fermi levels of the two contacts. In practice, the conductivity of an individual tube will be governed largely by the contact resistance between it and the metal contacts, as well as the Schottky barrier present between semi-conducting CNTs and the contacts. Nevertheless, nanotubes have been shown to support enormous current densities many times greater than metal wires are capable of [4].

1.3 Characterisation

Carbon nanotubes are notoriously difficult to study using most techniques which are traditionally relied on heavily by chemists. The physical nature of a sample of nanotubes, that is, degree of purity, amount of defects, and proportions of semi-conducting and metallic, can be determined using absorption, fluorescence, and Raman spectroscopy. Microscopy techniques such as STM, AFM, SEM and TEM can also provide invaluable information on the length, uniformity, crystallinity and morphology of nanotube samples. However, it should be noted that many of these techniques to not generally give a view of anything more than a small portion of the sample under inspection, or a small proportion which can be excited by a particular laser wavelength. The extent to which such results are representative of a whole sample is always a factor to be considered.

Electron-microscopy is probably the most important analysis tool for carbon nanotubes, and indeed, responsible for their discovery. SEM of CNT samples is highly useful for analysing their purity, the presence of other carbonaceous material, and the length and degree of alignment of the nanotubes. High resolution TEM allows detailed observation of the nanotube structure, such as diameter, degree of crystallinity in the walls, and the number of layers present in multi-walled tubes.

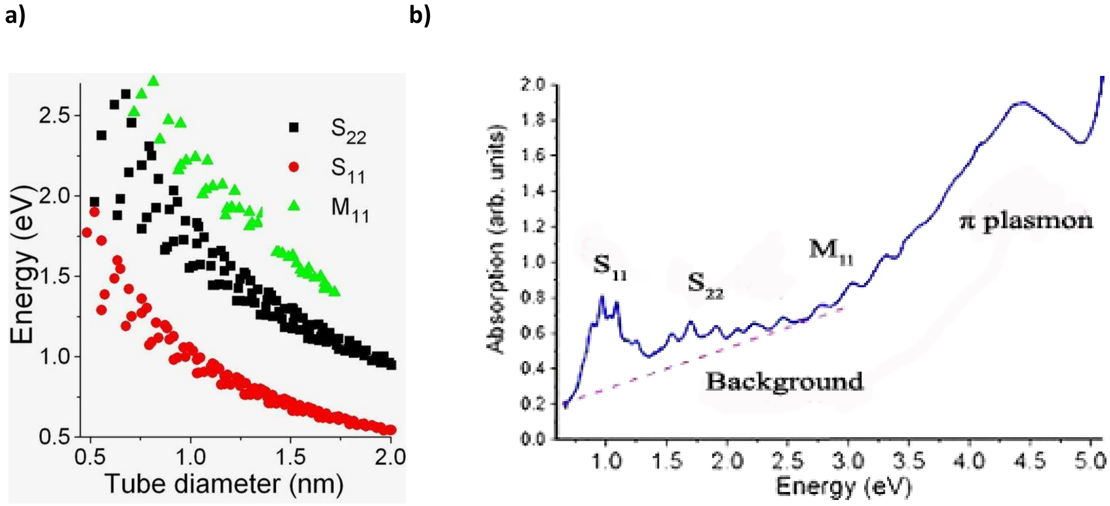

Figure 1.2 ***a)*** *Kataura plot and* ***b)*** *typical SWNT absorption spectrum [5]*

The electronic states of carbon nanotubes can be effectively studied by absorption spectroscopy in the optical and near IR regions. Any given sample of as-synthesised nanotubes will be a mix of semi-conducting and metallic tubes of various diameters. If excited with an appropriate wavelength laser, the sample will absorb in distinctive bands, which correspond to transitions between the Van Hove singularities closest to the Fermi level for metallic and semi-conducting tubes (commonly labelled S_{11}, S_{22}, and M_{11}). The range of nanotube chiralities and diameters present in any sample gives rise to broad band absorption in regions corresponding to each transition. A Kataura plot is a useful graphic representation of how the energy of each transition type varies with tube diameter [6]. It can be seen that these strongest nanotube transitions occur mainly in the near-IR and IR regions, with some metallic transitions observable in the visible. These absorption spectra are a useful means of assessing the relative metallic and semiconducting make-up of a nanotube sample, or degree to which semi-conducting tubes have been doped. Equally, the intensity of the absorption and resolution of individual peaks within each transition band is a good indication of the quality of a nanotube dispersion. Bundling together of tubes and interaction between them leads to less distinct resolution of peaks for individual tube transitions

Semi-conducting single walled carbon nanotubes can exhibit photoluminescence when excited with laser light of the appropriate wavelength. Electrons can be excited between

Van Hove singlurities in symmetry allowed transitions; usually from c_1 to v_1 (singularities either side of the band-gap: S_{11}) or from c_2 to v_2 (the next two singularities: S_{22}). The electron will then relax to the lowest state in the valence band (v_1) and decay to the c_1 level while emitting a photon of corresponding energy. This technique is highly useful as it can be used to determine exactly the m and n labels of the nanotubes present in a sample, and thus, their chirality, diameter and whether they are semi-conducting or metallic. A photoluminescence map is created by exciting the sample at a range of wavelengths in the red to near infra-red, and observing the various luminescence wavelengths emitted by the sample (figure 1.3). From the energy gaps, c_1-v_1 and c_2-v_2, for each tube can easily be determined the m and n vectors. This specific identification of nanotubes allowed by the technique sees it frequently put to use to assess the outcome of techniques to separate nanotubes by size or electronic properties; a highly important area of nanotube research.

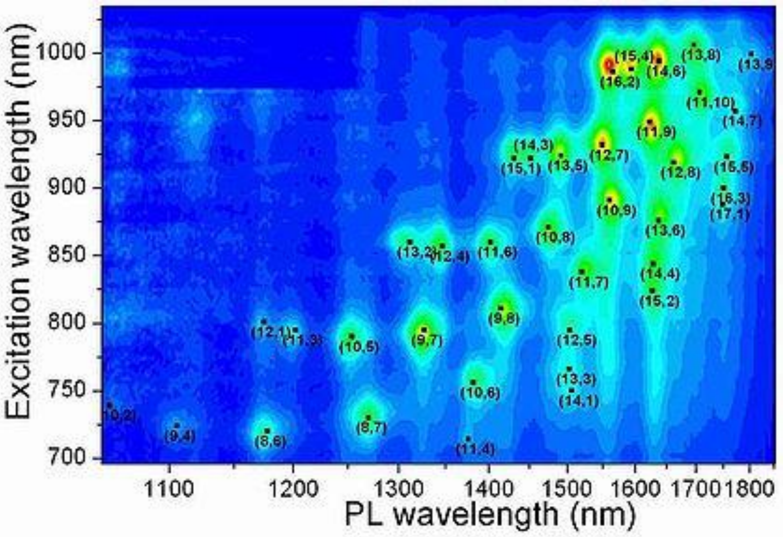

Figure 1.3 *A 2-dimensional fluorescence spectrum of SWNTs [9]*

Metallic nanotubes are not capable of photoluminescence, and they will quench the process in semi-conducting tubes if in contact with them as the electrons will simply move to fill the hole in the conduction band. In fact, interaction between any two tubes will disrupt the process and for this reason multi-walled tubes do not exhibit the phenomenon either. This requirement means that photoluminescence studies are also an effective means of assessing the degree of separation of tubes in a nanotube dispersion. The process is always of quite low efficiency, and is furthermore highly dependent on a good dispersion to work effectively.

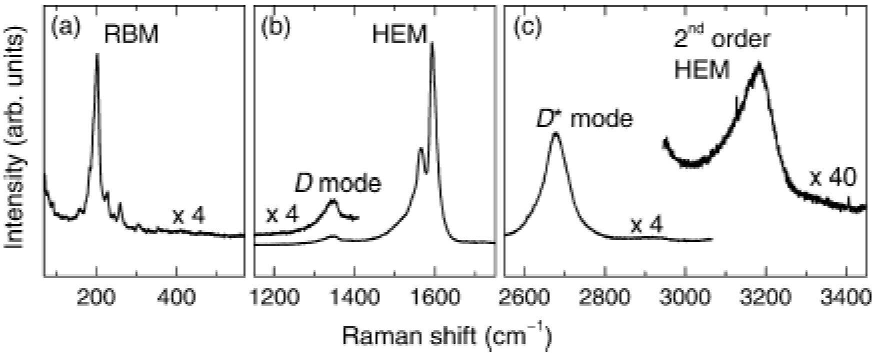

Figure 1.4 *A typical nanotube Raman spectrum [7]*

The pi-bonding structure of carbon nanotubes make them responsive to Raman spectroscopy, from which several important characteristics of a sample can be obtained. A typical Raman spectrum of a nanotube sample will display three distinictive absorption bands: at 1580 cm^{-1} a 'G mode' or high-energy mode (HEM) , at 1350 cm^{-1} the 'D mode' and at cm^{-1} the radial breathing mode (RBM) (figure 1.4). Other, higher energy peaks are overtones or combinations of these modes. The two higher energy absorption bands relate to stretching modes of the carbon-carbon pi bonds, while the lower frequency breathing mode clearly corresponds to the expansion and contraction of the entire tube. The D-band absorption, often known as the 'defect band', is associated with bond stretching at boundaries of a graphitic sheet, whereas the 'Graphitic' G-band relates to stretching within such a graphene sheet. For this reason, a strong D-band absorption is normally linked to either the presence of 'defects' in the nanotubes, such as sp3 carbons, or other graphitic material as impurities in the sample. Shorter tubes will also give a larger D-band absorption, as open tube ends are essentially defects in the pi-bonding structure. It is therefore the ratio between the D and G band absorptions which is quoted as a means of demonstrating either levels of purity or presence of sp^3 defects in a sample. The comparison is clearly not very quantitative or absolute, thus it is most effectively used as comparison between the same nanotube sample after and before a particular treatment or modification. Success of purification techniques can be assessed by reduction in the D-band, while introduction of sp^3 carbon during functionalisation of the tubes can be indicated by a D-band increase. Evidently, if both processes occur simultaneously, as they will do in any oxidative treatment of a sample, the change is less easy to interpret.

From the radial breathing mode can be estimated the diameters of nanotubes present in the sample; or more specifically, those which are electronically excited by the raman laser. The frequency of this vibrational mode (in cm^{-1}) is related to the diameter of a tube (in nm) by: $223/d + 10 = \nu$, although the constants are not known exactly [8]. The RBM band will therefore consist of several small peaks corresponding to the range of nanotubes excited by the laser.

The more detailed investigation of chemical adaptations to nanotubes is much less reliable, given that NMR and mass spectroscopy is difficult to carry out on nanotube samples and infra-red spectroscopy does not give reliable evidence of nanotube functionalisation.

1.4 Synthesis

Carbon nanotubes are produced to some extent in many commonly occurring combustion processes such as the burning of simple hydrocarbons. However, these processes offer only small yields of very irregular nanotubes, and provide no control over their size and quality. Controlled synthesis of carbon nanotubes follow three main methods: arc discharge, laser ablation, and chemical vapour deposition or hydrocarbon pyrolysis. The arc discharge method, in which a high current is passed between two high purity graphite electrodes in inert atmosphere, was that originally used by Iijima et al. for fullerene synthesis but found to give high yields of defect-free CNTs under certain conditions [1]. During the process, a deposit forms on the cathode while the anode is consumed. This deposit consists of a soft inner core of CNTs and other fullerenes, surrounded by a hard shell of graphene layers; nanotube yield is up to about 30% by weight. The production of single-walled nanotubes can be favoured by using graphite electrodes containing some proportion of metal catalyst, for which purpose a nickel-yttrium mixture has been found to give the highest SWNT yields [10]. The arc discharge method is in wide use partly because it was the first to be established, but it also provides a high quality of nanotube at lower costs than laser based methods described below.

The discovery that blasting a graphite target with a pulsed laser could result in synthesis of carbon nanotubes was made by the Smalley lab at Rice University [11]. The process is performed in a high temperature reactor under inert atmosphere, and the resulting nanotubes are formed in condensate of the vaporized carbon on the reactor walls. As for arc discharge, SWNT growth is favoured by use of metal catalyst particles in the graphite electrodes [12]; it has also been demonstrated that very fast picoseconds laser pulses promote SWNTs [13]. Laser ablation seems to offer a relatively controllable synthesis, in that reactor temperature and laser power can determine nanotube diameter, and products are of high purity and quality. However, high laser powers and high purity graphite means that it is easily the most expensive of the three techniques, and has a much smaller mass output of nanotubes.

Chemical vapour deposition is the most recent method to be recognised as a means to synthesise CNTs, although similar processes have been in use to produce carbon filaments long before it was possible to observe products on the nanoscale [14]. In CVD, nanotubes are grown on a substrate which is coated with metal catalyst nanoparticles. A carbon source gas such as methane or acetylene is fed into the reactor chamber with a process gas such as nitrogen or hydrogen while the substrate is heated to around 700 degrees. Carbon nanotube growth occurs at the metal nanoparticles, leaving them attached to the substrate. The mechanism for this growth is the subject of much study, but it is basically understood that the carbon source molecule is cracked on the surface of the metal particle, where carbon dissolves in the metal and then precipitates on the colder end in graphitic form. The diameters of the resulting tubes are thus strongly linked to the size of the starting particles. Two growth mechanism are recognised, ‘top-down’ and ‘bottom-up’, in which the particle moves upwards with the nanotube or stays at its root respectively [15]. The metal particles are usually prepared by a simple reduction of oxide solution on a substrate which is often silica, but a wide range of metals and substrates have been successfully used. The ability to grow nanotubes on a substrate is one of the method’s principle strengths, allowing direct integration of nanotubes with, for example, silicon based electronics, or carbon fibre materials. Growth of well-aligned vertical arrays of nanotubes is also possible, either by simply having dense enough metal coverage to force it sterically [16], or by forming a plasma in the reactor with a strong electric field; nanotubes will grow in the direction of an applied electric field [17].

As for the other syntheses, CVD conditions can effectively be optimised for single-walled nanotube growth. The most widely used technique is high-pressure carbon monoxide (HipCO), in which $Fe(CO)_5$ is injected into a stream of high pressure CO gas in the reaction furnace [18]. The iron forms clusters which catalyze the reaction of CO to form elemental carbon and CO_2. It is thought that initially spherical fullerenes are formed, but at a certain diameter the cylindrical nanotube structure becomes more favourable. Over 90% SWNT carbon can be achieved by this process, and they are typically of smaller diameter than those produced by other methods; around 1.1nm. One of the drawbacks of the process is the high quantity of Fe impurity present, largely encased in carbon, which it makes it particularly hard to remove.

CVD is widely regarded as the future of mass production of carbon nanotube due to its low cost, low temperature and versatility compared to the other methods. However, arc discharge and laser ablation tubes are still often used in nanotube research due to their superior purity and quality. CVD nanotubes often contain a high level of other carbon material, as well as the metal catalyst particles, and therefore require extensive purification after production. The nanotubes themselves also have a higher density of defects than those from the other syntheses, and consequently can show inferior performance in some applications [19].

1.5 Purification

As-produced nanotube samples will always contain some proportion of other carbonaceous material, graphitic or amorphous, as well as metal catalyst particles in the case of SWNTs or CVD synthesised tubes. This material is normally removed via aggressive oxidative treatment of the samples, using strong acids or other oxidants. Essentially, all the carbon material is steadily consumed by these strong oxidizing agents, but small spherical amorphous particles are consumed much more rapidly than nanotubes, which are merely cut-up and shortened during the process. Common purification procedures include reflux in piranha solution (H_2O_2/H_2SO_4), a mixture of sulphuric and nitric acids, or nitric acid alone [20]. The resulting nanotubes are also left with oxygen containing groups along their length, such as hydroxyls, carbonyls and carboxylic acids. Whilst the introduction of such sp^3 defects into the structure can negatively impact mechanical and electronic properties, they also present a convenient functionalisation with which to chemically attach other moieties. The oxidised CNTs themselves are also much easier to disperse in solvents such as DMSO or water. These acid treatments seem to also lead to chemical oxidative doping of the nanotubes; potentially increasing the conductivity of semi-conductors [21].

Of the various carbonaceous and catalyst materials present in most nanotube samples, amorphous carbon is the most easily removed by oxidative treatment, as it is much more readily oxidised than graphitic material. This kind of impurity can be removed by relatively mild processes such as gas phase oxidations in hot air or air and steam mixtures amongst others [22, 23]. These procedures are quite effective at purifying MWNT samples with little or no metal catalyst, and result in much less damaged nanotubes than acid treatments. However, for metal containing samples, the metal is not removed and furthermore will catalyse the rapid oxidation of carbonaceous material, particularly SWNTs. For this reason it is less effective for purifying HipCO samples, although more suitable gas phase protocols have been developed which are based on prior removal of metal particles [24].

Refluxing in nitric acid was one of the first liquid phase acid treatments to be tried and is still in wide use. Use of the appropriate acid concentration is important to avoid over oxidation and complete destruction of the nanotubes. Typically around 7M acid refluxing for about 6 hours has been shown to be effective for SWNT purification [25]. Hydrogen peroxide is another relatively mild oxidant used for purification, which likely is able to attack the carbonaceous material because of metal catalyst particles which lead to production of OH radicals [26]. In itself, H_2O_2 is not capable of removing metal particles so is frequently used in conjunction with HCl; in various ratios known as piranha solution [26]. The main drawbacks with these milder acid treatments their lack of efficacy in removing the more resistant graphitic materials, and metal particles encased in polyhedral carbon shells. For removing this kind of impurity, more strongly oxidizing acid treatments were developed.

Very strong acid procedures include the widely used mixture of concentrated sulphuric and nitric acids (3:1 ratio) which was originally shown by Liu et al. to produce short open-ended SWNTs [27]. This method can reportedly achieve 98% purity of SWNTs at a 40% yield, without removing small diameter tubes. Also in use are treatments with acidified $KMnO_4$ and acids in conjunction with microwave radiation [28,29]. Nitric acid or hydrochloric acid alone is able to efficiently breakdown metal particles while absorbing microwave energy.

Some physical procedures are also available to purify samples, such as centrifugation and filtration. These techniques are never as effective as the chemical oxidative processes, but have the advantage of not damaging the nanotubes at all. Filtration of samples works on the premise that smaller carbon impurities and metal particles are more soluble in certain solvents than the nanotubes. Upon filtration these impurities can easily be washed away, leaving the nanotubes and larger graphitic material without damaging them [30].

1.6 Electronic applications

The interest focussed on nanotubes for electronics owes both to their remarkable feature of being either metallic or semi-conducting, as well as their high conductivities and current densities they are capable of supporting. The numerous and diverse applications for which they are thought to be potentially beneficial can be loosely divided into two categories: those which employ individual nanotubes as components in an electrical device, and those which use bulk carbon nanotube materials in order to take advantage of their conductivity or some other advantageous property. The rational assembly of individual single-walled nanotubes of known properties into device architectures is the concept which has generated the most excitement as to the important role they could play in a new paradigm of ‘bottom-up’ molecular electronics. One can easily envision a nanoscale circuit which employs metallic tubes as minute wires and semi-conducting tubes as diodes and transistors. In a variation of this idea, they could be used alongside molecular devices such as molecular diodes or switches, as a means to connect molecules or to integrate them with macroscopic electrical contacts. Research into realising such novel nanoelectronic architectures has been intense and wide-reaching, the course of which has discovered unthought-of means in which to exploit the nanotube too numerous to describe here. Equally, the scale of the challenges faced has become ever more apparent. An important hurdle is the basic task of separating nanotubes by whether they are semi-conducting or metallic, and then the placement and organisation of individual tubes into appropriate assemblies is similarly problematic. Nevertheless, significant milestones have been reached by mastering or circumventing such difficulties, and some important proofs of principal have been demonstrated [31,32].

1.6.1 Nanotube circuitry

The first single nanotube field-effect transistor was demonstrated in 1998 by Dekker et al. [33] (figure 1.5). The device is formed by spreading a dilute solution of single-walled nanotubes over a pre-made microelectrode array on a standard substrate of silicon oxide on silicon. Some nanotubes will by chance find themselves bridging two platinum microelectrodes, which will act as a source and drain for the CNT transistor while the silicon substrate acts as a gate electrode, as in a conventional metal-oxide FET. Subsequent work has focussed on refining this concept into commercially viable microelectronics which can be mass produced in a similar manner to silicon chips [34]. As a means of eliminating metallic SWNTs from the sample, selective destruction of metallic tubes was demonstrated, by passing high currents through them whilst the semi-conducting tubes are made non-conductive with the gate electrode [35]. To a similar end, SWNTs can be grown directly on the substrate using CVD growth; specific conditions are able to produce high percentages of semi-conducting tubes [36]. Whole logic gates using CNT FETs have thus been achieved, and more complex architectures are likely to follow [37].

Figure 1.5 *Schematic of a SWNT field-effect transistor [33]*

The symmetric dispersion curve of nanotubes makes them neither p nor n type semiconductors, but a number of ways of doping them to create p-n junctions have been shown. Doping can be performed electrochemically or chemically- and can be region specific by selectively masking a portion of the nanotube with polymer [38]. Absorption of small atoms such as potassium or oxygen on exposed portions of nanotube can lead to doping, or selective chemical functionalisation of the ends can also lead to diode-like behaviour [39]. Such non-ambipolar nanotubes can be used as current rectifiers. Moreover, the altering electronic behaviour of the CNT upon absorption of reducing or oxidising molecules gives rise to very useful sensing properties. CNT FETs have been shown to exhibit sensitive behaviour as sensors for gases such as NO_2 and NH_3 [40,41].

As direct band-gap semi-conductors, SWNTs can also exhibit electroluminescence and photoconductivity. Using similar methods to those for single nanotube FETs, both phenomena have been observed. A standard semi-conducting nanotube has equal hole and electron mobility and there is no diode at which for light emission to be localised. Emission can therefore occur along the length of the tube, but the position can be controlled by altering the gate voltage or introducing some defect which causes a dramatic change in potential along the tube [42]. Emitted light is polarised along the tube axis. Photoconductivity in a single nanotube was first observed in 2003, where excitation by infra-red light generated a photocurrent or voltage in open-circuit configuration [43]. Resonant excitation between the second energy levels of the nanotube gave a quantum yield of around 10%, making the device a viable photodetector. These photoactive devices use the same structures as standard FETs, and one can forsee complex circuitry incorporating a variety of functions, such as photoswitching and emission.

Metallic SWNTs also have a part to play in future nanoelectronic devices. Ideally, they could be used to replace the metal contacts employed by most of the devices described above. An interesting concept is the possible change from metallic to semi-conducting which is theoretically possible upon change of chirality in a single tube. This has been observed by chance in a kinked single nanotube, and studied by scanning tunnelling spectroscopy along its length [44]. Meanwhile, Nuckolls et al. demonstrated the use of SWNTs as wires by which to interface molecular devices with macroscopic electrodes. Molecular switches can be covalently bound to SWNT ends via the carboxylic acid functionality present at their open ends [45].

The future of nanoelectronics based on the carbon nanotube is to a great extent dependent on the development of effective and consistent methods of synthesising or selecting nanotubes of a particular variety. To this end, much research has been directed towards developing novel chemical methods of selective nanotube separation. Some electroaddition reactions are found to occur more favourably with metallic nanotubes [46], while some molecules adsorb more favourably on certain chirality nanotubes [47]; both allow a means of differentiating CNT samples by bulk. It is perfection of these techniques which will likely allow the opening up of CNT based electronics.

1.6.2 Nanotube electrodes and composites

Used as a bulk material, rather than addressing individual nanotubes, CNTs can still offer some very useful properties for electronics; primarily their high conductivity and surface area. In this capacity they are often used as novel electrode materials for applications including photovoltaics, fuel cells, batteries and field emission displays. Nanotubes can be incorporated into such devices either by growing them directly onto relevant substrates by CVD, or by chemical functionalisation and dispersion in relevant media such as polymers. A paper-like form of CNTs often known as ‘buckypaper’ is made by filtering nanotube dispersions into flat, free-standing sheets, and has proved useful both for its mechanical and electrical properties [27]. These bulk uses are less restricted to use of single-walled nanotubes, to which the above discussion of nanoelectronics apply almost exclusively. Multi-walled nanotubes are effectively all metallic, normally including at least one metallic layer, making them suitable for applications which just require metallic behaviour.

The first application of nanotubes to really see commercial use is simply that of rendering other materials conductive via doping them with small amounts of CNTs. Nanotubes are particularly well suited to this function due to their good conductivity and very low percolation threshold- only a small concentration is required before the long structures form a coherent conductive network. This has been widely employed in conductive plastics needed for petrol transportation and in the semi-conductor industry [48,49].

Research into more efficient organic photovoltaic devices has experimented with various means of employing carbon nanotubes in high surface area electrodes as a means to facilitate exciton separation. In an organic photovoltaic device, photons are absorbed by a polymer or small molecule to form an exciton, which must be split into its constituent electron and hole to provide a photocurrent. This is achieved by using electron and hole accepting materials in some blend with a large interface to maximise the chance of an exciton forming near the interface. Carbon nanotubes themselves absorb poorly in the visible spectrum so would act entirely as nanoscale wires for absorbing molecules to pass electrons to. The device thus benefits from the electron transporting capability of the nanotubes which equally form a large interface with the organic medium. Interesting work has been done using CNTs as supports for light absorbing nanoparticles, dyes, as well as fullerene based molecules [50,51]. C_{60} derivatives such as PCBM are a frequently used and effective electron accepting media for organic photovoltaics. Li et al. used C_{60} molecules attached to CNTs to exploit the properties of both fullerenes- the C_{60} accepting electrons from an absorbing polymer, which then flow through nanotubes to an electrode

[52]. Thus superior charge transport is achieved than in the alternative scenario, where charge hops between molecules of C_{60} to the electrode.

Field emission displays are a yet to be realised technology which CNTs seem to be close to bringing to light. These displays work on the principal of constructing a pixel array from an array of individual electron emitting points- essentially tiny cathode ray tubes. The size, conductivity and aspect ratio of CNTs makes them perfect field emitters [53]. Pixel arrays of CNTs can be made by ink-jet printing water dispersion of them over microelectrode grids patterned via photolithography [54]. Ensuring that a large proportion of the CNTs are vertically aligned to act as field emitters can be achieved by surface treatments. Commercial prototypes of such displays have already been showcased, although they are likely to suffer from the simultaneous improvement in organic electronic displays.

1.7 Transparent electrodes from CNTs

The developing field of organic electronics promises a wealth of new technologies in which conventional inorganic semi-conductors are replaced by cheaper and flexible conducting polymers and organic small molecules. Of particular interest are organic light-emitting diodes (OLEDs) and photovoltaics, many examples of which have been demonstrated in the literature over the last several years. Such devices necessarily require an electrode which transmits light as effectively as possible, and they frequently make use of conductive metal oxides coated on glass for this purpose- most commonly indium tin oxide (ITO). This material offers very suitable properties with sheet resistances of up to 10 Ω/square for an optical transparency greater than 80%, and yet it possesses several drawbacks including its cost, lack of flexibility, and tendency to cause oxidation and degradation of organic films [55]. Essentially these materials do not fit well within the paradigm of organic electronics, as they negate many of the hoped for benefits which the switch to organics should provide.

Work over the past few years has shown that thin films of carbon nanotubes on a transparent substrate such as glass or PET, serve as very competitive transparent electrode materials [56,57]. The good conductivity and high aspect ratio of nanotubes makes them ideally suited to the formation of a percolating conductive network at very low coverages; allowing high optical transmission. Unlike the oxide films, which are prone to fracturing on bending of the substrate, these films are completely flexible when made on plastic substrates. Several procedures for the production of high quality CNT thin films have been demonstrated, nearly always involving the preparation of a dispersion of nanotubes in water and then transferring to a film via filtration, ink-jet printing or spraying [58,59]. Frequently, there is a step in which the film is transferred from a membrane to the transparent substrate either by dissolution of the membrane or stamping with a PDMS stamp [60].

These films show promising properties, with sheet resistances of around 200 Ω/sq. possible for visible transmittance of 85 % [61]. Since the discovery of this application for CNTs in organic devices, much work has been done on improving their properties. This has generally centered on trying to increase their conductivity by altering the type and purity of the nanotubes used, the quality of the dispersion, and the level of doping of semi-conducting tubes. Zhang et al. performed a comparison of films using HipCO, laser ablation and arc discharge SWNTs, showing conclusively that the arc discharge tubes yielded the most conductive films [62]. Highly oxidised nanotubes seem to perform better, demonstrating that the improvement in water dispersion quality which this provides outweighs any reduction in conductivity that disruption of the pi-conjugation may cause. The quality of the dispersion also relies heavily on the use of a surfactant, which aids the interaction of the hydrophobic tubes with water. Sodium dodecyl sulphate is frequently used for this purpose, but pi-rich polymers and the commercial surfactant triton-x have shown to result in higher performance electrodes [63]. Use of surfactants necessarily has a negative impact on the films as well, as the insulating molecules obstruct conduction between individual molecules; so a balance must be found. Indeed, several methods are commonly employed to try and reduce surfactant levels in the film after they have been made. This often involves simply washing with copious amounts of water or ethanol, but prolonged treatment with concentrated nitric acid also appears to be very effective in raising the film conductivity [64].

References

[1] S. Iijima, *Nature* **354** 1991 56
[2] Oberlin, A.; M. Endo, and T. Koyama, *J. Crystal Growth* **32** 1976 335
[3] Terrones M, *Inter. Mat. Rev.* **49** 2004 325
[4] Hong, Seunghun; Sung Myung, *Nature Nano.* **2** 2007 207
[5] http://en.wikipedia.org/wiki/Optical_properties_of_carbon_nanotubes
[6] H Kataura, Y. Kumazawa, Y. Maniwa, I. Umezu, S. Suzuki, Y. Ohtsuka and Y. Achiba *Synth. Met.* **103** 1999 2555
[7] C Thomsen, S Reich, *Topics Appl. Physics* **108** 2007 115
[8] H Kuzmany *Eur. Phys. J. B* **22** 2001 307
[9] http://en.wikipedia.org/wiki/Optical_properties_of_carbon_nanotubes
[10] C. Journet, W. K. Maser, P. Bernier, A. Loiseau, M. L. De La Chapelle, S. Lefrant, P. Deniard, R. Lee and J. E. Fischer, *Nature* **388** 1997 756
[11] C Guo,Y Ting, *J. Phys. Chem.* **99** 1995 10694
[12] A. Thess, R. Lee, P. Nikolaev, H. Dai, P. Petit, J. Robert, C. Xu, Y. H. Lee, S. G. Kim, A. G. Rinzler, D. T. Colbert, G. E. Scuseria, D. Toma`nek, J. E. Fischer and R. E. Smalley, *Science* 1996 **273** 483
[13] P. C. Eklund, B. K. Pradhan, U. J. Kim, Q. Xiong, J. E. Fischer, A. D. Friedman, B. C. Holloway, K. Jordan and M. W. Smith *Nano Lett*. **2** 2002 561
[14] M. S. Dresselhaus, G. Dresselhaus, K. Sugihara, I. L. Spain and H. A. Goldberg, in *'Graphite fibers and filaments'*, **3** chap. 2, 12; 1988, Berlin/New York/London, Springer (and references therein).
[15] R. T. K. Baker and P. S. Harris: *'Chemistry and physics of carbon'*, 83; 1978, New York, Marcel Dekker
[16] M. Terrones, N. Grobert, J. Olivares, J. P. Zhang, H. Terrones, K. Kordatos, W. K. Hsu, J. P. Hare, P. D. Townsend, K. Prassides, A. K. Cheetham, H. W. Kroto and D. R. M. Walton *Nature* **388** 1997 52
[17] Ren, Z. F. *Science* **282** 1998 1105
[18] P. Nikolaev, M. J. Bronikowski, R. K. Bradley, F. Rohmund, D. T. Colbert, K. A. Smith and R. E. Smalley, *Chem. Phys. Lett.* **91** 1999 313
[19] Q. Tang, X.Y. Chen, Z.P. Liu and Y.T. Qian *Carbon* **41** 2003 2613
[20] P-X Hou,C Liu, and H-M Cheng, *Carbon* **4** 2008 2003
[21] C. Aguirre, R. Martel, private correspondance
[22] P. M. Ajayan, T. W. Ebbesen , T. Ichihashi, S. Iijima, K. Tanigaki and H. Hiura, *Nature* **362** 1993 522
[23] G. Tobias, L. D. Shao, C. G. Salzmann, Y. Huh, and M. L. H. Green, *J. Phys. Chem B* **110** 2006 22318
[24] I. W. Chiang, *J. Phys. Chem. B* **105** 2001 1157
[25] H Hu , B Zhao, M. E. Itkis and R. C. Haddon, *J. Phys. Chem. B* **107** 2003 13838
[26] Y. H. Wang, H. W. Shan , R. H. Hauge, M. Pasquali, and R. E. Smalley, *J. Phys. Chem. B* **111** 2007 1249

[27] J. Liu, A. G. Rinzler, H. G. Dai, J. H. Hafner, R. K. Bradley and P. J. Boul, *Science* **280** 1998 1253
[28] J.F. Colomer, P. Piedigrosso, A. Fonseca and J.B. Nagy, *Synth. Met.* **103** 1999 2482
[29] C. M. Chen, M. Chen, F. C. Leu, S. Y. Hsu, S. C. Wang and S. C. Shi, *Diam. Relat. Mater.* **13** 2004 1182
[30] S. Bandow, A. M. Rao, K. A. Williams, A. Thess , R. E. Smalley and P. C. Eklund, *J Phys. Chem. B* **101** 1997 8839
[31] Ph. Avouris, Z. Chen and V. Perebeinos, *Nature Nano.* **2** 2007 605
[32] P. Sharma and P. Ahuja , *Mater. Res. Bull.* **43** 2008 2517
[33] H. Postma, T. Teepen, Z. Yao, M. Grifoni, and C. Dekker, *Science* **293** 2001 5527
[34] A. Vijayaraghavan, C. Sciascia, S. Dehm and A. Lombardo, *Nano Lett.* **7** 2007 1556
[35] P. G. Collins, M. S. Arnold, and P. Avouris, *Science* **292** 2001 706
[36] L. Ding, A. Tselev and J. Wang, *Nano Lett.* **9** 2009 800
[37] Y-C Tseng, *Nano Letters* **4** 2004 123
[38] H. Peng, V. A. Davis, W. Zhou, J. Sulpizio, Y. Wang, R. Booker, J. Vavro, and C. Guthy, *Science* **290** 2000 1552
[39] Z. Wei, M. Kondratenko, L.H. Dao and D.F. Perepichka, *J. Am. Chem. Soc.* **128** 2006 3134
[40] P. Bondavalli, P. Legagneux, D. Pribat and A. Balan, *Sensor. Actuat. B* **140** 2009 304
[41] M. Y. Faizah, *Eur. J. of Sci. Res.* **35** 2009 142
[42] J. A. Misewich, R. Martel, Ph. Avouris, J. C. Tsang, S. Heinze and J. Tersoff, *Science* **300** 2003 783
[43] M. Freitag, Y. Martin, J. A. Misewich, R. Martel and Ph. Avouris, *Nano Lett.* **3** 2003 1067
[44] Z. Yao, H. W. Ch. Postma, L. Balents and C. Dekker, *Nature* **402** 1999 18
[45] S. J. Wind, J. Hone, P. Kim, and C**.** Nuckolls, ***Science*** **311** 2006 356
[46] W. J. Kim, M. L. Usrey and M. S. Strano, *Chem. Mater.* **19** 2007 1571
[47] C. H. Liu, Y. Y. Liu, Y. H. Zhang et al. *Chem. Phys. Lett.* **471** 2009 97
[48] S. Yu, W. M. Wong, X. Hu and Y. K. Juay**,** *J. Appl. Polym. Sci.* **113** 2009 3477
[49] M. J. Biercuk, M. C. Llaguno, M. Radosavljevic and J. K. Hyun, *Appl. Phys. Lett.* **80** 2002 2767
[50] E. Kymakis and G. A. J. Amaratunga, *Sol. Energ. Mat. Sol. C.* **80** 2003 465
[51] P. R. Somani, S. P. Somani and M. Umeno, *Appl. Phys. Lett.* **93** 2008 033315
[52] C. Li, Y. Chen, Y. Wang et al., *J. Mater. Chem*. **17** 2007 2406
[53] Q. H. Wang, A. A. Setlur, J. M. Lauerhaas, J. Y. Dai et al., *Appl. Phys. Lett*. **72** 1998
[54] N. S. Lee, D. S. Chung, L. T. Han et al., *Diam. and Rel. Mat.* **10** 2001 265
[55] A.R. Schlatman, D.W. Floet, A. Hilberer, F. Garten et al., *Appl. Phys. Lett.* **69** 1996 1764
[56] Z.Wu, Z. Chen, X. Du, J. M. Logan et al., *Science* **305** 2004 27
[57] C. M. Aguirre, S. Auvray, S. Pigeon, R. Izquierdo, and R. Martel, *Appl. Phys. Lett*. **88** 2006 183104
[58] W. R. Small, *Small* **3** 2007 1500
[59] R. C. Tenent, T. M. Barnes, J. D. Bergeson et al., *Adv. Mat.* **21** 2009 3210
[60] L. Hu, G. Gruner, D. Li, R. B. Kaner and J. Cech, *J. Appl. Phys*. **101** 2007 016102

[61] M.W. Rowell, M.A. Topinka, M..D. McGehee, H.J. Prall et al., *Appl. Phys. Lett.* **88** 2006 233506
[62] D. Zhang, K. Ryu, X. Liu, E. Polikarpov et al., *Nano Lett*. **6** 2006 1880
[63] M.H.A. Ng, L.T. Hartadi, H. Tan and C.H.P. Poa, *Nanotechnology* **19** 2008 205703
[64] B.B. Parekh, G. Fanchini, G. Eda and M. Chhowalla, *Appl. Phys. Lett.* **90** 2007 12191

2. CONDUCTIVE POLYMERS

2.1 Introduction

Conducting polymers can be viewed as a convergence of two materials technologies which have dominated the latter half of the last century; that of inorganic semi-conductors and organic polymer materials. Organic materials which can offer similar electronic properties to the inorganics which dominate the electronics industry, promise the same significant advantages which has led to their current pervasion as materials in today's world; namely, lightness, processability, cost and durability. It is a significant impediment to possible silicon based technologies of the future, such as photovoltaics, that the material requires such high cost processing due to stringent purity requirements and relies heavily on vacuum deposition techniques. Consequently, organic materials and especially conductive, conjugated polymers are seen as a promising and necessary component of future large-area electronics.

It was first demonstrated in the seventies that polyacetylene behaves as a semiconductor, and then significantly, that upon oxidative 'doping' could be rendered many times more conductive; up to 10^5 S cm^{-1} [1,2]. Polyacetylene still exhibits the highest conductivity that can be obtained from a conjugated polymer [3], and yet possesses serious drawbacks concerning its stability (degrading in air) and poor processability. Attention turned to poly(heterocycles), particularly polypyrroles and polythiophenes, which can be thought of as cis-polyacetylene chains stabilized by the hetero-atom. These polymers offer much higher stability and versatility derived from the possibility of altering the monomer structure for different chemical and electronic properties. Conjugated polymers are synthesized either chemically or electrochemically; the latter method first having been demonstrated on polypyrroles in 1979, which proved harder to chemically synthesise due to their acidity [4]. Chemically synthesis typically yields polymers of slightly lower conductance than those made electrochemically, yet it is still predominantly used for large-scale production

2.2 Important examples and chemical synthesis

Polyacetylene

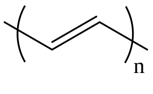

Poly(phenylvinylene)

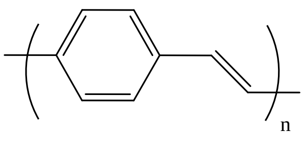

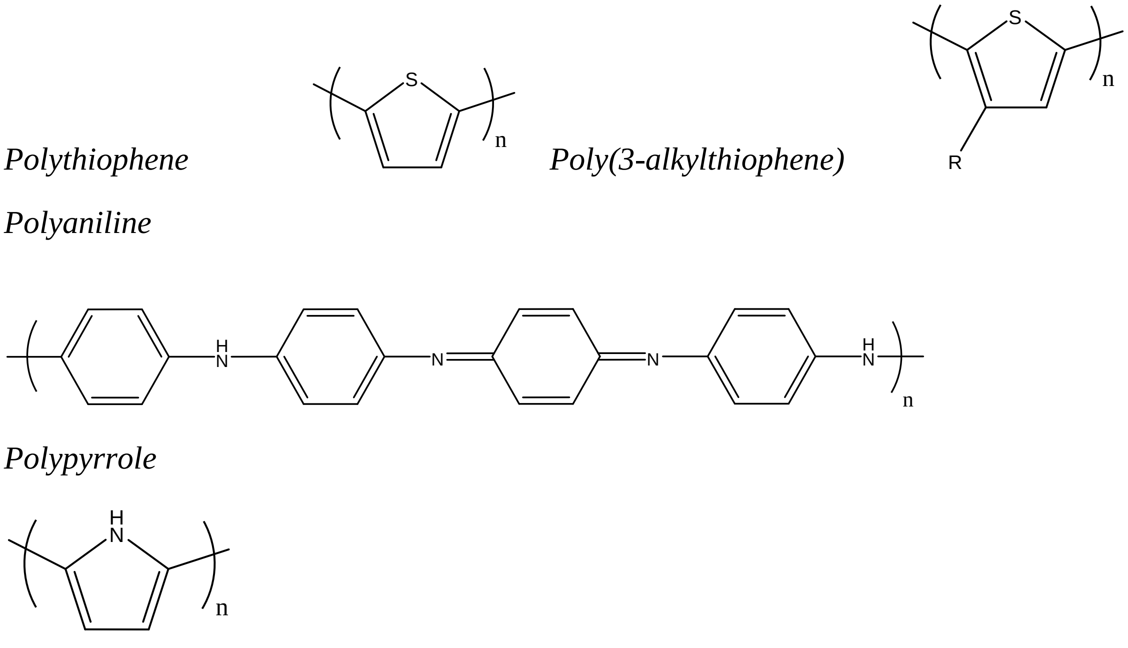

Polythiophene

Poly(3-alkylthiophene)

Polyaniline

Polypyrrole

Figure 2.1 *Some examples of widely used conjugated polymers*

General chemical synthesis of conjugated polymers can proceed by the chemical oxidation of the monomer in solution, or by organometallic coupling of substituted monomers. The former method generally uses an oxidizing agent such as ferric chloride, FeOTs, or persulfates [5,6]. The monomer is oxidized to radical cations which dimerize, form oligomers, and eventually precipitate out of solution as the polymer. Organometallic syntheses such as Grignard couplings are can be conducted on monomers with bromo-substitution at the alpha carbons, in the presence of a transition metal catalyst. For asymmetric monomers such as alkyl substituted polythiophenes, it is desirable to synthesise regioregular polymers which can exhibit superior electronic properties due to better packing. This can be achieved via the formation of asymmetrically substituted monomers for use in such Grignard couplings [7,8].

Polythiophenes are perhaps the most widely used and researched of all conducting polymers, seeing applications as both doped conducting and semi-conducting components in photovoltaics, light-emitting diodes, electrode materials and electrochromics [9-11]. The unfunctionalised polythiophene itself is rarely seen in practical use due its low solubility and processability caused by the strong pi-pi stacking between chains. Attention soon turned to synthesising polymers of thiophene derivatives; particularly those with alkyl chains substituted at the 3 carbon, collectively known as poly(3-alkylthiophene) (P3AT) [12]. The addition of short alkyl chains was shown to greatly improve solubility of the polymer, as well as lowering the oxidation potential of the monomer. Substituting at both the 3 and 4 positions has the further benefit of blocking polymerisation at these carbons and ensuring straight, regular chains linked at the alpha positions. Alkyl chain substituents can disrupt the planarity and conjugation of the heterocycle. However, addition of electronegative heteroatoms such as oxygen and sulphur at these positions can reduce the steric strain, as well as stabilising the oxidized forms of the monomer and polymer.

2.3 Doping and conductivity

Conjugated polymers can be n or p doped, referring to the process of adding or removing electrons from the conjugated pi bonding chain, but p-doped polymers prevail as by far the more stable variant. P-doping can be carried out either by chemical or electrochemical oxidation, with an anion always present to counter the positive charges formed in the polymer. This anion therefore forms an integral part of the doped polymer structure and thus has an important influence on its mechanical and electronic properties. Since polymerisation itself is an oxidative process, the polymer is often synthesised already in a doped state, but can be afterwards dedoped electrochemically by applying reducing voltages, or chemically with reducing agents such as hydrazine. The changes in electronic structure upon doping can be considered generally for heterocycles, as shown in figure 2.2. Removal of one electron from the chain forms the radical cation, for which it is energetically favourable for a portion of the chain (4 units) to adopt a quinoid structure. It is then more favourable for this unit to be further oxidized to a zero spin, doubly charged, bipolaron state. The course of this progression from neutral molecule to polarons with spin, to the bipolaron rich molecule, can clearly be followed using EPR. The new charged states create new energy levels in the band gap of the polymer, effectively reducing the band gap and creating mobile charge units which give the polymer electrical conductivity.

a)

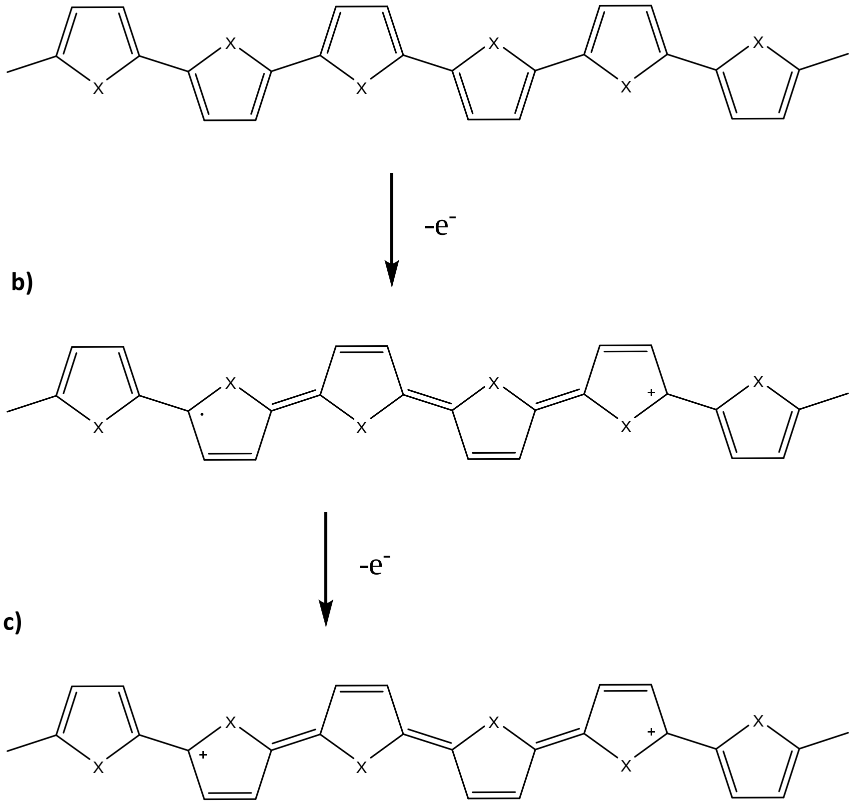

Figure 2.2 *Doping of conjugated poly(heterocycle)* ***(a)*** *from polaron* ***(b)*** *to bipolaron* ***(c)***

The extent of doping in fully doped polymers is usually between around 30% by moles. The charge carrier density is therefore very high, and many orders of magnitude higher than that in inorganic semiconductors. The fact that these polymers show conductivities only on a par with amporphous inorganics and considerably lower than crystalline ones, is due to low charge mobility. This is to be expected given the highly amorphous nature of most polymeric materials which hinders charge movement. Charge moves either along chains via the rearrangement of double bonds, or 'hops' between chains; the latter process presenting a much larger energetic barrier. Mobility of charge within a polymer chain is mainly hindered by conformational or chemical defects in the chain such as kinks or nonaromatic bonding. Poly(heterocylcle)s can often show linking at the 2 or alpha position on the cycle, which upsets pi orbital overlap in the chain.

Hopping of charge between polymer chains, as can occur when a defect is encountered within a chain, is governed by the extent of conformational order in the material. Unsubstituted conjugated polymers such as polythiophenes have quite a high degree of order due to strong pi-pi interactions between chains, and consequently high conductivities. It is likely that charge movement between molecules is greatly enhanced by numerous pi-pi interactions. For alkyl substituted thiophenes and pyrroles, regioregularity plays an important role in the conductivity. Interaction between regular alkyl chains can result in a highly crystalline polymer, but increased distance between the chains impedes charge mobility. Irregular polymers will form amorphous and poorly conductive materials. Mechanical stretching can be employed to enhance the conductivity considerably in the direction of the stretching [13].

2.4 Applications

2.4.1 Diodes and FETs

Diodes between two n and p doped polymer films are difficult to realise due to the inevitable diffusion of dopants between the two films [14]. Schottky diodes at polymer-metal interfaces have been demonstrated with a range of conjugated polymers, and shown to exhibit rectifying behaviour [15,16]. Conformational order from regioregularity and short substituents is important for obtaining good performance.

Field effect transistors based on organic molecules could offer a much cheaper and easier to manufacture alternative to silicon based technologies. A film of polymer or small molecules can be made via solution processing (printing, spincoating etc.) or evaporation, to act as the channel material between source and drain electrodes. Early work looked at polythiophene films which were capable of modest performances; modulating current by up to two orders of magnitude [17]. For these devices particularly, high charge carrier mobility is essential, and consequently attention has focussed on small conjugated molecules which can be evaporated into more crystalline films. Short oligomers of conjugated polymers such as sexithiophene and antradithiophene have been shown to give effective devices [18,19]. Polymer devices still possess the ever-important advantage of simple deposition, and thus work has focussed on using highly regular chains and surface treatments to encourage ordered deposition. As with many organic devices, amongst the principal drawbacks compared to inorganics are a slow response time and short lifetimes [20]. The potential for printing transistors simply onto flat and flexible substrates is nevertheless an enticing goal for this research.

2.4.2 Light-emitting diodes

Electroluminescence in a conjugated polymer was first observed in polyphenylvinylene (PPV) in 1990, which emits a yellow-green colour when a voltage is applied across a film of the polymer [21]. It was soon noted that, aside from the usual advantages of cost and flexibility which such a material could have over conventional, inorganic LEDs, they could also be chemically tuned to emit across the entire visible spectrum. Indeed, substitution at the 2 or 5 position of PPV gives a material which emits in the red region of the spectrum [22]. Other important electroluminescing polymers are polyfluorene, poly(p-phenylene) and alkyl substituted polythiophenes such as P3HT.

A conventional light-emitting diode functions using a junction between two inorganic semi-conductors with a direct band-gap; that is, a band-gap which has the correct symmetry for an optical transition to occur. As for any diode, there is a junction between n and p type semiconductors, at which electrons and holes will recombine under an appropriately directed voltage; in this instance, to produce a photon of light corresponding to the band-gap energy. In their simplest incarnation, such as that originally shown using PPV, a polymer LED can consist of one semi-conducting layer between two electrodes, one of which must be optically transparent. Holes are injected into the polymer film at the anode and electrons are injected at the cathode, they then recombine in the polymer to emit light of the polymer band-gap energy. Device architectures have since become significantly more complex in an effort to improve poor efficiency and tailor the emission wavelength; using blends of different polymers or small molecules to fulfil specific functions as n-type and p-type semi-conductors or a luminescent component.

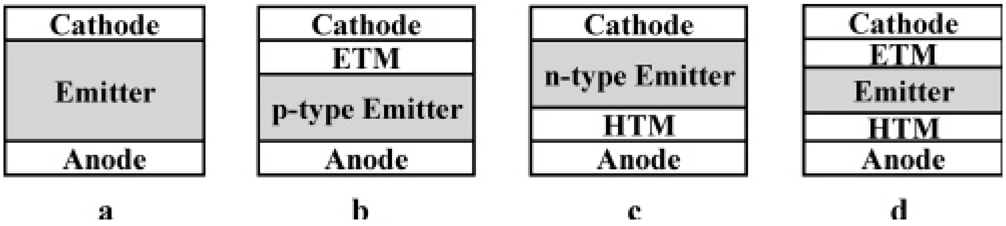

Figure 2.3 *Different possible architectures for organic LEDs, with electron and hole transporting (ETM, HTM) and light emitting materials.*

Most luminescent conjugated polymers are p-type in nature, often having a hole mobility orders of magnitude than their electron mobility. This is thought to be due to the relative lack of stability of anions in these polymers which permits easy trapping of electrons by oxygen or other impurities. It is largely this deficiency which has led to the development of these more complicated assemblies. Additionally, for good transport of charge through the device it is important that the HOMO/LUMO levels of the luminescent material match the p-type/n-type HOMO and LUMO, and equally that there is good matching to the levels of the electrodes. Large Energy barriers in the device of around an electronvolt can result in very poor quantum efficiencies. For this reason, additional hole or electron injection layers are also normally added to the anode and cathode to further improve energy level matching.

Common luminescent polymers used in OLEDs are P3ATs, PPV, polyfluorenes, and polyvinylcarbazole (PVK), the latter not a conjugated polymer but still showing hole mobility [23,24]. Clearly, different polymers will result in emission at different wavelengths, depending on their band-gaps, thus a range of molecules are the subject of work to optimise performance across the spectrum. Inter system crossing to the triplet state is to be minimised, and can be a problem in heavy atom containing molecules [25]. For this reason high conductivity polymers such as polythiophenes can be less effective for electroluminescence. Electronic interaction between polymer chains can also greatly decrease luminescence efficiency by increasing non-radiative decay.

The electron-accepting material can often be a small molecule, made processable in a polymer blend. Polymers with good electron transport properties include those consisting of oxadiazoles, other azoles, and polypyridines; generally electron deficient molecules which show reversible n-doping [26].

2.4.3 Photovoltaics

Organic photovoltaics are fundamentally not very different from OLEDs- the generation of photocurrent essentially being the reverse process of electroluminescence. An organic film between two electrodes absorbs a photon to form an exciton (a bound electron-hole pair), If the exciton can be separated before decaying, by the application of an electric field or materials of different electron affinities, the electron and hole travel to different electrodes and generate current.   The phenomenon was first observed in organic molecules with anthracene at the beginning of the last century, and much of the earlier work concentrated on dye molecules such as chlorophyll and pthalocyanine [27,28]. After the discovery of conducting polymers, observation of photoconductivity in them followed their progress from polyacetylene, to polythiophenes to PPVs [29,30]. Single material PVs show poor efficiencies because the excitons do not readily dissociate. Consequently, as for OLEDs, attention turned to two layer devices using electron donor and acceptor molecules. Much studied are blends of P3HT or PPV and soluble derivatives of C_{60} such as PCBM, in which the polymers are the light absorbing and hole carrying material, and the PCBM accepts and transports electrons [31,32]. Alternatively a donor-acceptor junction between two polymers is also possible, such as that between P3HT and poly(p-pyridylvinylene) [33].

The nature of the interface between the two layers is much more important than in OLEDs, as any exciton will only travel for around 10 nm before decaying, unless it is separated by the local field at the interface. Moreover, the organic film should be of a certain thickness (around 100 nm) to maximise the absorption of the solar radiation. To meet these requirements, research has focussed on ‘dispersive’ heterojunctions, in which donor and acceptor materials are blended together to form a highly interpenetrating and large area interface. This can be achieved with blends of polymer and fullerene derivatives with high solubility in the polymer; spin-coated in a single layer onto the electrode [34]. The downside is that conduction pathways to the electrodes through the blend can be more convoluted or blocked; ideally a film ordered into two highly integrated but contiguous layers is needed. To this end, organisation on a molecular level has been sought via use of discotic liquid crystals and diblock copolymers [35,36].

A priniciple challenge in the development of organic PVs is the fabrication of large areas beyond the relatively small constraints of spin-coating. As for all organic devices there are also important stability and lifetime issues, as the materials are highly sensitive to oxidation and degradation by air. Both OLEDs and organic PVs require highly effective sealing to retain their performance over time.

2.5 Poly(ethylenedioxythiophene)

2.5.1 Properties and morphology

Poly(ethyelnedioxythiophene) (PEDOT) is one of the most widely used polythiophenes due to its relatively low oxidation potential and band gap, and good stability [37]. Its development stems from a natural progression of alkyl derivatives of thiophene, undertaken as researchers have sought to lower the oxidation potential of the basic thiophene monomer, and improve its solubility. Simple alkyl chains achieve this purpose to some extent, but the chains also cause steric disruption of resulting polymer chains, and thus distort their pi-conjugation. Thiophenes with carbocycles at the 3 and 4 positions were found to overcome this steric disruption to, and introduction of heteroatoms such as sulphur and oxygen in positions next to the thiophene went a step further to reduce the distortion of the chain and stabilise the oxidized form.

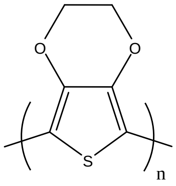

Figure 2.4 *Poly(ethylenedioxythiophene)*

The p-doped polymer of this EDOT monomer is a semi-transparent material, with conductivities of up to 850 S cm^{-1} for electropolymerised samples [38]. It changes from an opaque dark blue in its neutral state to transparent sky blue on doping, giving it considerable interest for use in electrochromic devices. These properties, together with the excellent stability of the doped polymer in air, make the material attractive for a variety of uses in organic electronics. It does, however, suffer from the same problems of processability as other polythiophenes whithout long alkyl substituents, being practicably insoluble in all solvents. This led to the development of the widely used PEDOT blend with polystyrene sulfonate (PSS) which forms stable dispersions in water [39]. It is in this processable form that PEDOT is used for nearly all of its current applications.

As for other thiophenes, PEDOT can be synthesised both chemically and electrochemically. The chemical synthesis is normally carried out using Iron (III) tosylate as the oxidising agent [40]. The process can be regarded as two steps: the oxidative polymerisation of the monomer followed by the oxidative doping of the polymer to form the conductive, charged polymer. The negatively charged tosylate ions act as counterions to the polymer and form an integral part of the polymer material. It is thought that the counterions form an alternating stack with layers of the polymer.

In the water dispersable PEDOT:PSS blend, the PSS serves both as a counterion to the PEDOT chains and a hydrophilic polymer which improves the material's interaction with water. The exact structure of the blended polymers is the subject of considerable research. It seems that the PSS is present in much longer chain lengths than the PEDOT, suggesting that short sections of PEDOT are tightly bound along the length of an individual PSS chain. In water, this material forms gel particles, largely consisting of water, with an inner core of PEDOT:PSS and a more PSS rich coating [41]. The size of these particles can be altered by varying the ratio of the polymers and the pressure treating the dispersion. Once the dispersion is spin-coated or cast, a film is formed from the gel particles, resulting in regions of PEDOT within a matrix of PSS and residual water. STM and photoelectron spectroscopy studies indicate that the surface of the film is also largely PSS rich [41, 42]. PSS is an insulating polymer, so its presence in the blend needs to be minimised for applications which require high conductivities.

Depending on the application, different blends and particle sizes are used in order to achieve an appropriate compromise of film conductivity and transparency. Smaller particles also lead to a less conductive film as more unfavourable particle boundaries are present.

A considerable improvement in the film's properties can be brought about by adding 'secondary dopants' to the PEDOT:PSS emulsion before processing. These are usually low boiling point solvents such as diethylene glycol, sorbitol, or DMSO [43,44]. They do not electronically dope the polymer or participate chemically in anyway, but act to alter the morphology of the film in such a way as to increase its conductivity. This change in the film then persists even after the solvent has evaporated away. It is thought that secondary dopants such as diethylene glycol act to phase segregate the polymers, so that rather than PEDOT rich particles surrounded by a PSS matrix, the PEDOT rich regions are merged together to form conductive pathways. Similarly, highly insulating PSS rich domains are formed within the film as well. Such treatments can increase the conductivity of a film by two to three orders of magnitude, up to 80 S cm^{-1}[44].

The PEDOT:PSS emulsion is a compromise between the advantageous properties of PEDOT and the processability offered by the insulating PSS counterion; even with secondary doping it does not approach the conductivities achievable in a pure PEDOT film. Its relative ease of processing has made it widespread for commercial uses of the material, and yet research is showing that pure PEDOT films made in-situ could also become practicable. The poor processability of PEDOT demands that it be synthesised directly in the device for which it is intended. Chen et al. demonstrated spin-coating of a solution of the EDOT monomer and $Fe(OTs)_3$, followed by heating to polymerise the film in-situ. Such films can show conductivities of up to 170 S cm^{-1} [45]. A drawback for some applications is the persisting presence of the metallic dopants in the film, which can lead to degradation of any organic layer which may be in contact with the film.

The third alternative is electropolymerisation of the PEDOT in-situ, which is largely the subject of this thesis and will be discussed in more depth in the following chapter. Electrochemical synthesis of PEDOT, as for other conducting polymers, offers easily the highest quality films and conducitivities, when performed under optimum conditions. It is of course restricted to applications in which a conducting substrated can be present upon which to form the polymer.

2.5.2 Applications of PEDOT

The primary importance of PEDOT is its combination of optical transparency and good electrical conductivity, leading to its use in photovoltaics, organic LEDs and antistatic coatings for screens. As a transparent conductor it is frequently considered as an alternative to the widely used indium tin oxide. Fig. 2.5 shows how films of pure PEDOT, oxidized in situ, and PEDOT:PSS compare to ITO as a function of film thickness. Although of lower performance than the inorganic material, the polymer offers advantages in terms of ease of processing and film smoothness.

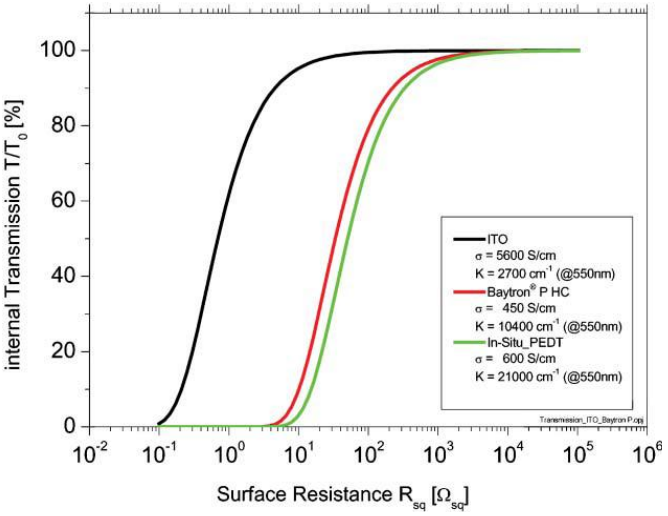

Figure 2.5 *A comparison of the performance of ITO, PEDOT:PSS, and chemically synthesised PEDOT as optically transparent electrodes [46]*

As discussed above, ITO presents a number of problems in terms of its expensive deposition and the rough, inflexible nature of the film. Theoretically, PEDOT could serve as a replacement for ITO in such devices as organic LEDs and photovoltaics, thus allowing entirely organic devices, and yet its lower conductivity presents difficulties for such applications. For organic devices with less stringent requirements for electrode conductivity, such as electrochromics and photosensors, highly conductive PEDOT films have been shown to be effective electrode materials [47,48]. Either in-situ polymerised PEDOT or a highly conductive grade of PEDOT:PSS is needed for this use of the polymer.

Consequently, PEDOT:PSS is more commonly used in conjunction with ITO, essentially as a means to ease the interaction between the inorganic and organic layers of the device, both electrically and physically. A thin coating of the polymer between the ITO and an organic semi-conductor improves hole transport between the two materials, as the LUMO of PEDOT comes somewhere between the other two. The polymer layer also serves simply to smooth out the ITO film, allowing more even spin-coating of the organic semi-conductor on top of it and preventing shorting of the device from protrusions in the film. In this capacity, the material is known as a ‘hole-injection layer’, and has become a crucial component of OLEDs as well as organic PVs in which it performs essentially the same function but in reverse [49,50]. In a LED holes and electrons are pumped into an organic semi-conductor where they recombine to form photons; whereas in a photovoltaic, holes and electrons formed by incident light are extracted at opposite electrodes. The PEDOT layer is mirrored by a counterpart ‘electron-injection layer’ at the anode of these devices, which matches the work functions of the metal electrode and the organic layer.

Another highly useful property of PEDOT is the colour change it undergoes between doped and dedoped states, which has led to its wide use in electrochromic devices [51,52]. These devices simply present a window which changes between two or more distinct colours upon the application of different voltages. The device consists of one transparent electrode coated with the electrochromic material, separated from another electrode by a solid electrolyte-gel. The second electrode is coated by an ‘ion-storage layer’ which is normally a redox active inorganic material which does not change its optical absorption between redox states. Together, the electrochromic and transparent conductor properties of PEDOT allow it to form an integral part of an entirely organic device, as demonstrated by Reynolds et al. [53].

The easy processing and relatively high conductivity of PEDOT:PSS also lends it to use as an electrode material in organic field-effect transistors [54]. These devices offer a cheap alternative to inorganic transistors in which films of semi-conducting organic molecules such as pentacene are used as a switchable electron/hole ‘channel’. The source, gate, and drain electrodes required for transistors are often formed by metal evaporation, but a cheaper alternative is to use printing techniques to pattern PEDOT:PSS as the electrodes. In this way large arrays of flexible devices can easily be fabricated.

References

[1] C. K. Chiang, C. R. Fincher, Y. W. Park, A. J. Heeger, H. Shirakawa, E. J. Louis, S. C. Gau and A. G. MacDiarmid, *Phys. Rev. Lett*. **39** 17 1977 1098
[2] H. Shirakawa, E. J. Louis, A. G. MacDiarmid, C. K. Chiang and A. J. Heeger, *J. Chem. Soc., Chem. Commun*. **16** 1977 578
[3] H. Naarmann and N. Theophilou, *Synth. Met*. **22** 1 11987
[4] A. F. Diaz, *Chemica scripta* **17** 1980 145
[5] R. Sugimoto, S. Takeda, H. B. Gu, K. Yoshino, *Chem. Express* **1** 1986 635
[6] V.M. Niemi, P. Knuuttilaand, J.E. Osterholm and J. Korvola *Polymer* **33** 1992 1559
[7] T. Yamamoto, K. Sanechika and A.J. Yamamoto, *Polym. Sci. Polym. Lett. Ed*. **18** 1980 181
[8] D.D. Cunningham, L. Laguren-Davidson, H.B. Mark, V. Pham and J.H. Zimmer, *Chem. Soc.,Chem. Commun*. **13** 1987 1021
[9] S. Glenis, G. Tourillon and F. Gamier *Thin Solid Films* **111** 1984 93
[10] D. Braun, G. Gustafsson, D. McBranch and A.J. Heeger, *J. of Appl. Phys.* **72** 1992 564
[11] Y. Ming, *Prog. Chem.* **21** 2009 1268
[12] Elsenbaumer, R.L., K.Y. Jen, and R Obodi. *Synth. Met.* **15** 1986 16
[13] Y. Nogami, J.-P. Pouget and T. Ishiguro *Synth. Met.* **62** 1994 257
[14] C.K. Chiang, S.C. Gau, C.R. Fincher Jr., Y.W. Park, A.G. MacDiarmid, A.J. Heeger, *Appl. Phys. Lett*. **33** 1978 18
[15] J. Lei, W. Liang, C.S. Brumlik and C.R. Martin, *Synth. Met*. **47** 1992 351
[16] M. Narasimhan, M. Hagler, V. Commarata and M. Thakur, *Appl. Phys. Lett*. **72** 1998 1063
[17] A. Tsumra, H. Koeza and T. Ando, *Appl. Phys. Lett*. **49** 1986 1210
[18] J.G. Laquindanum, H.E. Katz and A.J. Lovinger, *J. Am. Chem. Soc.* **120** 1998 664
[19] O. D. Jurchescu, S. Subramanian, R. J. Kline et al., *Chem. Mater.* **20** 2008 6733
[20] M.C. Gather, S. Ko¨ber, S. Heun, and K. Meerholz, *J. Appl. Phys.* **106** 2009 art. no. 024506
[21] P.L. Burn, D.D.C. Bradley, A.R. Brown, R.H. Friend and A.B.Holmes, *Synth. Met.* **41** 1991 261

[22] D. Braun and A.J. Heeger, *Appl. Phys. Lett*. **58** 1991 1982
[23] J. Kido, H. Shionoya, and K. Nagai, *Appl. Phys. Lett.* **67** 1995 2281
[24] I. Levesque, J. Stapledon and A. Donat-Bouillud, *Synth. Met.* **122** 2001 79
[25] C. Rothe, S.M. King and A.P. Monkman *Phys. Rev. Lett.* **97** 2006 art. no. 076602
[26] A.P. Kulkarni, C.J. Tonzola, A. Babel and S.A. Jenekhe, *Chem. Mater.* **16** 2004 4556
[27] C.W. Tang and A.C. Albrecht, *Nature* **254** 1975 507
[28] I.S. Shumov, V.I. Sevast'ianov, G.G. Komissarov, *Biofizika* **18** 1973 48
[29] C.W. Tang and A.C. Albrecht, *J. Chem. Phys*. **63** 1975 953
[30] D. Kearns and M..J. Calvin, *Chem. Phys*. **29** 1958 950
[31] N.S. Sariciftci, L. Smilowitz, A.J. Heeger and F. Wudl, *Synth. Met*. **59** 1993 333
[32] S. Morita, A.A. Zakhidov and K. Yoshino, *Jpn. J. Appl. Phys*. **32** 1993 873
[33] K. Tada, M. Onoda, H. Nakayama and K. Yoshino, *Synth. Met*. **102** 1999 982
[34] G. Yu, K. Pakbaz and A.J. Heeger, *Appl. Phys. Lett*. **64** 1994 3422
[35] L. Schmidt-Mende, A. Fectenk. Otter, K. M. Cullen, E. Moons, R.H. Friend and J.D. MacKenzie, *Science* **293** 2001 1119
[36] S.-S. Sun, *Sol. Energy Mater. Sol. Cells* **79** 2003 257
[37] (a) F. Jonas, G. Heywang, W. Schmidtberg, J. Heinze and M. Dietrich, EP 339 340 (Bayer AG), Prior: 1988-04-22; (b) G. Heywang and F. Jonas, *Adv. Mater* **4** 2 1992 117
[38] P. -H. Aubert, L. Groenendaal, F. Louwet, L. Lutsen et al. *Synth. Met.* **126** 2002 193
[38] F. Jonas and W. Krafft, EP 440 957 (Bayer AG), Prior: 1990-02-08.
[39] K.E. Aasmundtveit, E.J. Samuelsen, L.A.A Pettersson, O. Inganas and T. Johansson, T.,*Synth. Met.* **101** 1999 561
[40] F. Jonas and G. Heywang, *Electrochim. Acta*, **39** 1994 1345
[41] S. Timpanaro, M. Kemerink, F.J. Touwslager, M.M. de Kok and S**.** Schrader, *Chem. Phys. Lett.* **394** 2004 339
[42] G. Greczynski, Th. Kugler, M. Keil, W. Osikowicz and M. Fahlman, *J. Electron Spectrosc.* **121** 2001 1
[43] F. Jonas, A. Karbach, B. Muys, E. van Thillo, R. Wehrmann, A. Elschner and R. Dujardin, EP 686 662 (Bayer AG), Prior:1994-05-06/1995-03-03.
[44] B. D. Martin, N. Nikolov, S. K. Pollack, A. Saprigin, R. Shashidar, F. Zhang and P. A. Heiney, *Synth. Met*., **142** 2004 187
[45] J.H. Chen, C.A. Dai, W.Y. Chiu, *J. Polym. Sci. A: Polym. Chem.*, **46** 1662
[46] S. Kirchmeyer and K. Reuter, *J. Mater. Chem.*, **15** 2005 2077
[47] F. Zhang, M. Johansson, M. R. Andersson, J. C. Hummelen and O. Ingana¨s, *Adv. Mater*., **14** 2002 662
[48] T. Aemouts, P. Vanlaeke, W. Geens, J. Poortmans, P. Heremans, S. Borghs, R. Mertens, R. Andriessen and L. Leenders, *Thin Solid Films* **22** 2004 451
[49] A. Elschner, F. Bruder, H.-W. Heuer, F. Jonas, A. Karbach, S. Kirchmeyer, S. Thurm and R. Wehrmann, *Synth. Met.* **139** 2000 111
[50] T..M. Brown, J.S. Kim, R.H. Friend, F. Cacialli, R. Daik and W. Feast, *Appl. Phys. Lett.* **75** 1999 1679
[51] J. C. Gustafsson, B. Liedberg and O. Ingana¨s, *Solid State Ionics*, **69** 1994 145.
[52] H.-W. Heuer, R. Wehrmann and S. Kirchmeyer, *Adv. Funct. Mater*. **12** 2002 89.
[53] S. A. Sapp, G. A. Sotzing, J. R. Reddinger and J. R. Reynolds, *Adv. Mater*. **8** 1996, 808
[54] T. Kawase, H. Sirringhaus, R. H. Friend and T. Shimoda, *Adv. Mater*. **13** 2001 1601

3. ELECTROPOLYMERISATION OF CONDUCTIVE POLYMERS

3.1 Procedure and mechanism

Electrochemical synthesis of conducting polymers offers a number of advantages over chemical oxidative synthesis. It requires only small amounts of starting monomer, is precise and easily reproducible, and allows immediate analysis via electrochemical studies. For these reasons, electropolymerisation is frequently used for scientific studies of conducting polymers, although its main drawback is the relative difficulty in making large quantities of material. The resulting polymers are also generally highly insoluble, making other analysis techniques difficult to perform.

The electropolymerisation is cathodic, with the electrochemical oxidation of monomers leading to polymer formation. The synthesis is carried out in a standard three electrode electrochemical cell, normally with in an organic medium with an appropriate soluble electrolyte salt and a quantity of the monomer. The oxidation potential of the monomer is applied at the working electrode and current flows between the counter and the working electrodes as monomer is oxidised and polymerises. Formation of the polymer on the working electrode of the cell then follows a process of nucleation and phase-growth, but is subject to a large amount of variation in terms of chain length, orientation, morphology and crystallinity of the film. These factors have an important impact on the electronic and film's mechanical properties. Altering the electrical conditions of the polymerisation, solvent, electrolyte, monomer concentration and electrode material all can have a significant effect on the growth of the polymer film and its properties [1,2].

The mechanism of electropolymerisation of conducting heterocycle polymers has not been definitively elucidated, but several convincing theories exist to describe the process. It is known that the oxidation of one heterocycle monomer requires 2 electrons, leading to the proposed mechanism (figure 3.1) based on coupling reactions of aromatic compounds.

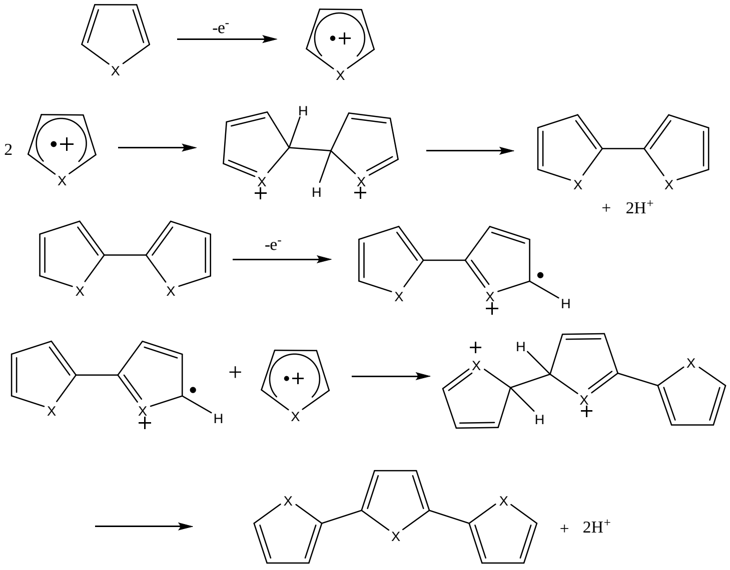

Figure 3.1 *Electropolymerisation mechanism for poly(heterocycle)s [2].*

The first step is the removal of one electron to form the radical cation. The coupling of two monomers gives the dimer dication which then regains aromaticity via the loss of two hydrogens. The resulting dimer is more easily oxidized than the monomer, so it is itself converted to a radical cation before similar coupling and rearomatization. In this fashion, oligomers are formed in solution until they are sufficiently long to become insoluble and precipitate on the electrode. Although it there is quite clear evidence for the presence of oligomers in solution at the beginning of the electropolymerisation, it is still not entirely apparent whether they are a crucial step in the formation of the polymer. The alternative view is that the process begins with absorption of thiophene to the surface, and this is supported by various experimental evidence; not least of which, the fact that commencing the polymerisation with oligomers as starting material leads to very poor quality polymer films [3]. Time resolved STM images of electrode surfaces during polymer growth also seems to support the view that growth occurs on the surface from the beginning [4]. It is likely that the growth of the polymer consists of a mix of both processes, with relative contributions depending on the various growth conditions.

The continued growth of the polymer film can proceed in a layer by layer or island forming mode, depending largely on its solubility in the solvent and the electrical condtions used. As the polymer is formed it will become doped, at oxidative potentials, or successively doped and de-doped if a cycling voltage is applied. This behaviour can clearly be observed in polymer grown by successive cyclic voltammetry scans (figure 3.2), in which the current corresponding to the doping and dedoping of the film increases with the quantity of polymer. As the film is doped, electrons are removed onto the electrode and the positive charge remaining is countered by electrolyte salt anions. For this reason the nature of the salt can also play an important role in the resulting properties of the film; forming as it does, an integral part of the materials structure.

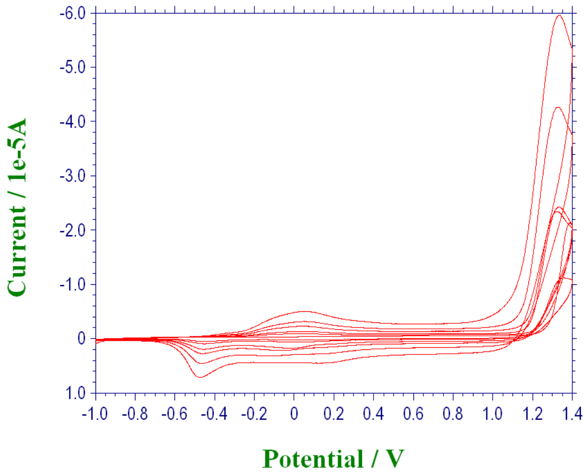

Figure 3.2 *Growth of PEDOT via cyclic voltammetry showing the oxidation of the monomer at 1.2 V and the electrochemistry of the resulting polymer; the current increasing as film thickness increases (potential vs. Ag/AgCl).*

3.2 Electropolymerisation conditions: polythiophenes

Several studies have been directed at investigating the effects of altering the diverse variables present in the electropolymerisation on the properties of the resulting films; most particularly their conductivity. Such studies often make use of in-situ conductivity measurements, in which a bi-potentiostat is used to measure conductivity of a polymer film across a microelectrode gap during the course of its deposition [5,6]. This avoids the need to remove the film from the electrode for conductivity measurements, which can significantly damage the film and reduce its performance. Here, discussion will focus on electrodeposition of polythiophenes, which to a large extent are representative of other conjugated polymers, and are relevant to the work described herein.

On a molecular level, electropolymerisation conditions have an effect on which of various growth mechanisms of the polymer chain will predominate. As discussed, the polymer can nucleate on the surface and continue to grow on the surface, or oligomers can form in solution. These oligomers will inevitably become physically incorporated into the growing polymer matrix; forming part of the film without being chemically bound to it [3]. Their presence in the film will clearly have a negative impact on overall conjugation length, density and cohesiveness; factors which relate directly to the overall film conductivity. In general, a closely packed, more ordered film will give better electric performance, largely due to the fact the order in itself derives from well ordered chains with long conjugation length. The impact of short oligomers on the film's properties can be seen in the growth of films using bisthiophene of terthiophene as a starting monomer. These conditions always lead to poorer quality films, likely owing to the decreased reactivity of the starting units, which leads to more short oligomers being incorporated.

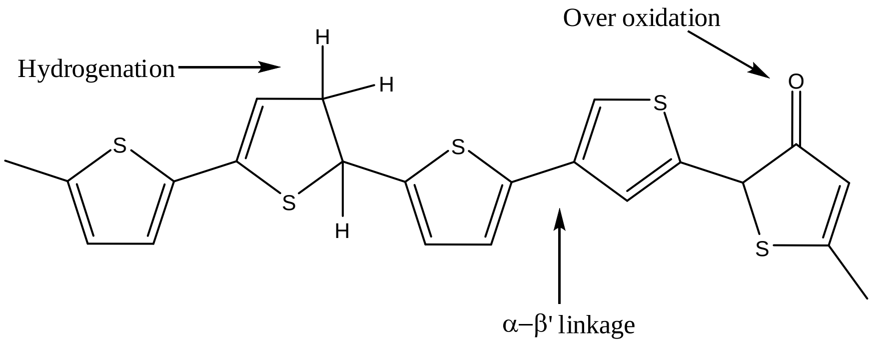

Figure 3.3 *Typical defects in polythiophenes*

The formation of defects in the chain is the other process which needs to be kept to a minimum. Apart from the formation of chemical defects such as oxidised carbons, it is favourable that kink free, fully conjugated and regioregular chains are produced. A common defect for unsubstituted polythiopenes is the α-β' linkage between units, rather than the regular α-α' linkage. This constitutes a break in the conjugation of the polymer and introduces a kink which can further disrupt adjacent chains. It seems that the chance of such unwanted linkages occurring increase as chain length increases (as relative reactivities decrease), which is supported by the general reduction in film quality for thicker films [7, 8]. Singularly substituted thiophenes such as P3ATs have less chance of such linkages occurring, but their regioregularity, and hence the ordered stacking of the side groups has a more important effect on film order. Regioregular synthesis is achievable in chemical syntheses but much more difficult to control electrochemically. The priniciple factors controlling this appear to be the electrical conditions and the monomer concentration [9].

A number of different formats are available for the application of the oxidation potential; widely used are potentiostatic or galvanostatic conditions, potential cycling and voltage pulses [10-12]. The voltage applied can also be greater than the actual oxidation potential required by the monomer. Indeed, it appears that high voltages can favour the rapid nucleation of polymer on the electrode and thus create denser, more ordered films [13]. On the other hand, control of the current flowing through the cell is of greater importance for the continuing regular and defect free growth of the chains [14]. Essentially, faster deposition leads to more chaotic, rapid growth of the film in certain areas, and even, homogeneous films are not favoured. High monomer concentration will have a similar negative effect as it accelerates the deposition. Potential sweeps as in cyclic voltammetry, up to or beyond the oxidation potential are often used to grow the polymer film. While this technique is appealing as it allows continuous monitoring of the growth of the polymer film from the growth of the polymer redox peaks, it does not allow any systematic control over the current or rate of deposition. Froberg et al. studied the change in morphology of PEDOT films with the change in the upper switching potential of voltage sweeps with interesting results [15]. At very low switching potentials films were dense (slow growth) but completely amorphous. On the other hand, switching at 1100mV gives highly crystalline films, whilst further increases lead to increasingly porous, less crystalline films. Sakaguchi et al. used voltage pulses of 150ms to favour slow and systematic growth of polythiophene chains on a gold substrate; observable by STM (figure 3.4) [4]. Conclusive proof of the growth of the chain on the surface rather than in solution is given by switching monomers and observing the block copolymers formed as a result.

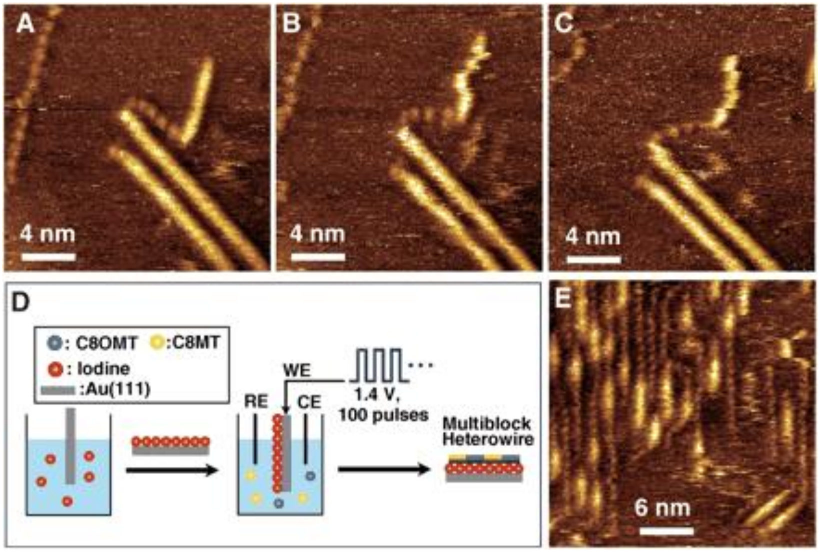

Figure 3.4 *Growth of polythiopene wires on gold by Sakaguchi et al. [4]*

The solvent in which the electopolymerisation is carried out proves to be one of the most influential factors on the polymer morphology. Strictly anhydrous conditions are necessary to avoid incorporation of carbonyl groups into the polymer, and thus reduction in conjugation length [16]. Anhydrous, aprotic solvents which also have high dielectric constants and stability at high voltages are therefore required: acetonitrile, benzonitrile, nitrobenzene and propylene carbonate are all commonly used for these reasons [17-19]. The solubility of the polymer in a given solvent will influence the growth mechanism of the film. Low solubility will clearly favour growth of chains directly on the electrode surface, whilst a degree of solubility of oligomers will favour the growth in solution and later precipitation of longer oligomers.

The anode material on which the polymer is grown is normally an inert conducting material such as platinum, gold, ITO, or glassy carbon. It has been found that polythiophenes will tend to form better films on platinum, probably because of the high number of active sites allowed for nucleation of the monomer, which will lead to a denser film [20].

The conductivity of the electrodeposition medium is insured by the presence of electrolyte salts soluble in the organic solvents used. These are normally small anions such as ClO_4^-, PF_6^-, or BF_4^-, which are associated with cations such as lithium or alkylated ammonium. It is the anion which becomes directly incorporated into the polymer film as a counterion to charged polymer, and thus that which has the greater impact on the film properties. In-situ conductivity measurements of polythiophene films formed with different anions have shown that ClO_4^- and PF_6^- generally give higher conductivity films [21, 23]. In-situ measurements of PEDOT films by Reynolds et al. showed that in fact the cation used appeared to make a greater difference; with lithium salts out performing films made using ammonium salts by an order of magnitude [5].

Several studies have looked at the effect of substituting different alkyl chain lengths to polythiophene or PEDOT. Short chain lengths cause steric hindrance and disorder in the polymer backbone, lowering conductivity of the polymer films as the conjugation length is decreased. However, longer alkyl substituents (>6) start to have a positive effect on conductivity, presumably due to interdigitation between adjacent chains leading to a greater degree of order in the polymer [22].

References

[1] Roncali J.*Chem. Rev.* **92** 1992
[2] E**.** Genies, G. Bidan and A.F..Diaz, *J. Electrwnul. Chem*. **149** 1983 113
[3] J. Roncali, F. Gamier, M. Lemaire and R. Garreau, *Synth. Met*. **15** 1986 323
[4] H. Sakaguchi, H. Matsumura, H. Gong and A.M. Abouelwafa, *Science* **310** 2005 1002
[5] M.C. Morvant and J.R Reynolds, *Synth. Met.* **92** 1998 57
[6] E.W. Paul, A. J. Ricco and M. S. Wrighton, *J. Phys. Chem.* **89** 1985 1441
[7] G.M. Garnaggi, G. Deluca and A. Tundo, *J. Chem. Soc Perkin Trans***. 2** 1972 1594
[8] A. Yaaaar**,** J. Roncali, and F. Garnier, *Macromolecules* **22** 1989 804
[9] C. Pozo-Gonzalo, T. Khan, J.W. McDouall, P.J. Skabara. et al. *J. Mater. Chem.* **12** 2002 500
[10] S.B. Saidman and M.E. Vela, *Thin Solid Films* **493** 2005 96
[11] P. Ocón and P. Herrasti, *Polymer* **42** 2001 2439
[12] S. Aeiyach, A. Kone, M. Dieng and J. Aaron, *Chem. Comm.* **12** 1991 822
[13] L. Pigani, A. Heras, A. Colina and R. Seeber, *Electrochem. Commun.* **6** 2004 1192
[14] J. Roncali, A. Yassar and F.J. Garnier, *Chim. Phys.* **86** 1989 241
[15] L. Niu, C. Kvarnstrom, K. Froberg and A. Ivaska, *Synth. met.* **122** 2001 425
[16] D. Delabouglise, R. Garreau, M. Lemaire and J. Roncali, *New J. Chem*. **12** 1988 155
[17] R.J. Waltman, J. Bargon and A.F. Diaz, *J. Phys. Chem.* **8** 1983

[18] K. Kaneto, Y. Kohno, K. Ycehino and Y.J. Inuiahi, *J. Chem Soc*. *Chem Commun*. 1983 382
[19] M. Sato, S. Tanaka and K.Y. Kaeriyama, *Chem. Soc*, *Chem commun*, 1985 713
[20] J. Roncali, A. Yaaaar and F.Z. Garnier, *J. Chem. Soc.*, *Chem. Commun*. 1988 581
[21] Giurgin, K. Zong, J.R. Reynolds, W.-P. Lee, K.R. Brenneman et al., *Synth. Met***. 119** 2001 405
[22] L. Groenendaal, G. Zotti and F. Jonas, *Synth. Met.* **118** 2001 105

4. A TRANSPARENT ELECTRODE FROM ELECTRODEPOSITION OF PEDOT ON CNT THIN FILMS

4.1 Introduction

The aim of the work described in this chapter is to make a high perfomance transparent electrode from a film of PEDOT electrochemically deposited onto a carbon nanotube film. As discussed above, PEDOT forms an essential role in many organic devices, improving charge transport between electrode and organic material, and smoothening the electrode. Electrochemically grown PEDOT films are known to offer higher conductivities than chemically synthesised films or films cast from aqueous dispersions such as PEDOT:PSS. Films made from chemical oxidation of the monomer necessarily contain metal catalyst which would likely play a role in degradation of active organic semi-conducting layers. As discussed above, PEDOT:PSS films are known to suffer from a large proportion of the insulating PSS at film surfaces and surrounding conductive PEDOT particles. Moreover, the inevitable presence of water in these films is also a stability hazard for active organic layers and the cathode (usually Al) in a device. An electropolymerised film necessarily requires a conductive and transparent substrate on which for the deposition to take place, and carbon nanotube films present a new alternative to conventional ITO films, which are better suited to the development of organic devices.

By this rationale, we propose an electrode which uses a carbon nanotube film as a conductive scaffold on which to grow a pure and highly conductive PEDOT film. The resulting material should benefit from the properties of both materials; namely, the high conductivity of the nanotubes and the smoothness and work-function of the polymer.

4.2 Results and discussion

4.2.1 Nanotube purification and dispersion in water

HipCO SWNTs

For this work, two commercial sources of carbon nanotubes were used; HipCO CVD CNTs from Carbon Nanotechnologies and P3 arc-discharge nanotubes from Carbon Solutions. The HipCO tubes underwent oxidative purification before use in order to remove amorphous carbon, as well as to improve their water solubility via functionalisation of sidewalls. Several different procedures were followed to purify these nanotubes:

1. Heating to 100 ºC in air
2. Heating to 100 ºC under humid air
3. Reflux in various concentrations of Nitric acid (10%, 50%), 4 hours

The resulting tubes were washed with copious amounts of distilled water to achieve a neutral dispersion. Although water solubility of the nanotubes usually increases after oxidation, the surfactant sodium dodecyl sulphate (SDS) (1% solution) was added to improve the water dispersions. The dispersions were then sonicated, centrifuged, and the supernatant sonicated again to break down any remaining nanotube aggregation. Ultrasonication is a useful technique for solubilising CNTs, but will also damage and cut tubes if continued for too long, so must be used in moderation for applications requiring a high degree of nanotube integrity.

These purification protocol's were chosen to be relatively mild and therefore retain a high degree of nanotube integrity; as longer nanotubes should form more conductive films for low coverages. On the other hand, a high degree of oxidation of nanotube walls will increase their solubility and therefore yield better dispersions in water and more homogeneous films. Moreover, it is known that reaction of SWNTs with nitric acid can oxidatively dope semi-conducting nanotubes and thereby render them more conductive. Our aim is therefore to determine which of these factors should prove the most influential in the fabrication of competitive transparent electrodes.

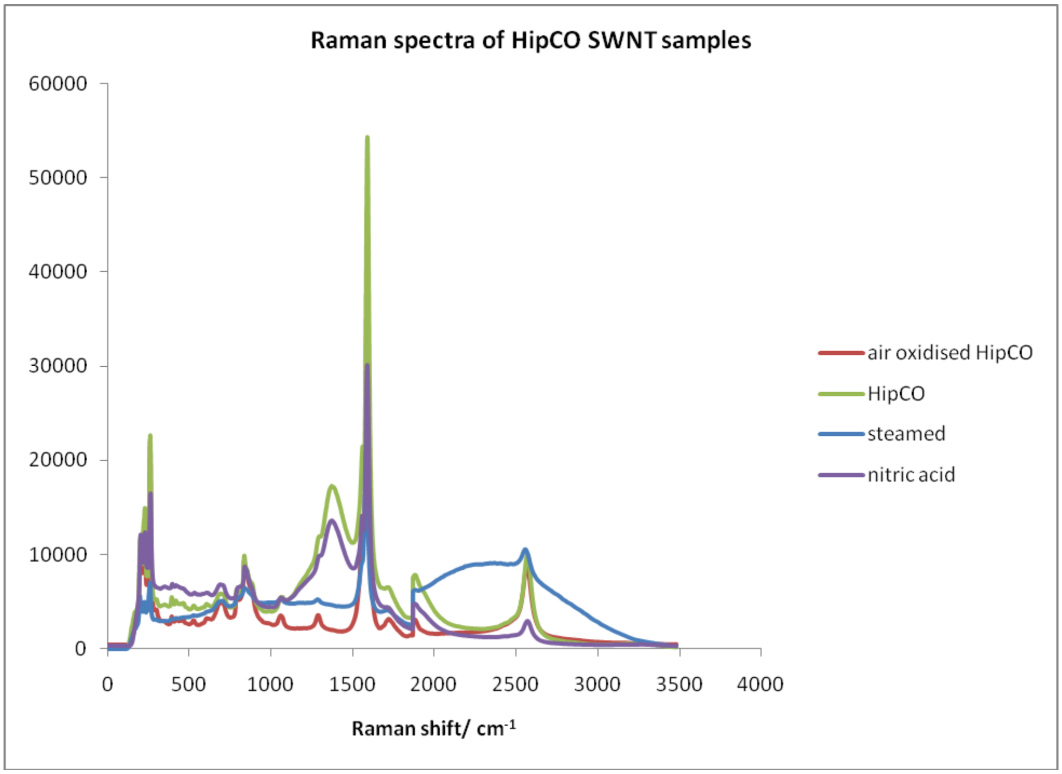

Figure 4.1 *Raman spectra of HipCO nanotube samples, as supplied and purified*

Raman spectroscopy of purified samples, filtered (where necessary) and oven-dried, are shown in figure 4.1. It can clearly be seen that the two gaseous oxidations carried out result in a dramatic reduction of the large D mode absorption present in the as-bought samples. This is a strong indication that both these procedures are quite effective at removing carbonaceous impurities yet at the same time retaining the integrity of the nanotube side-walls. This agrees with work by Tobias et al. who first proposed steam oxidation as a means to reduce damage to SWNTs during purification [1], though it should be noted that 100 ºC represents an exceptionally low temperature for this process.

The Raman spectrum of the SWNTs refluxed in 10% nitric acid shows a more prominent D peak, and considerably smaller G/D intensity ratio at 2.3, compared with the as-purchased nanotubes (ratio of 3.6). The increase in apparent amount of sp^3 defects in the sample is likely due to extensive oxidation of the nanotube side-walls by the acid.

The radial breathing mode absorption for all samples are very similar, which is to be expected as it relates to the diameters of those nanotubes in the sample which have electronic transitions in resonance with the Raman laser. Three clear peaks are visible, corresponding to nanotubes with diameters from around 0.93 to 1.2 nm.

Unsurprisingly, the gas oxidised nanotubes were found to be poorly soluble in water, even after sonication and the addition of surfactant. Consequently, films made from filtrations of these dispersions were visibly inhomogeneous. Upon transfer of these films to glass slides, adhesion to the glass was noticeably poorer; making the transfer itself difficult to perform. It seems clear that the purification of the SWNTs to a near pristine state, with minimal sidewall oxidation is highly unfavourable for the subsequent processing required for film preparation.

Of the nitric acid treated SWNTs, those refluxed in 50% acid were possible to disperse in water, yet filtration of these dispersions often gave patchy films. The SWNTs refluxed in 10% acid were easily dispersed, could be filtered into smooth, homogeneous films, and showed reasonable adhesion to glass. The visible-NIR spectra of these dispersions shows some clear groups of peaks for semi-conducting and metallic transitions, indicating a good degree of separation between individual tubes (figure 4.3). We infer that the lower oxidation strength of more concentrated acid resulted in less oxidised nanotubes which yielded relatively poorer dispersions. All further work on HipCO was conducted on samples modified in 10% nitric acid.

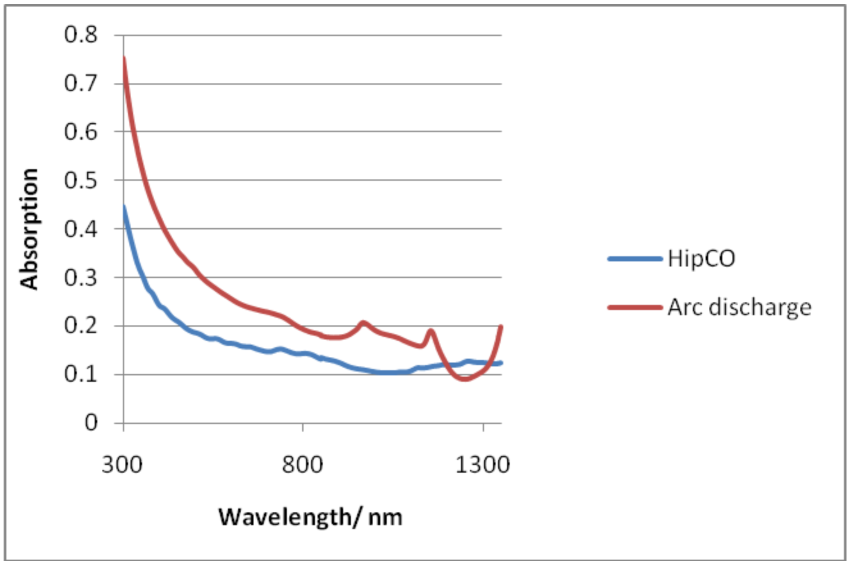

Figure 4.2 *Vis-NIR spectra of SWNT dispersions*

P3 functionalised arc-discharge SWNTs

Attention was turned to arc-discharge synthesised SWNTs as potentially a source of longer and purer nanotubes. Work by Zhang et al., has shown that these SWNTs yield much higher performance transparent films than other nanotube sources, the obvious negative being their much higher cost [2]. The P3 arc discharge nanotubes obtained were of a high purity and already highly oxidised, so they were used without chemical treatment. The Raman spectrum of the as-bought nanotubes is shown in figure 4.3. A high intensity D mode absorption is likely due to the high level of functionalisation in the nanotubes as they are pre-purified. The purity of these nanotubes with respect to the HipCO samples can be further assessed by electron microscopy (figure 4.4). Thin films of arc-discharge films show sharply resolved thin tubules, whereas HipCO films appear to have a matrix of non-nanotube material surrounding larger SWNT bundles. This material is probably amorphous carbon impurities.

The broad absorption for the radial breathing mode suggests that there is a wide range of nanotube diameters in the sample analysed. The peak RBM absorption correlates to an average nanotube diameter of 0.73 nm. The Raman intensity from these nanotubes is generally much lower, likely due to much denser packing of SWNTs within the material

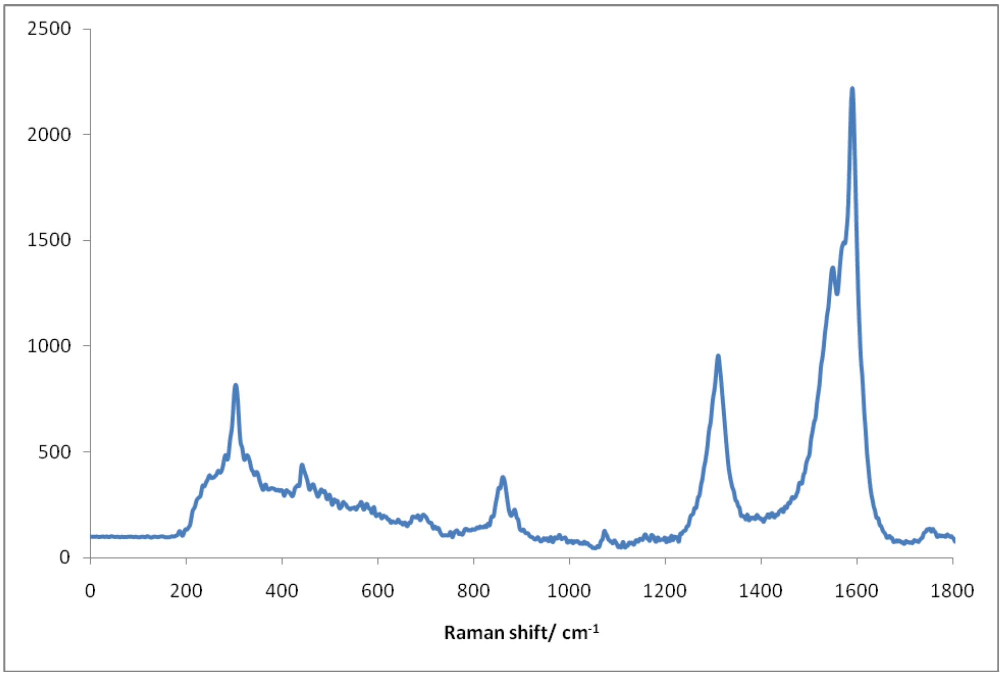

Figure 4.3 *Raman spectrum of P3 arc-discharge SWNTs*

Dispersions in water were again made in 1% SDS (1:10 ratio, CNTs:surfactant), followed by the same cycle of sonication and centrifugation. These high purity nanotubes appear to give better quality dispersions than any of the HipCO samples, although the absorption spectrum of the solution shows less clear peaks, probably owing to the high level of oxidation (figure 4.2).

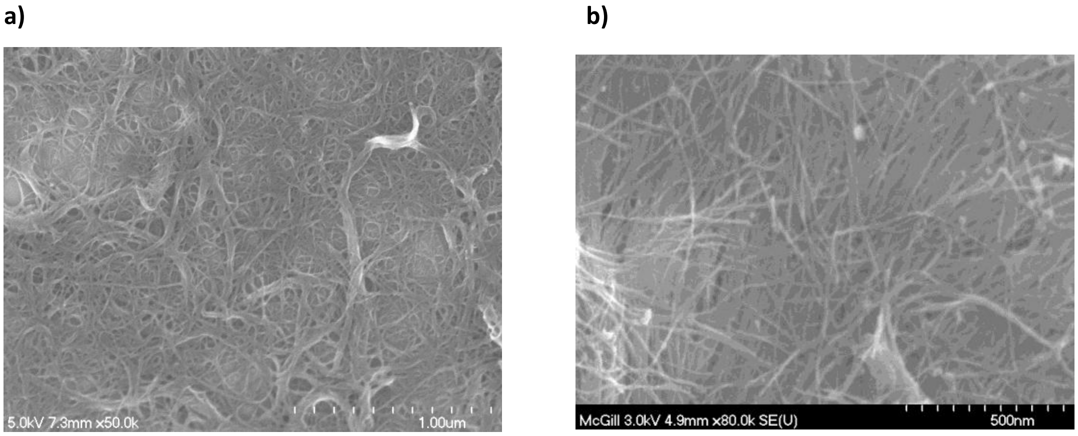

Figure 4.4 *Scanning electron microscopy of **a)** HipCO film on glass and **b)** arc discharge film on glass*

4.2.2 Transparent Nanotube films

Glass substrates

Appropriate quantities of the SWNT dispersions were filtered, after diluting with a large excess distilled water to ensure an even film. Filtration is performed through mixed ester cellulose membranes, resulting in a thin and homogeneous nanotube film on the membrane. The thickness and optical absorption of the films can be controlled and predicted to reasonable accuracy based on the optical absorption of the solution and the volume filtrated.

Portions of SWNT films on the membrane are placed in chlorobenzene for one minute before placing onto glass microscope coverslips. This step is carried out to avoid formation of air bubbles between the membrane and the substrate, which can damage the CNT film. The substrates are placed in a large acetone bath for several hours to dissolve the cellulose membranes. Resulting nanotube films on transparent substrates are rinsed in isopropanol and dried under nitrogen. Heating to 300 ºC on a hot plate for one hour is carried out to improve bonding between the glass and the nanotubes. This step proved to be imperative for rendering the films resistant to subsequent electropolymerisation process, in which they come into close, abrasive, contact with the electrical contact metal. Not heating frequently resulted in films being completely removed where they are contacted, whereas the annealing seems to render them to a great extent impervious to scratching. This is particularly true for arc-discharge films, which adhere less well to glass than HipCO nanotubes; likely owing to their higher purity. Excessive heating can result in total oxidation and removal of the nanotube film. Even the treatment to 300 ºC is likely to be causing some oxidative damage to the nanotubes within the film, and could perhaps be improved by performing under nitrogen.

The films are then placed in a concentrated nitric acid bath for one hour and then rinsed in isopropanol to remove SDS and oxidatively dope the nanotubes, thus increasing their conductivity. This treatment is capable of reducing the sheet resistance of a film by several times, and is therefore a very effective means of vastly improving film performance. It is uncertain whether this enhancement comes primarily from solubilising and removing the surfactant, or from chemical doping of the nanotubes. Studies on the change in absorption spectra of the nanotubes from semi-conducting transitions to predominately metallic transitions seem to suggest the latter plays an important role.

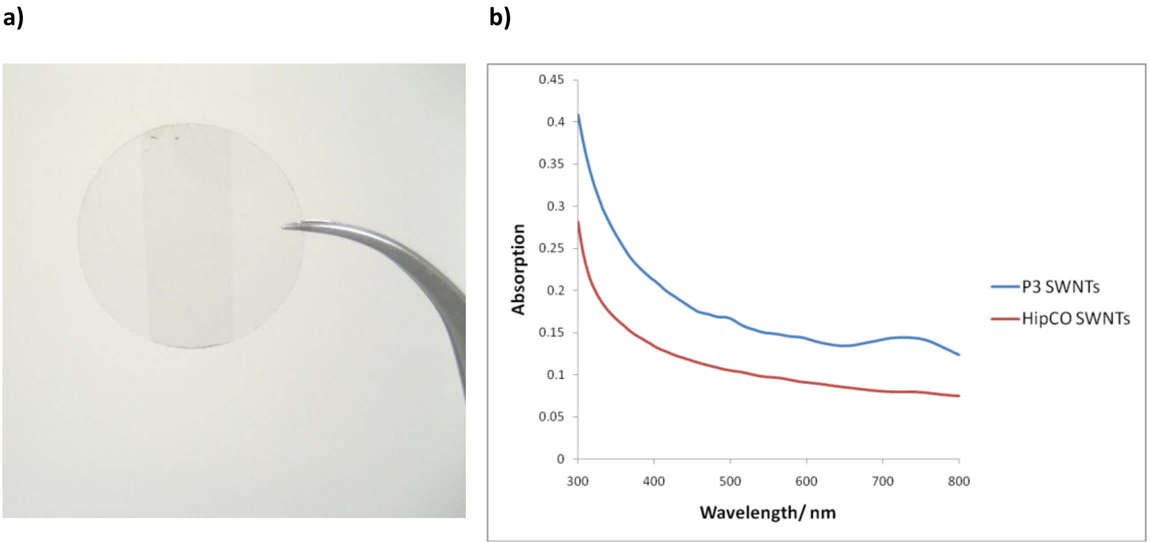

Figure 4.4 a) *Photo of P3 CNT film on glass cover-slip and* ***b)*** *absorption spectra of HipCO and P3 films*

Plastic substrates

The possibility of fabricating fully flexible organic devices is one of the primary benefits of using carbon nanotube electrodes. A number of suitable transparent plastics exist, with various advantages with regards to their clarity, chemical resistance, and mechanical properties. Studied here are standard laser printing transparencies (a polyacrylate based copolymer) and Polyethylene terephthalate (PET).

SWNT film transfer to circles of the polyacrylate was carried out in the same manner as described above, except without the nitric acid treatment or annealing. Carbon nanotubes adhere to the hydrophobic polymer surface much better than they do to glass, so the heating of the films proved entirely unnecessary.

PDMS stamping on PET

The transfer of carbon nanotube films from filtration membranes using a polydimethylsiloxane (PDMS) stamp was first shown by Zhou et al. in 1996 [4]. It has several advantages over the dissolution process, particularly the possibility of patterning the films, and the use of less solvent resistant substrates. The SWNT films for these electrodes were made by filtering through alumina membranes (not needing a soluble membrane material). A PDMS stamp with a grid of rectangular protusions was pressed against the nanotube film, removed and then pressed against a polyethylene terephthalate sheet, transferring the nanotubes completely to the new substrate. These SWNT films were made specifically for the easier fabrication of organic LED devices, and were therefore patterned as three strip electrodes on larger PET substrates.

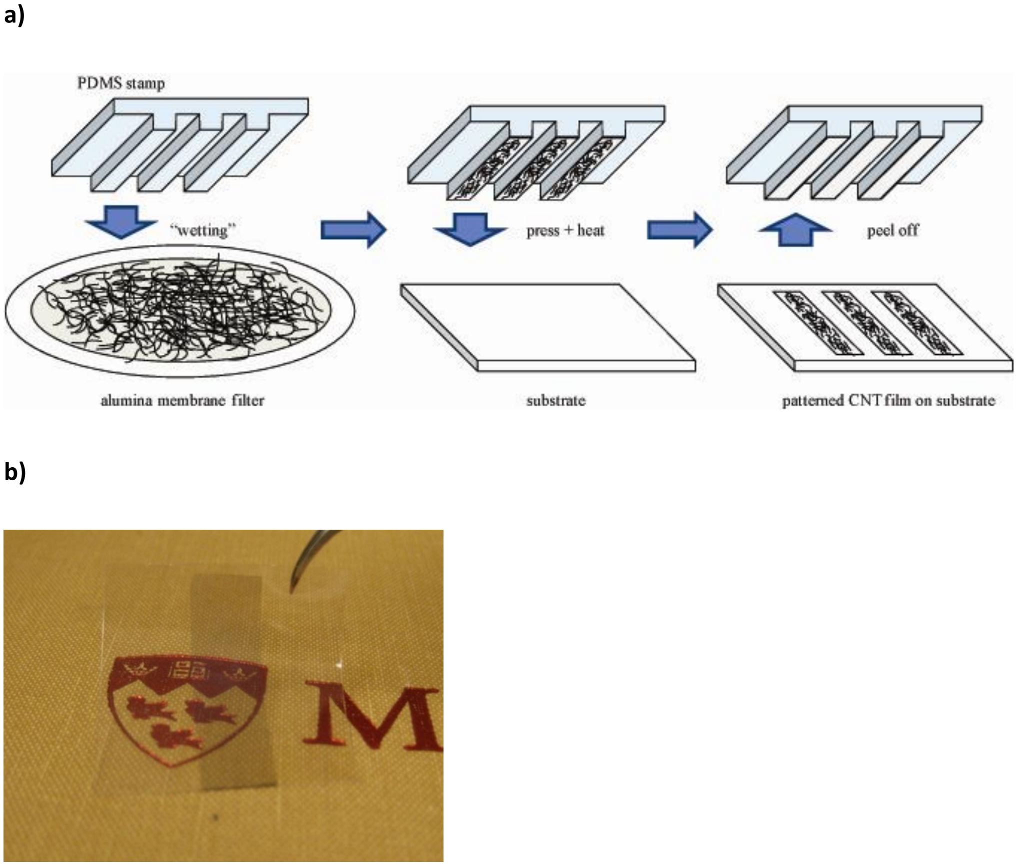

Figure 4.6 ***a)*** *PDMS stamping of films on PET* ***b)*** *a single strip of nanotubes on PET [5]*

4.2.3 Electropolymerisation

The electropolymerisation of PEDOT onto a transparent nanotube electrode on glass was carried out in a specially designed, three electrode electrochemical cell (figure 4.7 a)). The nanotubes electrode acts as the working electrode, and is connected to the potentiostat probe via a brass ring around the edge of the CNT film, inside of which is a Teflon ring to seal the electrolyte from this metal contact. The counter electrode is a platinum disc place parallel to and above the CNT film, and an aqueous Ag/Ag$^+$ electrode is used as a reference. The electrolyte is a solution of TBAPF$_6$ in anhydrous propylene carbonate. To ensure anhydrous conditions, the electrolyte salt is dried by heating and then cooling under argon; the polymerisation is similarly carried out under argon atmosphere. Figure 4.7 b) shows a potentiodynamic deposition of PEDOT where the voltage is cycled past the oxidation potential of the monomer and back. The growth of the polymer film is clear from the increase doping and de-doping current at lower potentials.

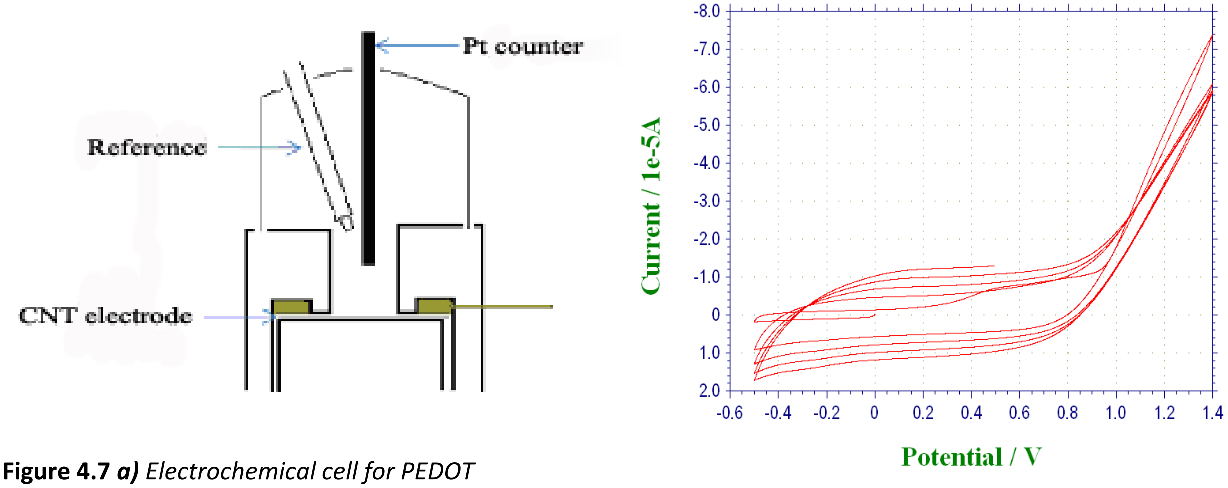
a)

b)

Figure 4.7 ***a)*** *Electrochemical cell for PEDOT deposition and* ***b)*** *cyclic voltammetry scans showing the growth of the polymer film (potential vs. Ag/AgCl). The oxidative polymerisation current starts at 0.9V and increases linearly- showing limitation from the film resistance (ohmic) rather than the electrolyte.*

However, for a more quantifiable deposition a potentiostatic method was used, by applying a constant potential of 1.1V over varying periods of time. The duration of the deposition depends on the rate at which charge is accumulating on the electrode, but a sufficiently thick film is generally formed after 50 to 100 s at this potential. For a given deposition rate, the duration can be used to control the polymer thickness to a certain extent. The transmission spectra in figure 4.8 show how PEDOT thickness increases with deposition time: here, 80 s of deposition yields a film 33% more absorbing (at 550 nm) than 60 s of deposition. The electrodes are removed from the cell and rinsed in acetone and isopropanol before drying in nitrogen. Using this technique, it was possible to achieve thin, homogeneous PEDOT films across the nanotube film (figure 4.8 a) and b)). Electron microscopy shows similar images to those of pristine films, although some organic material is visible; the polymer is apparently poorly resolved in EM.

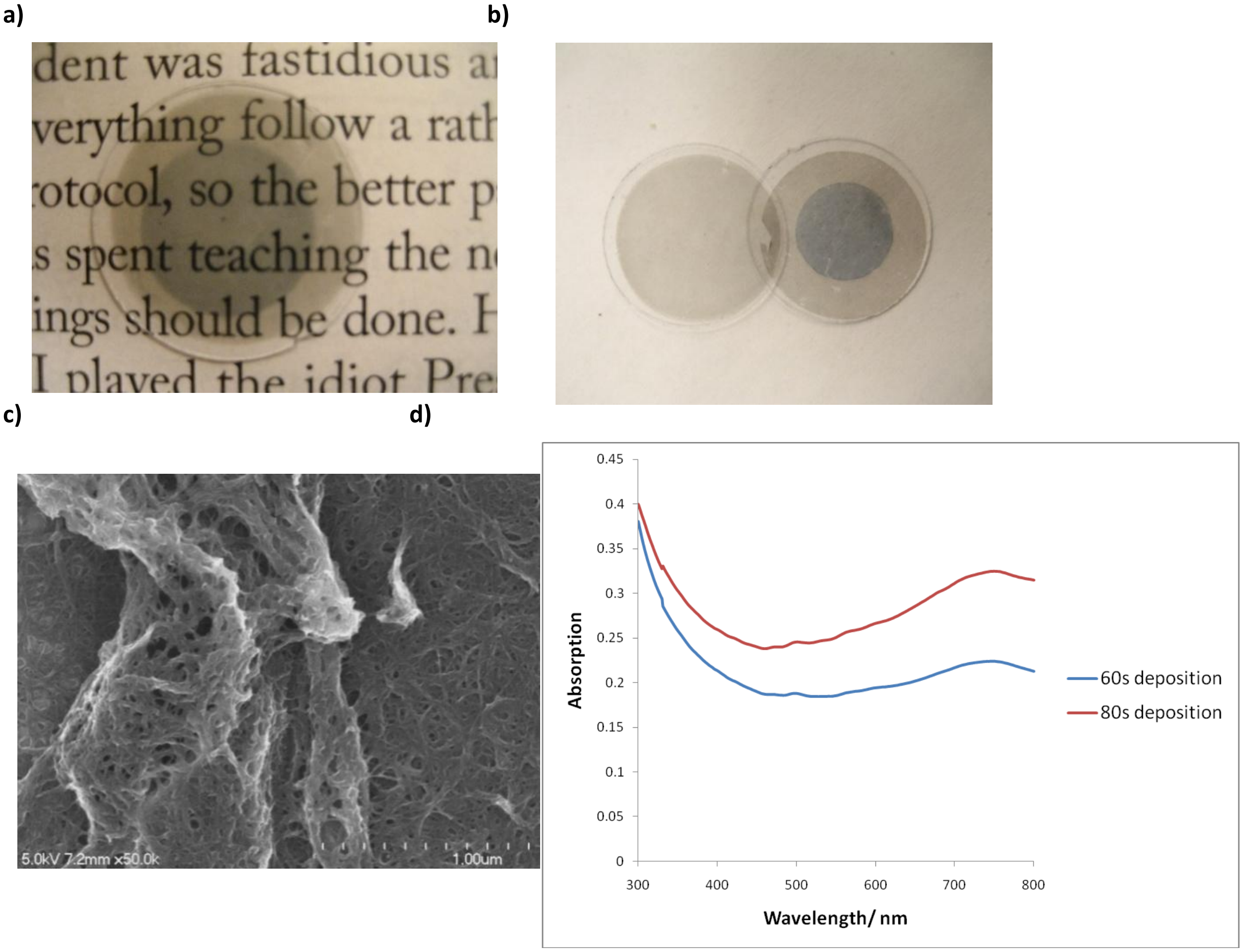

Figure 4.8 *PEDOT on CNT films **(a)(b)** and **c)** SEM, **d)** Transmission spectra for films of different deposition times.*

Electropolymerisation on PET films

The nanotube films on PET were aimed at compatibility with existing LED analysis instruments, and it was not possible to integrate them with the electrochemical cell described above. Instead, a layer of palladium was evaporated along one end of the rectangular strips of nanotubes, to act as a contact during polymerisation and also for later device operation. The other end of the nanotube strips was then dipped into electrolyte, whilst a parallel piece of ITO coated glass of similar dimensions was used as the counter electrode. This confirmation of electrodes is less ideal than the designed cell, as there is less exact control over exposed electrode area, electrode separation and importantly, the exposed edges and extremities of the nanotube film receive the majority of the electrochemical current, and thus the polymer. It is nonetheless possible to grow relatively homogeneous polymer films in this manner.

4.2.3 Optical and electrical properties of PEDOT films

The suitability for devices of all the electrodes was assessed by measuring their sheet resistance and absorption in the visible region. The first electrodes made with HipCO SWNTs were not generally of high conductivity; rarely attaining below 1000 Ohms/sq. even with the polymer coating. Figure 4.9 a) shows the performance of the films without PEDOT. As should be expected the sheet resistance of the film decreases in roughly logarithmic proportion with its transmittance.

The sheet resistance of nanotube films was also measured before and after the nitric acid bath which is thought to increase conductivity of films by removing SDS and oxidatively doping semi-conducting nanotubes. Indeed, large drops in sheet resistance of up to 40% were observed after employing an acid bath for several hours.

A series of PEDOT films of varying thickness were grown on CNT films of constant properties, made by filtering a constant volume of the same CNT dispersion. The performance of these PEDOT coated films for both HipCO and arc discharge nanotubes is plotted in figure 4.9 b). The increase in conductivity for a given transparency offered by the P3 nanotubes can easily be seen- at several kΩ/sq. difference for the same transparency. As might be expected, increasingly thick layers of PEDOT correspond to an increase in the absorbance of the film as well as a reduction in sheet resistance. These first series of films were made according to the paradigm of an electrode based largely on the polymer, in which the nanotube film serves mainly as a means to grow the polymer, rather than the principle conduction pathway for the electrode. However, using this proportion of the two materials, for either nanotube source, gives electrodes which consistently fall short of the required properties for an electrode in a working device. Looking for a sheet resistance of less than 500 Ohms/sq. corresponds to a quantity of PEDOT with too much absorbance for the electrode to function well.

With a view to obtaining device viable electrodes, the P3 nanotubes were employed in the making of electrodes of different proportions of the materials. A thicker nanotube film, with a thin layer of PEDOT corresponds more closely to the parameters of conventional nanotube electrodes with spin-coated PEDOT hole-injection layers. The high conductivity of the CNTs generally allows a relatively high performance transparent electrode in itself, whilst a thin polymer layer serves mainly to smooth the electrode surface. Nanotube films of about three times the thickness of the previous films were made, on top of which were grown PEDOT films of varying thicknesses, generally much thinner than previous electrodes, in order to arrive at total absorbance similar to the first series of electrodes. Figure 4.10 shows absorbance spectra typical of the two electrode paradigms- it can be seen that in terms of absorbance, the first electrodes have a roughly 1:6 ratio of CNTs to PEDOT, whilst this ratio tends towards 2:3 for the films aimed at device production.

This second series of P3 films were made in a slightly different fashion from previous films. Rather than carrying out a single small scale filtration for each film, larger area films of nanotubes were formed on large membranes, which were then cut into smaller pieces for transfer to glass or plastic substrates. This ensures consistency between each nanotube film, and allowed the use of different electrode geometries, particularly rectangular strips rather than circles, with a view to facilitating later device measurement.

a)

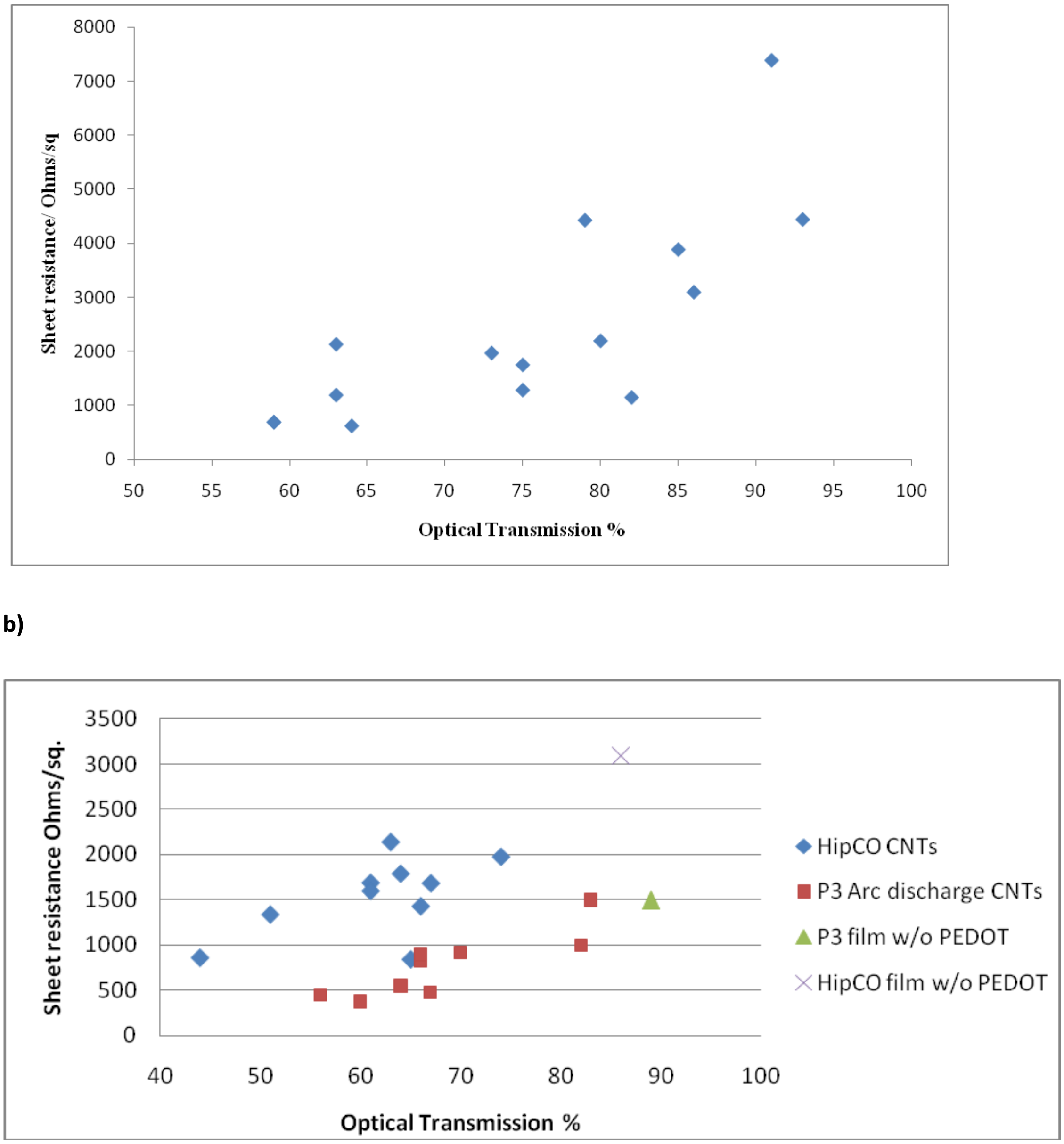

Figure 4.9 ***a)*** *HipCO CNT films of varying thickness and* ***b)*** *PEDOT coated films compared for arc discharge and HipCO films*

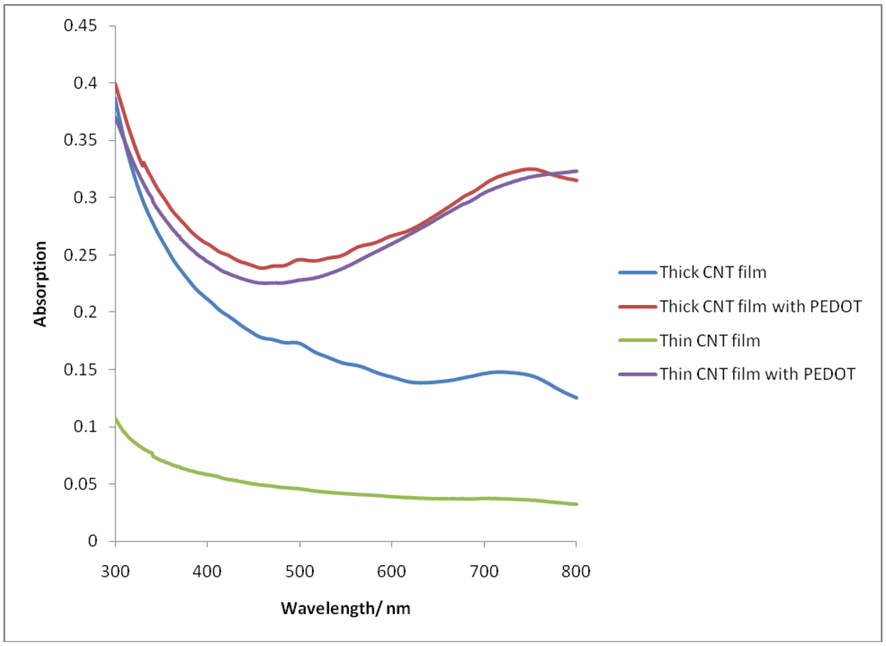

Figure 4.10 *Absorption spectra for two extremes of electrode- a thin nanotube layer with a thick PEDOT coating, and a thick nanotube layer with a thin layer of polymer for smoothening purposes.*

These higher conductivity, device oriented electrodes were produced on a variety of substrates as described in the previous section. For comparison with conventional device production, PEDOT was also spin-coated on to the same nanotube films at two different rotation speeds (5000 and 6000 rpm), giving different PEDOT thicknesses. Figure 4.11 plots the performance of these various electrodes in terms of their transparency and sheet resistance for different thicknesses of PEDOT. The data point for a bare CNT film shows how this thicker P3 film on its own has a relatively low sheet resistance of 300 Ω/sq. However, what is most striking about these data is that the addition of PEDOT to the electrode actually appears to reduce the conductivity of the film, with increasingly thick polymer layers giving more sheet resistance to the electrode. This is quite unexpected, given that the opposite trend is observed for the previous series of electrodes, and that increasing the thickness of the conductive layer should necessarily decrease the sheet resistance. Two possible conclusions can be drawn from this difference in behaviour. Firstly, the more conductive nanotube film could be such that the thin layer of less conductive polymer acts only as a resistive layer in between the measuring probes and the CNT film through which the current is flowing. This would imply that for the thinner nanotube films the PEDOT layer is thick enough to have a comparably low sheet resistance, which allows it to augment the total conductivity of the film. Presumably there is some intermediate ratio of the two materials at which the addition of PEDOT goes from being detrimental to beneficial. It is nonetheless quite unexpected that such a thin layer of PEDOT should prove to be such a marked hindrance to the flow of current between the probes and the nanotubes, rather than just increasing the total conducting area available in the film. A second conclusion could be that the polymer in these films is less highly doped, and therefore less conductive than those in the previous electrodes. Polymer which is de-doped to some extent at the end of the electrodeposition would indeed be only detrimental to the electronic properties of the electrode. In order to investigate this possibility, the conductivity of the electrodes under different doping potentials was studied, as detailed in section 4.2.5.

The spin-coated films of PEDOT:PSS show similar behaviour to their electropolymerised counterparts, yet higher performing electropolymerised films achieve lower sheet resistances (by up to 100 Ω/sq.) for the same thickness of PEDOT.

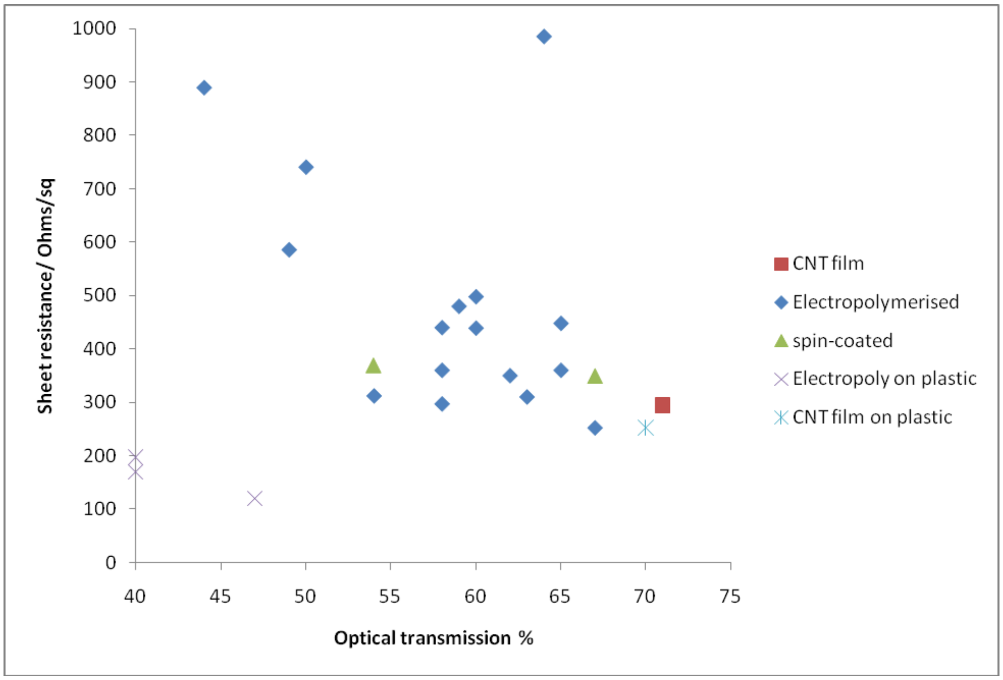

Figure 4.11 *The performance of higher conductivity arc-discharge SWNT electrodes for device applications, on glass and polyacrylate substrates.*

Some data for similar electrodes transferred to the polyacrylate sheets is also included in figure 4.11. Whilst the nanotube film alone on this substrate behaved much the same as a similar film on glass, the addition of PEDOT led to quite different results for the plastic electrodes. The polymer layer actually leads to quite a dramatic decrease in the sheet resistance, although is also accompanied by a proportionately large drop in transparency. The drop in optical transparency of these films is likely due to the slight denaturing of the plastic by the electropolymerisation solvent. In fact, this is probably overstated by the spectrophotometer measurement, as to the eye the electrodes appear of similar transparency to the glass films. However, the plastic surface is visibly roughened by the process, which will increase the degree of scattering of the transmitted light, and have a negative impact on the amount of light detected by the machine. The impressive conductivity of these films, and the fact that they show an opposing trend of the polymer being beneficial to the conductivity, is of more uncertain origin. It should first be noted that the adhesion of nanotubes to plastic substrates is much better than it is to glass, and the nanotubes appear to some extent to integrate themselves into the polymer sheet. The subsequent layer of conductive polymer could then plausibly be forming less of a discrete layer on top of the nanotubes, creating instead a much higher degree of inter-mixing of the two materials. In this way, it seems probable that the current impeding properties of the PEDOT layer resting on top are to some degree negated, whilst the benefits from having conductive material in the spaces between nanotubes is enhanced. In any case, one can conclude that plastic substrates, as well offering the sought after device flexibility, actually have quite an important favourable impact on electrode performance, as long as their optical clarity can be maintained throughout processing.

4.2.4 Morphology of films

An important property of the PEDOT film as a hole-injection layer is the smoothing of the rough electrode surface. This allows for more homogeneous spin-coating of the luminescent organic layers and reduces the chance of the device electrically shorting from contact between the electrodes. This is as necessary with a CNT electrode as with an ITO one, as the long nanotubes can potentially protrude from the surface and penetrate the organic layers. Detailed atomic force microscopy (AFM) was thus performed on all the electrodes in various stages of preparation, in order to assess them in this regard, and compare with equivalent spin-coated PEDOT electrodes.

Glass substrates

a)

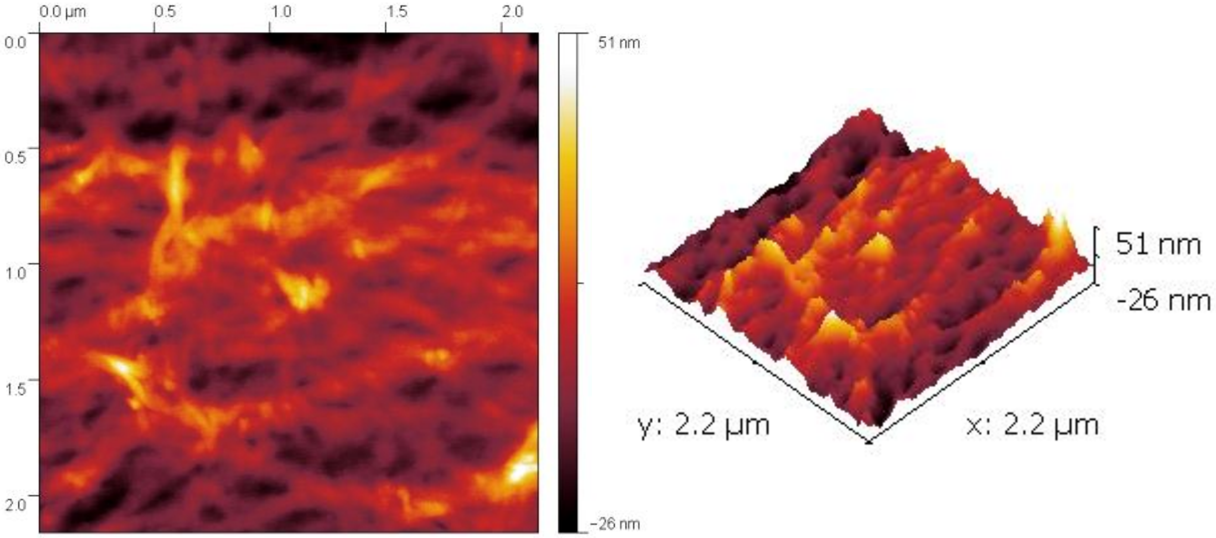

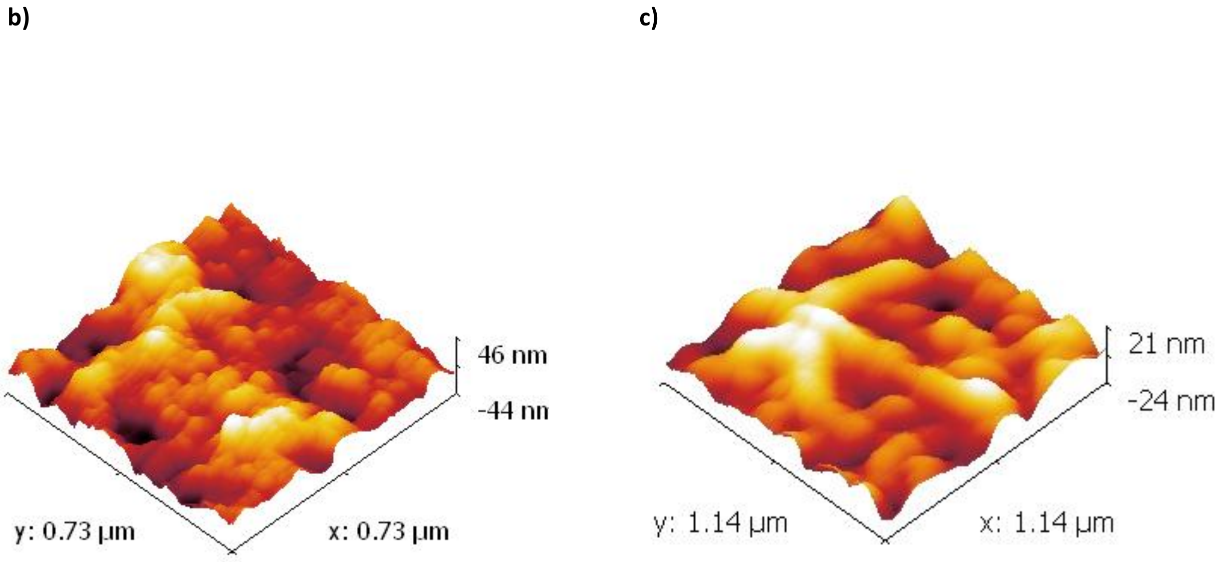

Figure 4.12 *AFM images of* ***a)*** *arc discharge SWNTs on glass,* ***b)*** *spin-coated PEDOT:PSS on SWNTs on glass, and* ***c)*** *electropolymerised PEDOT on CNTs on glass. Root mean square roughness for these surfaces:* ***a)*** *8.5 nm* ***b)*** *6.2 nm* ***c)*** *8.5 nm*

The fibrous film formed by the SWNTs is quite apparent in the image in figure 4.12 (a), and its relatively elevated surface roughness is indication of the need for smoothing by the polymer layer. The topography of a PEDOT:PSS film spin-coated at 6000 rpm shows how this is achieved to some extent by the small reduction in the rms roughness. The electropolymerised film is visibly less homogeneous than the spin-coated one; it is likely that the growth of the film follows to some degree the topography of the CNT film. Regions where the nanotubes are aggregated or protruding into the electrolyte should offer lower resistance pathways and form nucleation sites for growth of the film, which then spreads out over the rest of the electrode. Moreover, as a more crystalline polymer it will naturally grow faster in less stable crystal directions, where as the amorphous spin-coated material will evenly distribute itself. The increase in roughness is nevertheless relatively minimal compared to the advantage gained in conductivity.

Plastic substrates

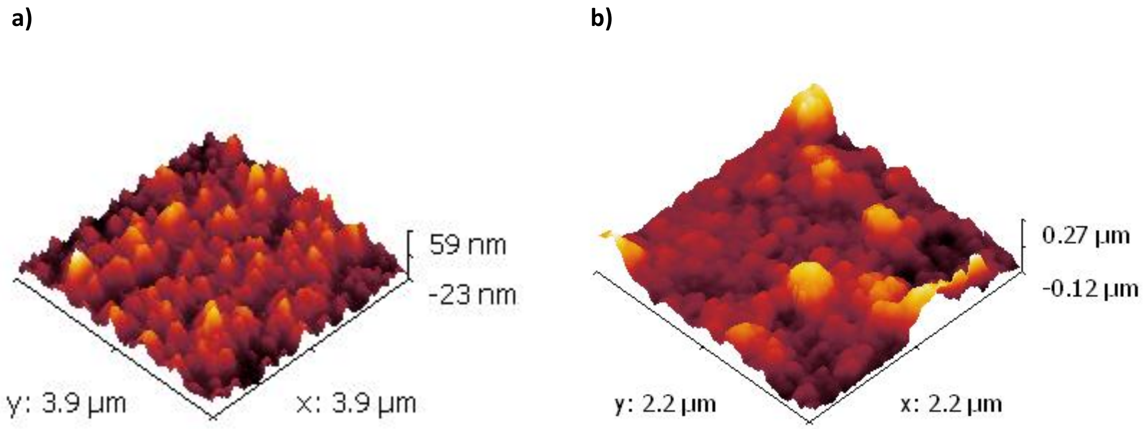

Figure 4.13 ***a)*** *Laser transparency plastic: rms roughness =8 nm* ***b)*** *Electropolymerised PEDOT on SWNTs on polyacrylate: rms roughness =25 nm*

The polyacrylate plastic film possesses an inherent roughness which is already quite considerable relative to glass. This clearly has a knock-on effect on the subsequent layers of nanotubes and polymer; with the final electrode showing very high roughnesses around 25 nm. This is an indication that, although cheap and readily available, this material is not entirely well suited to device purposes.

PET and PDMS stamping

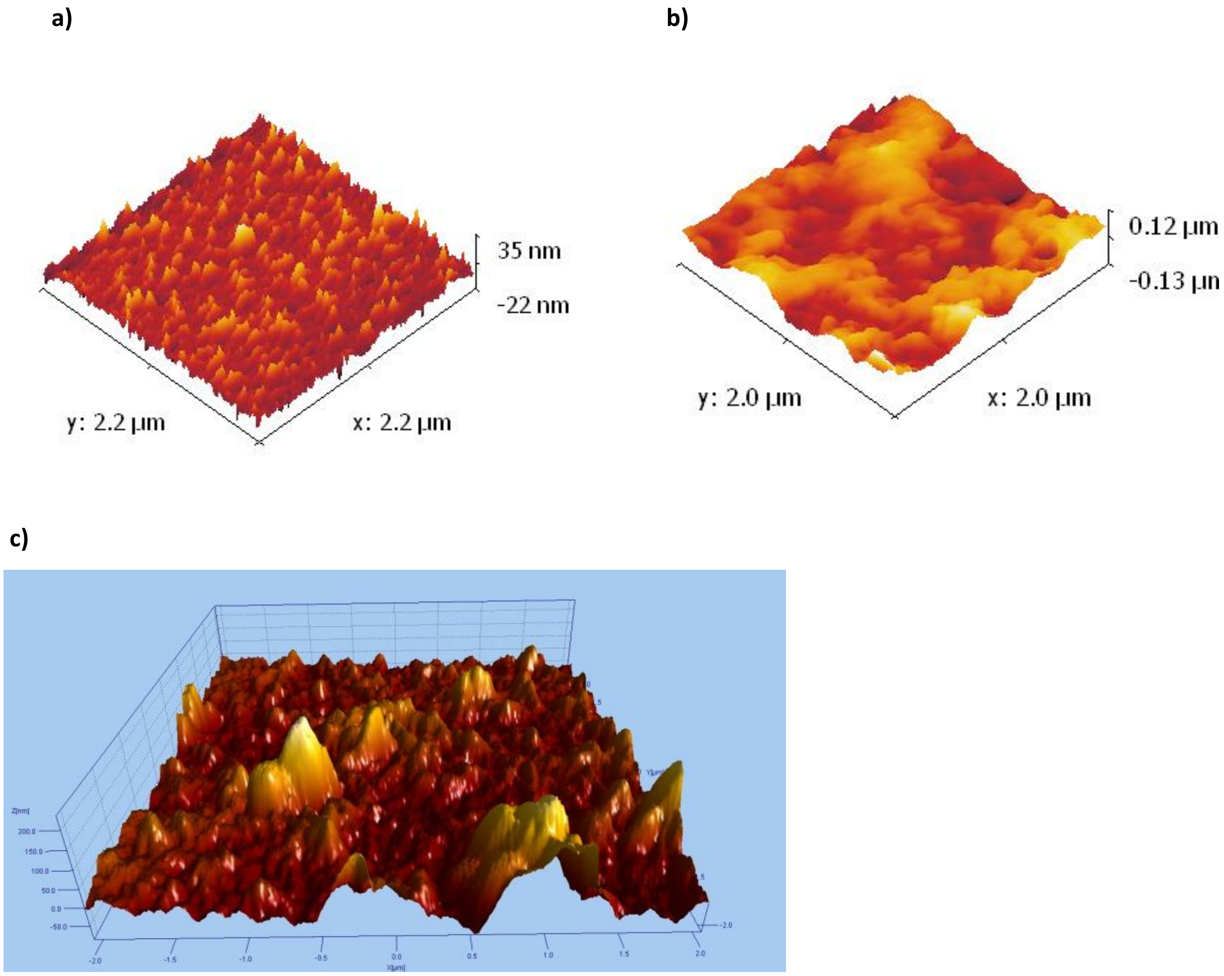

Figure 4.14 ***a)*** *SWNTs on polyethylene terephthalate (rms roughness=3 nm) and* ***b,c)*** *electropolymerised PEDOT on this surface (rms roughness= 18 nm)*

PET displays a remarkably smooth surface under the AFM tip; even with a nanotube layer the roughness is half that of the similar film on glass. It can be inferred that the substrate softness and improved interaction with the nanotubes allows them to become embedded in the surface to a certain extent. Upon electropolymerisation of the PEDOT layer, the roughness increases quite substantially, and several large agglomerations of the polymer can be seen in the topography of the film. The reason for this disproportionately large increase in roughness is likely linked to the different polymerisation conditions used for these samples. As the strips of nanotubes were dipped into electrolyte, and contacted from one end, a much less homogeneous growth pattern develops over the course of the polymerisation. Polymer visibly grows quicker at the exposed film boundaries, furthest from the electrical contact. Achieving total coverage of the nanotubes requires continuing the polymerisation for some time and therefore necessitates an excess of polymer in some regions of the film. Moreover, the growth of the film likely follows a much less layer-by-layer mechanism than the previously described films. The PEDOT will rather grow up along the film edges and then outwards from these more conductive regions, instead of depositing evenly along the CNT strip. Essentially, the growth mechanism is more disordered for this kind of cell geometry, and an excess of PEDOT is deposited, both of which lead to a relatively rough topography.

4.2.5 In-situ conductivity measurements

To investigate the effect of doping levels on the conductivity of PEDOT and the nanotubes in the electrodes, in-situ conductivity measurements were taken at a range of doping conditions [6,7]. Parallel strip gold electrodes were evaporated onto CNT films on glass, and PEDOT-CNT films on glass, and contacted to two separate working electrodes of the potentiostat. This electrode was dipped in the electrolyte solution where doping of the film was in turn controlled by the Ag/Ag^+ reference and Pt counter electrode. Conductivity measurements were then taken by applying a constant doping potential to one working electrode and the same voltage +10 mV to the second working electrode. In this manner, after the doping or de-doping of the film has reached completion, the current passing through the electrodes should correspond solely to the current passing through film between the two electrodes. In practice, at some potentials, particularly those below zero, there is other electrochemistry occurring at the electrodes which proved difficult to eliminate and interfered with the conductivity readings somewhat.

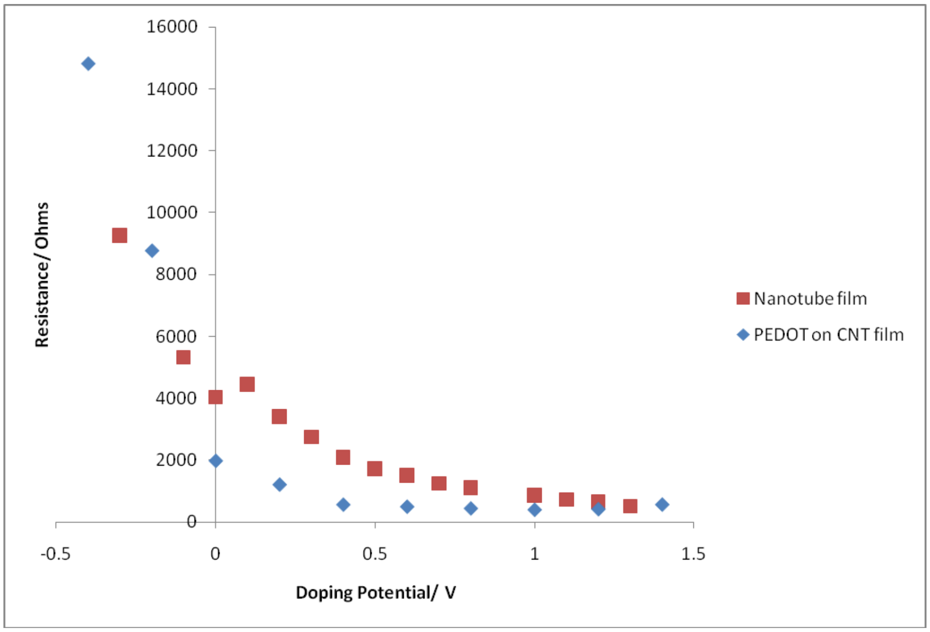

Figure 4.15 *In-situ conductivity for CNT film and PEDOT on CNT film*

The oxidative doping of both the nanotubes and the polymer can clearly be seen from figure 4.15, in which the resistance across the electrode gap markedly decreases as the doping potential is made increasingly positive. The resistance of both electrodes starts to level off after a certain degree of doping is reached. For the simple CNT film, this levelling-off should be linked to the electronic band structure of the semi-conducting nanotubes in the film (Kazoui et al [8]). The oxidative doping corresponds to removal of electrons from the valence band of these nanotubes, and the impact of this process on the conductivity will be related to the density of states at the doping potential applied. Thus, the slowing of the increase in conductivity at higher potentials is linked to a vanHove singularity in the semi-conducting band structure, which once being depleted of electrons, further removal of electrons will require relatively greater jumps in doping potential.

The polymer coated electrode shows a more distinct plateau in conductivity. This is typical of doping conductive polymers and corresponds to saturation in the material of the charge-carrying bipolaron units. Past a certain concentration of bipolarons it becomes more difficult to remove electrons from the material and the concentrated radicals can start to undergo reactions with each other [9].

These results emphasise the need to maintain a high doping potential after the deposition of the polymer film in order to obtain the maximum performance from the electrode.

4.2.6 Spectroelectrochemistry

To qualify the suitability of PEDOT on CNT electrodes for electrochromic applications, some electrodes were made for spectroelectrochemical measurements. Figure 4.16 shows the change in absorption of the polymer-CNT electrodes as the applied doping potential is varied. At -1.2 V the polymer is fully dedoped and a strong absorption band between 400 and 770 nm is clear, corresponding to a visible dark blue colour in the film. The 770 nm edge of this band corresponds to the band gap of the undoped polymer (1.6 eV); lower energy transitions than these are not available to the molecule. As the doping potential is made more positive, polarons and their bipolarons are created which introduces new energy states within the band gap of the undoped molecule. The absorption therefore shifts to lower energies as the transitions occurring take place between these doped, mid-gap states.

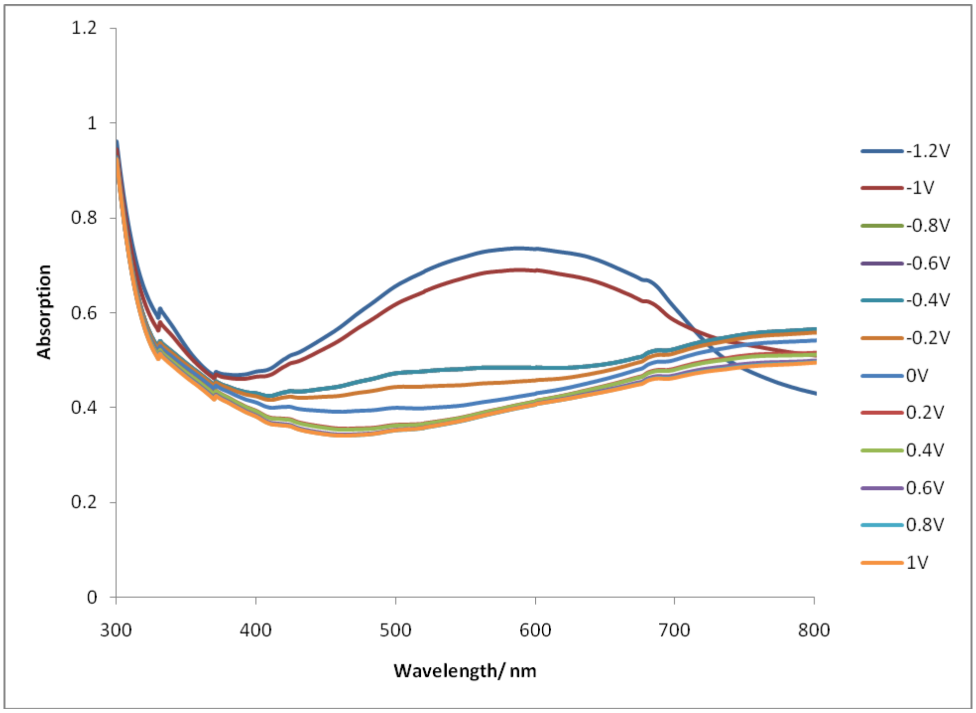

Figure 4.16 *The change in the absorption spectrum of a CNT-PEDOT film at doping potentials from -1.2 to 0.8V against a silver wire quasi-reference electrode.*

4.2.7 OLEDs

Organic light emitting diodes were assembled by both spin-coating and evaporation of a luminescent organic layer. A metal contact to the nanotube anode is first made by evaporation of a narrow strip of palladium across one end of the film. P3 films on circular glass substrates were used for spin-coated devices. A luminescent polymer blend (see experimental) was spin-coated over the whole substrate. This essentially consists of n-type and p-type emitting materials, as well as the phosphorescent dye $Ir(ppy)_3$, which increases efficiency by allowing phosphorescent transitions (normally spin-forbidden). This was followed by the evaporation of the electron-injection layer (LiF) and cathode (Al) over a region on top of the nanotube film. The polymer layer is removed from a portion of the palladium contact, in order to make contact with the anode. The performance of the device can then be tested by applying voltage sweeps across the two electrodes and measuring the current response and emitted light. Of two devices assembled in this fashion, one emitted a very faint light. The failed device was shorted, probably due to a region of aggregated nanotubes puncturing through the polymer layer to the cathode.

Evaporated devices used the widely used small molecule blend of the electron accepting tris(8-hydroxyquinolinato)aluminium (Alq_3) and electron donating N,N'-diphenyl-N,N'-bis(1-naphthyl)-(1,1'-biphenyl)-4,4'-diamine (NPB). The anode contact, LiF and Al layers are evaporated in the same manner described above. Unsurprisingly, these devices were slightly more successful than spin-coated ones; for which surface inhomogeneity is exacerbated in the spin-coated film. One of the two devices made emitted clearly visible light.

CNT electrodes patterned on to PET were aimed at creating devices with appropriate geometry for determination of emitted light intensity and efficiency. The PEDOT coated electrodes made on PET proved to be too rough to assemble a working device. The extent of the effect of the roughness on subsequent layers can be seen from the evaporated palladium contact, which is not even reflective on the PEDOT covered region (figure 4.17).

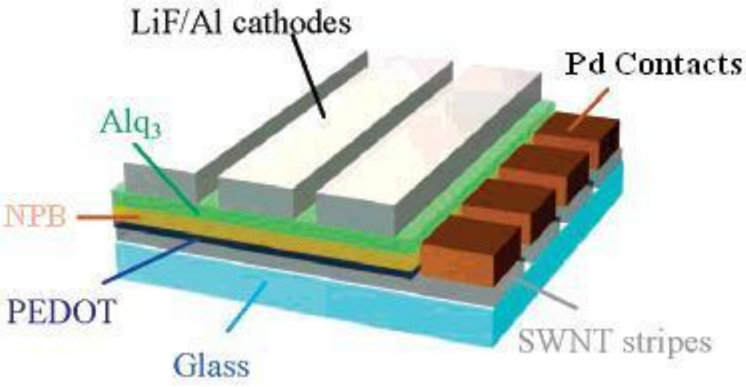

Figure 4.17 *Structure of evaporated organic devices [2]*

4.2.8 Spectroelectrochemistry in the Infra-red

Transparent carbon nanotube electrodes are transparent throughout much of the infra-red region of the spectrum as well as the visible, and thus offer a singular conductive substrate for IR studies on polymers and small molecules. Steckler et al. [10] demonstrated this by using CNT electrodes to electrodeposit low band-gap polymers and then investigating their absorption edge in the NIR. We propose using transparent CNT electrodes in electrochromic studies in which the change of a polymer's absorption spectrum with doping potential is observed into IR frequencies. This is particularly useful for low band-gap, highly conjugated molecules which exhibit electronic transitions in this part of the spectrum. The obvious alternative transparent electrode, ITO films on glass, can't be used in this manner because of the absorption of longer wavelengths. Typically, spectroscopy with such electrodes is rendered impossible much beyond 2000 nm [11].

For this purpose, CNT films had to be made on an IR transparent substrate such as KBr. The films were transferred to polished KBr windows as described above, via dissolution of the membrane in acetone. These nanotube films on KBr showed sheet resistances of around 1.3 kΩ (thin CNT films were used). Two CNT coated windows, to act as working and counter electrode were placed parallel to each other, and separated by a rubber seal to form a 1.5 mm thick electrochemical cell. A silver wire was introduced between them to act as a quasi-reference electrode.

As a preliminary study, spectra were taken of electrolyte solutions using this apparatus, to demonstrate the availability of a transmission window in the IR. The absorption of a solution of $TBAPF_6$ in dichloromethane (DCM) is shown in figure 4.18. Between the intense solvent absorption peaks at 3000 and 1500 cm^{-1} there is a transmission window containing small peaks from the electrolyte salt, which can easily be subtracted.

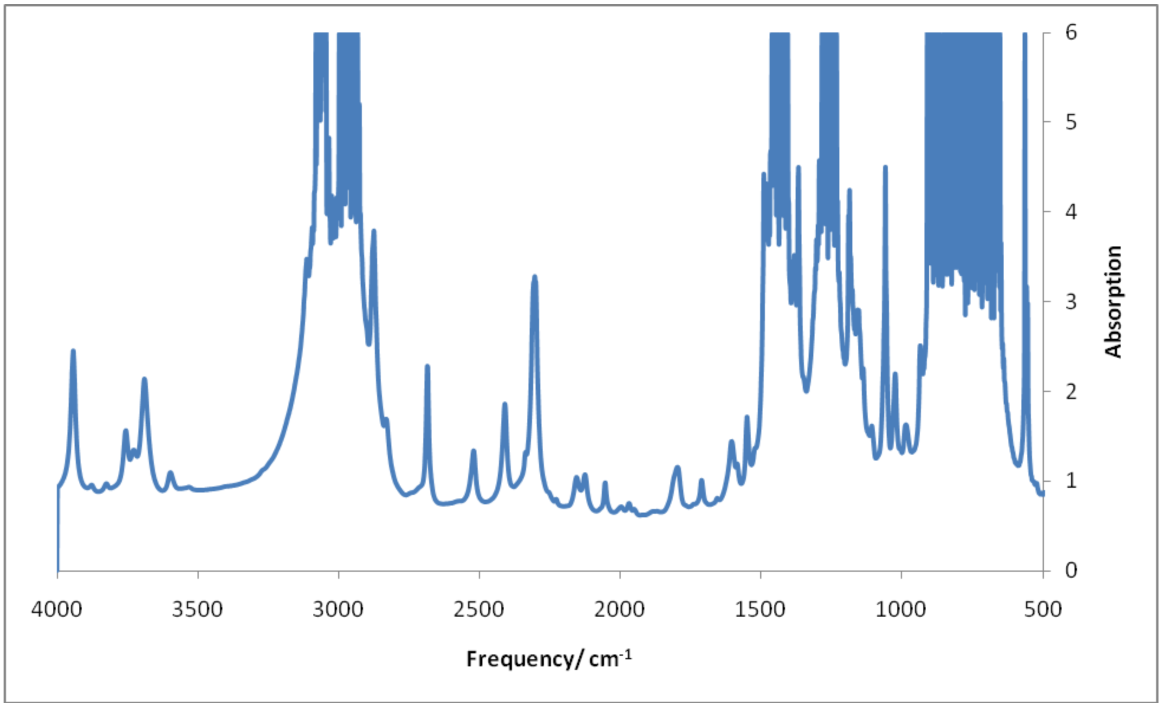

Figure 4.18 *FT-IR spectrum of an electrochemical cell based on CNT coated KBr windows, containing 0.5M* $TBAPF_6$ *in DCM.*

It would be desirable to widen the transmission window available by a judicious choice of solvent and electrolyte. Propylene carbonate and acetonitrile were also looked at as alternative solvents, but show more absorption in the region of interest. These solvents were chosen with a view to permitting subsequent electropolymerisation, or not solublising monomer films, whilst not having a detrimental effect on the rubber seal. Using a different sealant material could permit the use of less IR absorbing solvents such as CCl_4, depending on the analyte in question.

This cell was then successfully used to electrochemically deposit a PEDOT film on the CNT working electrode.

4.3 Conclusions

Transparent electrodes for device applications were made by the electrochemical deposition of PEDOT on thin SWNT films on several substrates. Appropriate conditions have been demonstrated for attaining homogeneous and complete thin PEDOT films which are suitable for electrodes in devices such as OLEDs and organic photovoltaic. Two regimes of polymer-CNT electrode are possible: one in which a very thin CNT film is used merely to grow what is essentially a conducting polymer electrode, and one in which the a thin PEDOT hole-injection layer is electrochemically grown onto a highly conductive CNT film. Whilst electrodes using very thin CNT films were found to be too resistive for device applications, electrochemically grown thin PEDOT layers exhibited sheet resistances up to 100 Ω/sq. lower than equivalent thickness spin-coated PEDOT:PSS films. The roughness of the PEDOT films on glass is comparable to that of spin-coated films, and functioning OLEDs were demonstrated using these electrodes. However, films grown on polyacrylate and PET were even lower resistance, but high roughness made them entirely unsuitable for device fabrication. Attempts should be made to improve the PEDOT deposition on these flexible substrates.

These electrodes present themselves as a useful tool for the study of the spectroelectrochemistry of various molecules in the IR. To this end, conductive, transparent films were made on KBr windows and used in the assembly of a working electrochemical cell with a transmission window in the IR. Future work should pursue this avenue to further the study of PEDOT and other low band-gap polymers in this region of the spectrum.

4.4 Experimental

4.4.1 CNT purification

HipCO SWNTs were purchased from Carbon Nanotechnologies Incorporated, and arc discharge SWNTs from Carbon Solutions. For air purification, 10 mg of HipCO SWNTs were heated to 100 degrees while air was passed through the vessel. Purification in nitric acid was carried out on 5 mg of SWNTs in 10 ml of 10 percent nitric acid, refluxed for three hours. Raman spectroscopy of starting materials and purification products was conducted with a Hololab 5000 Raman microscope (Kaiser optical systems), with a laser wavelength of 785 nm.

4.4.2 CNT dispersions and films

SWNT dispersions in water were made with 0.1 wt% SWNTs and 1% SDS, sonicated with a vibra-cell ultrasonic probe from Sonics, and centrifuged at 20000 rpm for half an hour with an Avanti J-E centrifuge (Beckman Coulter). UV-visible spectroscopy of solutions was performed with a Jasco V-670 spectrophotometer using 1% SDS solutions in water as a reference.

Filtration of SWNT dispersions into nanotube films was done under vacuum through mixed ester cellulose membranes (0.1 or 0.22 um pore size) from Millipore. The resulting nanotube film on the membrane was immersed in chlorobenzene for one minute, before placing on a glass coverslip. The coverslip and nanotube film was then placed in a large acetone bath for three to four hours. Upon removal from the bath, the films are rinsed in acetone and isopropyl alcohol, dried in nitrogen and then heated on a hot-plate at 300 degrees for several hours. The films are then placed in concentrated nitric acid for 3-5 hours.

Polyacrylate copolymer laser printing transparencies (PP2950) were purchased from 3M and PET sheets were purchased from Padtech. Transfer of nanotube films to these substrates was conducted as for glass, except without heating and acid treatment. PDMS stamps were also used to transfer nanotube films to PET. Moulds for the stamps were made in photoresist on a silicon wafer substrate.

Sheet resistance measurements of nanotube films were taken with a Lucas Labs 302 four-point probe. Optical absorbance of films was measured with the Jasco spectrophotometer, using a clean glass coverslip as a reference.

4.4.3 Electropolymerisation

Electropolymerisation of PEDOT onto nanotube films was performed in a tailor-made three probe electrochemical cell. The electrolyte consisted of 0.1M $TBAPF_6$ in dry propylene carbonate, with roughly 0.01M EDOT. Before use the electrolyte salt is dried in an oven at 200 degrees for 15 minutes, and then cooled under argon. After adding the dry PC, argon is bubbled through the solution for ten minutes. A platinum disc was used as the counter electrode, Ag/Ag^+ aqueous reference electrode, and the SWNT film acts as the working electrode. These were connected to a CH Instruments electrochemical workstation. Polymerisation was performed both by CV scans between -0.5 and 1.2 V and by a potentiostatic deposition at 1.1 V . The number of scans or time held at the polymerisation voltage was dictated by the deposition rate, indicated by the growth in polymer doping signal or the total deposited charge, as well as by eye. An inert atmosphere is maintained throughout the polymerisation process. The finished films were removed and washed in isopropyl alcohol and dried in nitrogen. Sheet resistance and absorbance of these films was measured as for SWNT films.

Atomic force microscopy of all samples was carried out on a DI AFM, or a Nanoink AFM (for larger samples on PET). Scanning electron microscopy was performed on a Hitachi S4700 FE-SEM.

4.4.4 OLEDs

Organic LEDs were made both by spin-coating and evaporation (UQ Physique 0335 evaporator) of the active organic layer. Metal contact to the CNT-PEDOT electrode was made by evaporating a thin strip of palladium. Spin-coated devices used a polymer blend consisting of: polyvinylcarbazole (PVK) (0.32 wt %), 2-(4-biphenylyl)-5-(4-*tert*-butylphenyl)-1,3,4 oxadiazole (PBD) (0.32 wt %), tris(2-phenyl-pyridinato) iridium [Ir(ppy)$_3$] (0.03 wt %), and *N*,*N*'-diphenyl-*N*,*N*'-bis(3-methylphenyl)-1,1'-biphenyl-4 ,4'-diamine (TPD) (0.10 wt %) into a mixed solvent of 1,2-dichloroethane and chloroform. On top of this layer, a LiF electron-injection layer is evaporated over a small (2x2 mm) area of the device, followed by an aluminium cathode.

Evaporated devices were made following a similar protocol, except the active organic layer was deposited by evaporation of a thin film of Alq$_3$ and NPB.

4.4.5 In-situ conductivity

Electrodes for in-situ conductivity measurements had parallel gold strips 2 mm wide and 2 mm apart evaporated on to them with an Edwards Auto 306 evaporator. These gold strips were contacted to two separate working electrodes of the potentiostat, and the electrode was placed in a standard electrochemical cell (0.1M TBAPF$_6$ in PC), with a Pt coil counter electrode and Ag/Ag$^+$ reference.

4.4.6 Spectroelectrochemistry

For spectroelectrochemistry measurements, long CNT films (30 x 5 mm) were transferred to a piece of glass microscope slide. Contact to this film by the working electrode of the potentiostat was made via a coating of silver paste over on end of the slide. The electrode was placed in a glass cuvette with a Pt wire as counter and silver wire as reference. The Pt wire was cleaned in a flame and the silver wire with sandpaper and in concentrated HCl. The cuvette was filled with standard electrolyte solution (0.1M TBAPF$_6$ in PC). For a reference cuvette, a similar glass slide, without nanotubes was placed in a cuvette filled with the electrolyte solution. The SWNT and polymer working electrode was held at a series of potentials while the absorbance spectra were recorded.

For spectroelectrochemical measurements in the infra-red, CNT films were transferred to KBr windows as described above, via acetone dissolution of the membrane. An IR transmission cell was made from two parallel CNT coated windows, which constitute the working and counter electrodes. Electrolyte and the polymer under study are introduced into the sealed space between them, with a silver wire to act as a reference electrode. FT-

IR spectra were taken with a Nicolet 6700 FT-IR spectrophotometer (Thermo), whilst doping potentials were applied to the electrodes with the potentiostat.

References

[1] G. Tobias, L. Shao, C. G. Salzmann et al., *J. Phys. Chem. B* **110** 2006 22318
[2] D. Zhang, K. Ryu, X. Liu et al., *Nano Lett*. **6** 2006 1880
[3] M. E. Itkis, D. E. Perea, S. Niyogi et al., *Nano Lett.* **3** 3 2003 309
[4] Y. Zhou, L Hu and G. Gruner, *Appl. Phys. Lett.* **88** 2006 123109
[5] Figure courtesy of Y-M Chien
[6] G. Schiavon, S. Sitran and G. Zotti, *Synth. Met.*, **32** 1989 209
[7] M. Morvant and J. Reynolds, *Synth. Met.*, **92** 1998 57
[8] S. Kazaoui, N. Minami, N. Matsuda et al., *Appl. Phys. Lett.* **78** 22
[9] W. Domagala, B. Pilawa and M. Lapkowski, *Electrochim. Acta* **53** 2008 4580
[10] T. Steckler, K. Abboud, M. Craps, A Rinzler et al., *Chem. Commun*. **46** 2007 4904
[11] M. Nikolou, A.L. Dyer, R. Steckler, E.P. Donague et al., *Chem. Mater*. **21** 22 2009 5539

5. COVALENTLY BOUND SWNT MONOLAYERS ON SILICON

5.1 Introduction

The successful integration of SWNTs with silicon chips is an important step in their development as components in future nanoelectronics. Common methods such as casting nanotube dispersions over silicon substrates and then patterning contacts do not necessarily create well defined contacts to the nanotubes, and the process is random and inefficient. Exploiting the chemistry of SWNTs to form covalent bonds between them and a silicon surface would create useful oppurtunities for the mass-fabrication of organised SWNTs arrays in direct electrical communication with the substrate. Some work has been done towards the fabrication of self-assembling monolayers (SAM) of SWNTs on silicon and other substrates in order to create vertically aligned nanotube arrays [1,2,3]. The spontaneous self-assembly of electronic components into organised structures is one potentially huge advantage that the use of molecular devices can bring to electronics; avoiding complicated and costly patterning procedures. Vertical arrays of SWNTs on gold and silicon have already shown to be effective as electrochemical probes and current rectifiers [2,3].

Work in this group demonstrated how the attachment of SWNTs to a gold surface via a thiol SAM has the added advantage of allowing chemical functionalisation of just one end of the nanotubes; that which remains unattached to the substrate. This opportunity to manipulate the electronic nature of the two ends of a nanotube allows the formation of diode-like SWNTs which exhibit current rectification.

a) **b)**

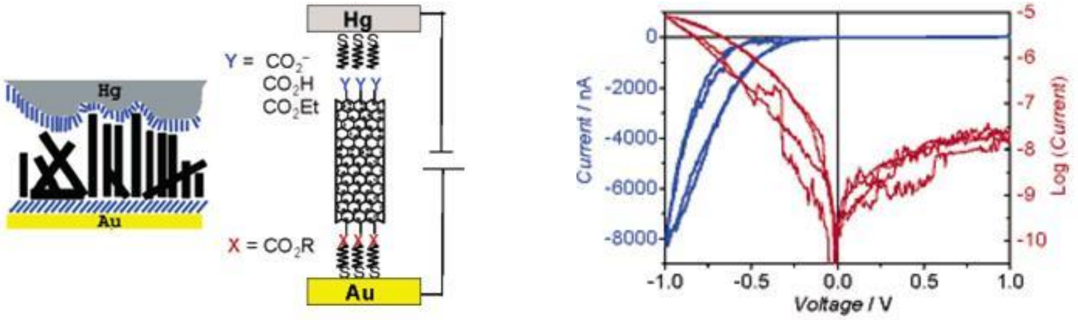

Figure 5.1 ***a)*** *Vertical array of SWNTs covalently attached to a gold thiol SAM; a mercury drop electrode with a similar thiol layer is used to take electrical measurements across the SWNT monolayer;* ***b)*** *only with asymmetric functionalisation of the ends is current rectification observed [3]*

Nevertheless, whilst this kind of chemistry is relatively easy at the gold surface, through readily formed thiol SAMs, the transposing of such SWNTs architectures to silicon substrates is less straight-forward. The benefits of reproducing these devices onto silicon are not only the added relevancy to current electronics, but also the relative stability of the surface which should allow easier testing of more diverse structures. The mercury drop electrode used for characterisation of these nanotube monolayers is notoriously difficult to manipulate with a gold substrate, with which it easily forms alloys.

Some work has been performed on the covalent attachment of SWNTs to silicon oxide surfaces, through thioester chemistry [2]. Bonding to a hydride terminated silicon substrate is more appealing for electronic applications due to its semi-conducting nature. Whilst chemistry at this surface is more challenging, the formation of covalently bound alkyl monolayers was shown in 1995 by Linford et al., using a radical reaction of 1-alkenes [4,5]. The reaction requires thermal, chemical, or photochemical intiation for the homolytic cleavage of a Si-H bond. The resulting surface radical can attack a double bond, binding the carbon chain and leaving a new carbon radical which can abstract a surface hydrogen and thus propagate a chain-reaction of alkene binding [4].

This chemistry has opened up a huge range of further possibilities through the introduction of different functionalities to the alkyl chains [6]. Attachment of a SWNT monolayer to a hydroxyl or amine functionalised surface should be possible through straight-forward ester or amide coupling to the ubiquitous carboxyl groups at cut CNT

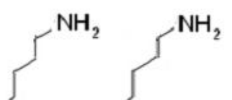

ends. Figure 5.2 shows one proposed route to attachment of an aligned SWNT monolayer to silicon hydride.

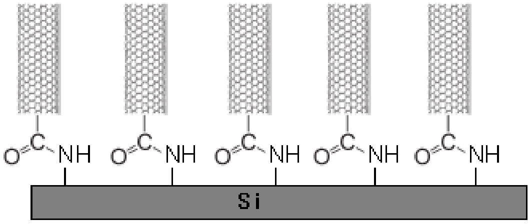

Figure 5.2 *Proposed Reaction scheme: Alkenes with a terminal amine or alcohol moiety can be coupled to a silicon hydride surface and then amide or ester coupled to oxidised SWNTs.*

5.2 Results and Discussion

5.2.1 Silicon oxide etching

An important first step towards performing chemistry at the silicon hydride surface is the removal of the silicon oxide layer present on all silicon wafers. The oxide is efficiently etched by hydrofluoric acid, but this fast process can leave ‘overetched’ surfaces, where the silicon itself is pitted and uneven. The microelectronics industry tends to use a milder, and less acidic etchant known as buffered-oxide etch which includes ammonium fluoride. The use of ammonium fluoride alone is also possible, and has been shown to create more even surfaces, although other factors such as the orientation of the silicon crystal and the level of doping are also significant [8,9]. This work looked at HF and NH_4F etching of both Si(100) and Si(111) crystals.

The progress and success of etching treatments were monitored by ellipsometry, contact angle measurements and AFM. The contact angle of water drops on the wafer surface is a rough but simple indicator of the success of the etching process- the hydrophilic oxide surface will give a lower contact angle (~24 degrees) compared to the hydrophobic hydrogen terminated surface (~70 degrees). Ellipsometry provides a means of measuring to a high degree of accuracy (to a fraction of an angstrom) the thickness of layered materials from the change in polarisation of reflected light, and is useful for monitoring the progress of the oxide etch. However, it requires an exact knowledge of the refractive indices of the substrate and the oxide layer in order to provide the desired level of accuracy in thickness. Silicon oxide has well known optical parameters, but the silicon itself can vary slightly according to the level of doping in the wafer. To determine the refractive indices, n and k, of the silicon wafers used, general silicon indices were used to monitor the change in a sample over different etching times (figure 5.3 b)). When the oxide thickness given stayed constant upon further etching, a hydrogen terminated surface was assumed and its indices measured with the ellipsometer. Indices of n= 3.83 and k= -0.14 were found for this Si(111). This also allowed determination of the etching rates and the time required for full etching. Prolonged etching of the wafers can also lead to overly rough surfaces. Furthermore, the etching is always carried out in strictly deoxygenated conditions, as oxygen will inevitably oxidise exposed silicon, thus leading to further roughening.

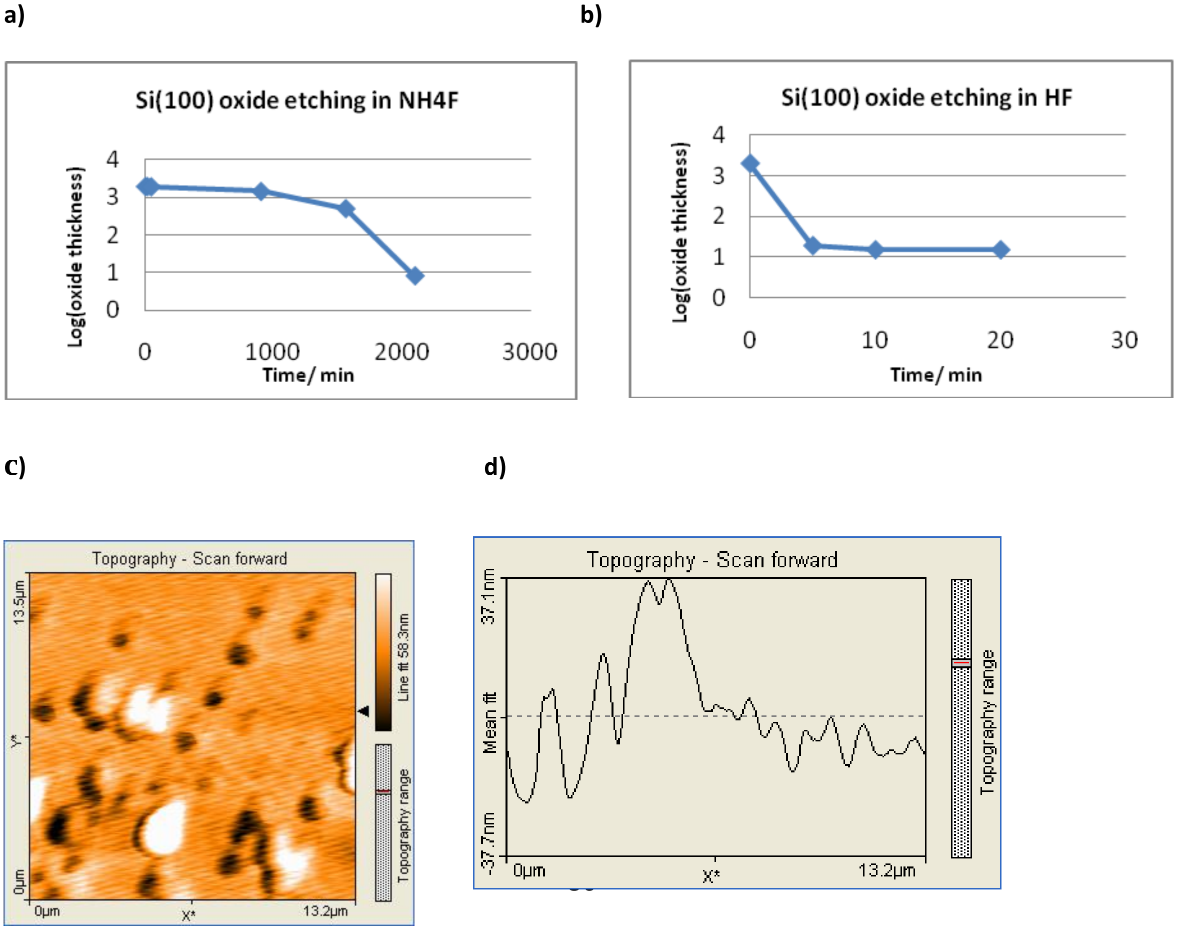

Figure 5.3 *Etching of Si(100):* ***(a) (b)****Etching rates in different etchants and* ***(c) (d)*** *the rough etched surface after etching in HF, rms roughness= 8.2nm*

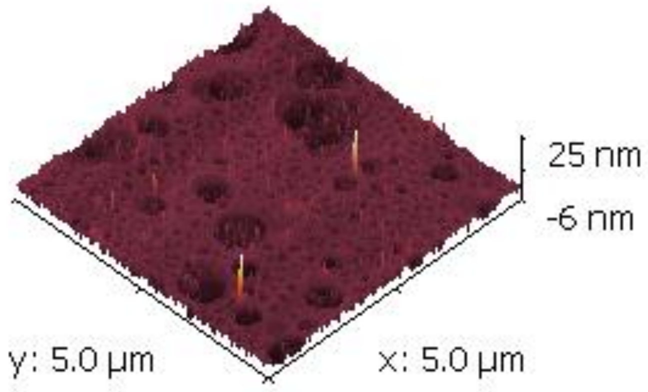

Figure 5.4 *A Si(111) surface after etching in 40%* NH_4F*, rms roughness= 0.9nm*

The Si(100) crystals used were for microelectronic applications so had a 2000 Angstrom thick layer of oxide which required removal. In 50 % HF this could be achieved quite rapidly (10-15 minutes), but left slightly rough surfaces with characteristic pyramid shaped etch marks. Milder etches in 40% ammonium fluoride were so much slower as to become unpractical, requiring over 24 hours to achieve what appeared to be a fully etched surface, although the etch rate appears to increase steadily over time. A switch of substrates to Si(111) was aimed towards using a wafer tailor-made to the requirements of the subsequent investigations. Si(111) is known to etch in a much more anisotropic manner than Si(100), in the crystal direction, giving generally more atomically flat silicon surfaces [10]. These wafers had only a thin layer of oxide, always present in ambient conditions, and were degeneratively n doped to a high conductivity. Studies of alkyl monolayers on silicon by Cahen et al. have shown that p doped substrates can interfere with electronic measurements on the monolayer by themselves creating a Schottky barrier between the substrate and the organic layer which causes current rectification [11]. This would confuse attempts to determine the electronic behaviour of the SWNT monolayers.

The thin oxide layer on Si(111) could be completely removed in NH_4F in five to ten minutes. AFM imaging of the resulting surface shows them to be not completely flat, with circular pits, and a roughness of 0.9 nm (figure 6.4).

5.2.2 Alkyl monolayers on silicon hydride

Before attempting the attachment of a hydroxyl functionalised 1-alkene to the silicon surface, trials on simple alkenes of two different lengths were carried out. The surface coupling reaction was run with 1-dodecene and the twenty-two carbon alkene 1-docosene. The alkenes are deoxygenated by freeze-pump-thaw cycles with nitrogen, before addition of the etched silicon directly from the etching solution. The reaction vessel is kept under inert atmosphere and heated to 200 ºC for 4 hours. After reaction the wafers are removed and rinsed repeatedly in toluene and DCM. The success of the reaction was again monitored by ellipsometry and contact angle measurements. The ellipsometry measurements were extremely sensitive to unwanted organic material which can easily adsorb to the organic functionalised surface, so a strict washing protocol was developed to reveal the actual molecular monolayer for measuring. Successful measurements showed appropriate thicknesses for monolayers of both alkenes as shown in table 6.1. The tilt angle of the molecules within the monolayer, relative to the surface normal, can be inferred from this data (~30º). The contact angle of water drops on the functionalised surface was expected to increase significantly compared to the etched surface, as the hydrophobic alkyl chains are introduced. This was observed to some extent for both alkenes, particularly for the longer chain molecule. AFM imaging of the resulting surfaces was problematic, likely due to quick contamination by organic material. The surfaces displayed unexpectedly high roughness in the images taken.

Monolayer	Ellipsommetry thickness/ A	Contact angle/ degrees

Si-$C_{12}H_{25}$	10±2	98º±1
Si-$C_{22}H_{45}$	23±3	105º±1
Si-$C_{11}H_{22}OH$	10±2	78º±1

Table 5.1 *Characterisation of various alkyl chain monolayers on silicon hydride*

5.2.3 Coupling of SWNTs to silicon

Functionalisation with hydroxyl alkene

For linking CNTs to the silicon surface, ω-undecenyl alcohol was used a means of providing hydroxyl groups at the surface. The coupling of a hydroxyl functionalised alkene to the hydride terminated service proved to be more challenging than the reaction with basic alkenes. Using similar conditions to those described above (200 ºC) persistently yielded much thicker organic films than appropriate for a monolayer. The reaction of the alkene with the surface proceeds via a radical mechanism, and therefore it is likely that a number of unwanted longer chains can be formed. Moreover, in the presence of base, the alcohol moiety could attack the alkene and form polyether chains. It is probably owing to the suppression of this reaction that carrying out the reaction at lower temperatures was more successful for monolayer formation . Heating to 80 ºC for 24 hours yielded surfaces with an organic layer thickness of around 10 angstroms. The contact angle of water drops on these surfaces showed them to be less hydrophobic than those functionalised with simple alkenes, as would be expected for a hydroxyl functionalised surface.

Cutting CNTs

The formation of a well ordered vertical monolayer of carbon nanotubes is favoured by nanotubes which are short as possible whilst still retaining their electronic properties. Short tubes which are closely bound together at the surface are more likely to pack together vertically due to the steric interaction between them, than long nanotubes which will be less rigid and tend to form a disordered ‘spaghetti-like’ layer. Cutting of nanotubes is generally achieved by the same kind of aggressive oxidations which are used to purify them; making use of strong acids, sonication and sometimes adsorbed metal particles which can catalyse cutting at particular points [12,13]. For the coupling of nanotubes to the hydroxyl functionalised silicon surface, two different types of nanotubes were looked at. The first were HipCO SWNTs sonicated for 24 hours in a hydrogen peroxide and concentrated sulphuric acid solution (1:3) (piranha solution), the second was the arc discharge P3 SWNTs, merely sonicated in the reaction solvent, DMF, for several hours. P3 nanotubes are already highly functionalised, so oxidation of the tube ends for the subsequent reaction should not be necessary- the sonication serving only to cut the tubes. Figure 5.7 shows SEM images of the shortened HipCO tubes cast in a dilute solution over silicon. Most of the tubes visible in the images are much less than a micrometre long, which is considerably shorter than the as-purchased tubes.

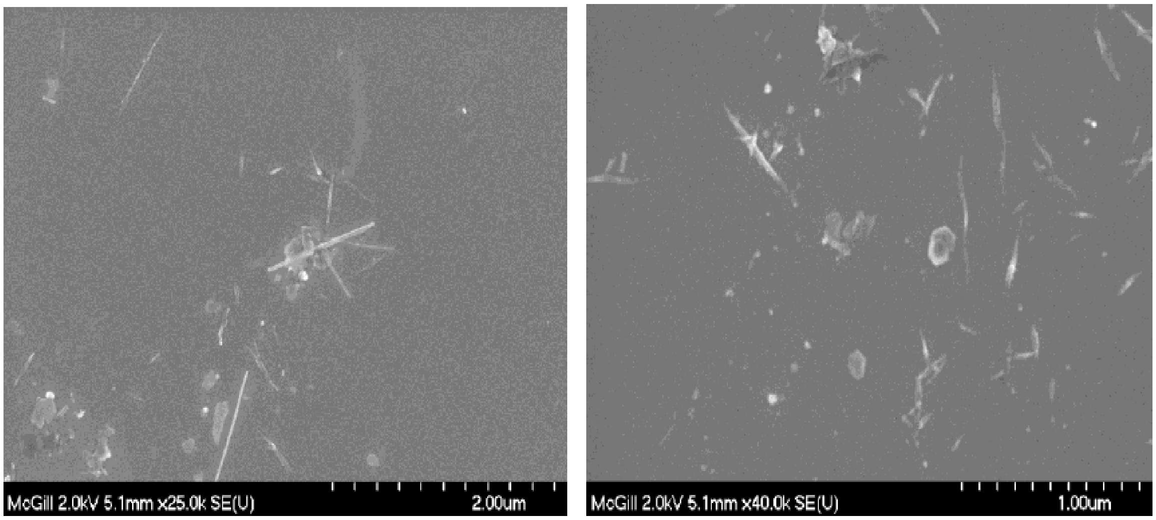

Figure 5.7 *SEM images of HipCO SWNTs shortened via sonication in piranha solution for 24hrs*.

DCC coupling

The solid-state DCC coupling was carried out in DMF, as for the similar reaction on gold substrates [3], due to the favourable CNT solubilising properties of this solvent. Cut HipCO nanotubes, kept as a water dispersion, were filtered, oven dried, and the redispersed in DMF by sonication. The P3 nanotubes were dispersed directly in DMF. These nanotube dispersions were stirred for 2 hours with DCC in a dry flask under inert atmosphere, before the addition of the functionalised silicon wafer and the DMAP catalyst. The vessel was then heated to 80 ºC for two hours. After completion of the reaction the wafer was removed and washed in copious IPA, toluene, and sonicated in IPA for several minutes to ensure the removal of non-covalently bound adsorbates. The wafers were analysed by AFM and SEM.

a)

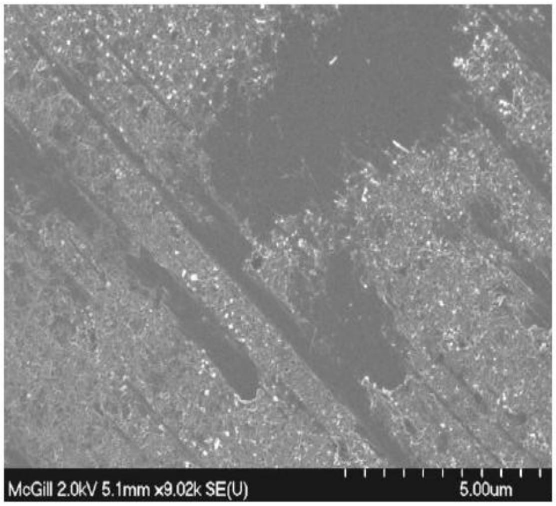

b)

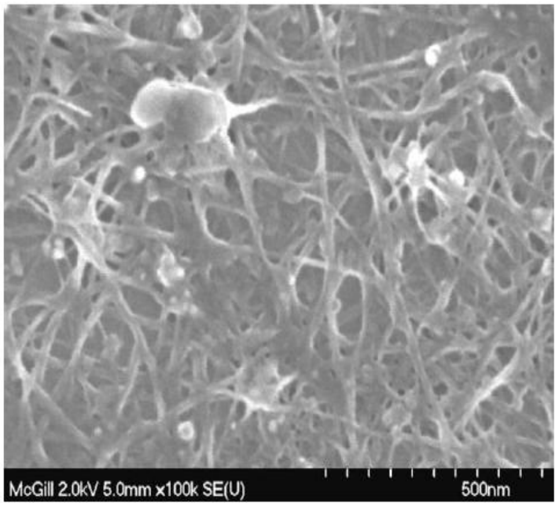

c)

d)

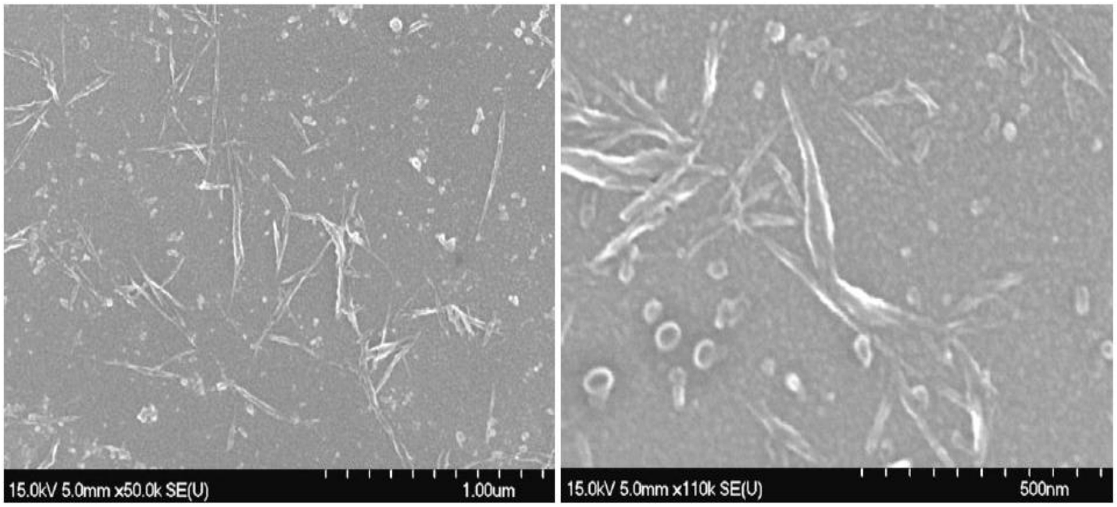

Figure 5.8 *Scanning electron microscopy of CNTs coupled to Si(111):* ***(a)(b)****P3 nanotubes cut via intense sonication, and* ***(c)(d)*** *HipCO nanotubes cut via sonication in piranha solution.*

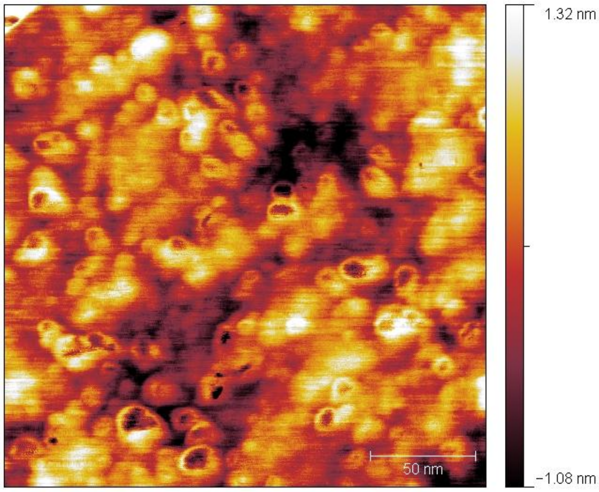

Figure 5.9 *AFM of the Si-CNT surface: a region without flat-lying nanotube bundles.*

Figure 5.8 shows SEM images of the two types of nanotube attached to the silicon surface. The arc-discharge nanotubes are clearly much longer than the piranha-cut HipCO nanotubes, and form a tangled network over portions of the surface. Most of the surface is covered, but the covered regions resemble straight parallel ribbons, presumably corresponding to a crystal direction of the Si(111) surface. The tubular structures visible in the cut HipCO functionalised surfaces are mostly too large to be individual SWNTs, and they are more likely bundles of several nanotubes. Both samples appear to contain a considerable amount of non-nanotube impurities, and the nanotubes themselves appear quite damaged. The HipCO nanotubes have probably not been purified effectively enough before or during the cutting process, and the arc-discharge nanotubes may have been damaged during sonication.

It is worth noting that it would be difficult to detect a true vertically aligned array of SWNTs looking down on to the surface with an SEM. It is possible that the bundles and portions of nanotubes visible in the images are resting on top of an array or sticking up out of one. Indeed, the background of the images has a spotted appearance which could correspond to packed SWNTs. The nature of these apparently flatter regions was further elucidated by AFM (figure 5.9). With a rms roughness of 0.5 nm, these images discount the possibility of a vertically aligned nanotube layer which would be at least as rough as the polydispersity of SWNT length. The bright ring features seen in both types of microscopy are unusual and are probably associated with some impurity such as polyethers present from formation of the alcohol monolayer, or dust from molecular sieves (present in DMF).

5.3 Conclusions

The attachment of short single-walled nanotubes to a silicon hydride surface has been demonstrated, as a step towards the creation of vertically aligned and ordered arrays of SWNTs on silicon. The nanotubes are covalently bound to an Si(111) surface via an ester coupling to an alkyl monolayer with terminal hydroxyl moieties. Flat silicon hydride surfaces were achieved via etching in deoxygenated ammonium fluoride, and the functionalisation of this surface with hydroxyl terminated alkenes was shown for the first time. The resulting nanotube films appear disordered, unaligned and probably thicker than a monolayer, but are not removed by long periods of sonication. It is likely that many nanotubes are couple to the surface at points along their length, rather than their ends, which would result in those lying flat which are visible in SEM imaging. Further improvements to these monolayers should focus on cutting short sections of nanotubes of relatively regular size and achieving superior dispersions in the reaction solvent. A higher degree of purity in the films would also be desirable, and could be achieved by more rigorous purification of the CNT samples before attachment.

Electronic characterisation of these films should also be performed; to test whether they can exhibit the same current rectifying properties as similar aligned monolayers on gold.

5.4 Experimental

5.4.1 Silicon etching

Si(100) wafers were purchased from University wafer and Si(111) wafers from PCA silicon; both p-type and degeneratively doped ($<0.02\ \Omega\ \mathrm{cm}^{-1}$). All solvents and reagents are from Sigma-Aldrich except ammonium fluoride from Alfa Aesar.

Silicon wafers were cleaned in isopropanol and in a plasma cleaner (Harrick Plasma PDC 32G) before etching. 50% HF solution was deoxygenated by nitrogen bubbling and kept under nitrogen during the etching of the wafers. The silicon was then removed and washed in copious distilled water and isopropanol, and then dried in nitrogen. Ammonium fluoride etchant was prepared at 40% from the solid, and deoxygenated as for HF.

AFM of Si(100) was carried out on a Nanosurf AFM, and AFM of Si(111) on a DI nanoscope.

5.4.2 Alkene coupling to silicon hydride

For the synthesis of monolayers of dodecene and docosene on silicon hydride, the alkenes were first deoxygenated by freeze-pump-thaw cycles. The etched wafer was added directly after etching and washing. The reaction vessel was then heated to 200 degrees under nitrogen for 4 hours. The silicon was then removed and rinsed repeatedly in dichloromethane and toluene, as well as sonicating in both solvents. Ellipsometry measurements were conducted with a Gaertner ellipsometer and contact angle measurements with a HG-DM goniometer (CHIU Technical Corporation).

The hydroxyl terminated alkene, ω-undecenyl alcohol, was also deoxygenated by freeze-pump-thaw cycles. Attachment to silicon was achieved by heating to 80 degrees for 24 hours.

5.4.3 Carbon nanotubes

P3 arc discharge SWNTs were prepared for attachment to silicon via sonication with a sonicator probe for several hours in dimethyl formamide. HipCO SWNTs were sonicated in 3:1 conc. sulphuric acid:hydrogen peroxide solution for 24 hours, before filtering, drying and redispersing in dry DMF by more sonication.

Ester coupling of CNTs to hydroxyl functionalised silicon was achieved via a DCC coupling. Excess dicyclohexylcarbodiimide (300 mg) was added to about 1 mg of CNTs in dry DMF (5 ml) and stirred under nitrogen for 2 hours. The functionalised silicon was then added with a catalytic quantity of dimethylaminopyridine (DMAP) and the vessel heated to 80 degrees for two hours. The reacted silicon was rinsed and sonicated in IPA for ten minutes.

SEM was performed on a Hitachi S4700 FI-SEM.

References

[1] J. Yu, D. Losic, M. Marshall, T. Bocking, J.J. Gooding and J.G. Shapter, *Soft Matter* **2** 2006 1081
[2] Z. Poh, B. Flavel, C. Shearer et al., *Mater. Lett.* **63** 2009 757
[3] Z. Wei, M Kondratenko, L. Dao and D.F. Perepichka, *J. Am. Chem. Soc.* **128** 2006 3134
[4] M. Linford and C Chidsey, *J. Am. Chem. Soc.* **117** 1995 3145

[5] M. Linford, P. Fenter, P. Eisenberger and C. Chidsey, *J. Am. Chem. Soc.* **115** 1993 12631
[6] T Böcking, A Salomon, D Cahen et al., *Langmuir* **23** 2007 3236
[7] O. Seitz, T. Bocking, A Salomon et al., *Langmuir* **22** 2006 6915
[8] U. Neuwald, H. Hessel, A. Feltz et al., *Surf. Sci. Lett.* **296** 1993 L8
[9] P. Allongue, C Henry de Villeneuve, S Morin et al., *Electrochim. Acta* **45** 2000 4591
[10] J. H. Ouyang, X. S. Zhao et al.**,** *J. Appl. Phys*. **93** 7 2003
[11] F**.** Thieblemont**,** O. Seitz, A Vilan and H. Cohen, *Adv. Mat.* **20** 2008 3931
[12] K. J. Ziegler, Z. Gu, H. Peng and E. Flor, *J. Am. Chem. Soc.* **127** (5) 2005 1541
[13] X. X. Wang and J. N Wang, *Carbon* **46** 2008 117

Abbreviations

AFM	**Atomic force microscopy**
CNT	**Carbon nanotube**
CVD	**Chemical vapour deposition**
DCC	**Dicyclohexylcarbodiimide**
DCM	**Dichloromethane**
DMAP	**Dimethylaminopyridine**
DMF	**Dimethylformamide**
DOS	**Density of states (electronic)**
ETM	**Electron transporting material**
FET	**Field-effect transistor**
HOMO/LUMO	**Highest occupied/Lowest unoccupied molecular orbital**
HTM	**Hole transporting material**
IR	**Infra-red**
ITO	**Indium tin oxide**
MWNT	**Multi-walled carbon nanotube**
NPB	**N,N'-diphenyl-N,N'-bis(1-naphthyl)-(1,1'-biphenyl)-4,4'-diamine**
OLED	**Organic light-emitting diode**
P3HT	**Poly(3-hexylthiophene)**
PCBM	**[6,6]-phenyl-C_{61}-butyric acid methyl ester**

PEDOT	**Poly(ethylenedioxythiophene)**
PEDOT:PSS	**Emulsion of PEDOT with poly(styrenesulphonate)**
PET	**Polyethylene terephthalate**
PPV	**Poly(phenylene vinylene)**
PV	**Photovoltaic**
PVK	**Poly(vinylcarbazole)**
RBM	**Radial breathing mode (Raman spec.)**
SDS	**Sodium dodecylsulphate**
SEM/TEM	**Scanning/Transmission electron microscopy**
STM	**Scanning tunnelling microscopy**
SWNT	**Single-walled carbon nanotube**
$\mathbf{TBAPF_6}$	**Tetrabutylammonium hexylfluorophosphate**